University of Crete
School of Sciences
Department of Physics

Master Thesis

Biomedical Applications via Nonlinear Lithography

Vasileia N. Melissinaki

Supervisor: Prof. C. Fotakis
Advisor: Dr. M. Farsari

Heraklion, Crete
July 2011

Πανεπιστήμιο Κρήτης
Σχολή Θετικών Επιστημών
Τμήμα Φυσικής

Μεταπτυχιακή Εργασία

Βιοϊατρικές εφαρμογές μη γραμμικής λιθογραφίας

Βασιλεία Ν. Μελισσινάκη

Υπεύθυνος Καθηγητής: Καθ. Κ. Φωτάκης
Επιβλέπουσα: Δρ. Μ. Φαρσάρη

Ηράκλειο Κρήτης
Ιούλιος 2011

Acknowledgments – Ευχαριστίες

Για την διεκπεραίωση της εργασίας αυτής συνέβαλαν πολλοί άνθρωποι, τους οποίους θα ήθελα να ευχαριστήσω, τόσο για την υλική υποστήριξη και για τις γνώσεις που μου προσέφεραν, όσο και την ψυχολογική υποστήριξη στις δύσκολες στιγμές.

Καταρχήν, θα ήθελα να ευχαριστήσω τον υπεύθυνο καθηγητή της εργασίας αυτής, κ. Κωνσταντίνο Φωτάκη, διευθυντή του Ι.Η.Λ.Δ. του Ι.Τ.Ε., ο οποίος μου έδωσε την ευκαιρία να εργαστώ στα εργαστήρια λέιζερ κατά την διάρκεια διεκπεραίωσης των πειραμάτων.

Στη συνέχεια, θα ήθελα να ευχαριστήσω την επιβλέπουσα της εργασίας αυτής, κα. Μαρία Φαρσάρη, ερευνήτρια του Ι.Η.Λ.Δ., για την πολύτιμη υποστήριξη της τόσο υλικά όσο και επιστημονικά. Επίσης, να ευχαριστήσω θερμά την κα. Ανθή Ρανέλλα για την άψογη συνεργασία που είχαμε στο βιολογικό μέρος αυτής της εργασίας, τόσο στο πειραματικό κομμάτι όσο και στις γνώσεις βιολογίας που μου μεταλαμπάδευσε.

Επιπλέον να ευχαριστήσω θερμά τον κ. Παναγιώτη Τζανετάκη για την συμμετοχή του στην τριμελή επιτροπή της παρούσας εργασίας.

Να ευχαριστήσω ακόμα, την κα. Μαρία Βαμβακάκη για την συνεργασία μας στην κατασκευή των υλικών που χρησιμοποιήθηκαν στο πρώτο μέρος της εργασίας, αλλά και για τις πληροφορίες σε θέματα χημείας, ενώ για το υλικό στο δεύτερο μέρος της εργασίας αυτής θα ήθελα να ευχαριστήσω τον λέκτορα Frederik Claeyssens από το Kroto Research Institute και το τμήμα Μηχανικής και Επιστήμης Υλικών του Πανεπιστημίου του Sheffield. Να ευχαριστήσω επίσης, τον διδακτορικό φοιτητή του, Andrew Gills για την συνεργασία μας στο δεύτερο μέρος αυτής της εργασίας.

Θα ήθελα επίσης να ευχαριστήσω θερμά τα παιδιά της ομάδας μου, Ελένη – Ασημίνα Καμπουράκη για την βοήθεια στη σύνθεση τον χημικών διαλυμάτων αλλά και για τις συζητήσεις μας όσον αφορά τα πειράματα, την Αναστασία Γιακουμάκη για την βοήθεια στη σύνθεση τον χημικών διαλυμάτων και τον Στέλιο Ψυχαράκη για την βοήθεια στις καλλιέργειες κυττάρων. Θα ήθελα ακόμα να ευχαριστήσω θερμά τον Αλέξανδρο Σελίμη, καθώς επίσης και την Μαρία Συγλέτου για την βοήθεια που μου προσέφεραν στην χρήση του Excimer Laser.

Να ευχαριστήσω ακόμα, τις κυρίες Αλεξάνδρα Σιακούλη και Αλέκα Μανουσάκη για την βοήθεια τους στην μελέτη των δειγμάτων με την χρήση του Ηλεκτρονικού Μικροσκοπίου Σάρωσης, καθώς επίσης και των κύριο Γιώργο Βρέντζο από το Ινστιτούτο Μοριακής Βιολογίας και Βιοτεχνολογίας για την καθοδήγηση σε τεχνικά θέματα στις καλλιέργειες κυττάρων .

Τέλος, το μεγαλύτερο και θερμότερο ευχαριστώ θα ήθελα να το πω στην οικογένεια μου, η οποία με στήριζε και με στηρίζει με υπομονή και κατανόηση σε κάθε μου βήμα.

Σας ευχαριστώ πολύ όλους σας!

Abstract

In the past few years, direct laser writing technology has been extensively studied, due to its ability for direct fabricating of complex 3D structures, which scale varies from several nanometers to some millimeters. This technology is based on nonlinear lithography and specifically, on two-photon polymerization process induced with a femtosecond laser. In this thesis, two-photon polymerization process was used for creating scaffolds with photosensitive biomaterials, for biomedical applications.

In the first part, the 3D scaffolds' fabrication using photosensitive, non-biodegradable materials has been investigated. The ability to develop 3D cell cultures on these scaffolds for tissue engineering applications has also been studied. Tissue engineering is a technology based on developing biological substitutes for the repair, reconstruction, regeneration or replacement of tissue. In this study, two organic-inorganic hybrid photosensitive sol-gel materials were used; a Zirconium based and a Titanium based material. The next step after the successful results of fibroblast cultivation on 2D thin films, was the fabrication of 3D complex porous structures, with the same materials and by using the same process of cultivation, inspiring results were given.

In the second part, a new biodegradable polylactide-based material was used for fabricating tissue engineering scaffolds. In cooperation with the Kroto Research Institute and specifically the Department of Materials Science and Engineering of University of Sheffield, where the material was synthesized, neuronal cells (cell line PC12), as well as fibroblast cells (cell line 3T3), were cultivated on two dimensional thin films for checking the cells viability and proliferation and after the encouraging biocompatibility results, 3D complex porous structures were fabricated. The cells cultivation on the 3D scaffolds had successful results.

TABLE OF CONTENTS

CHAPTER 1
INTRODUCTION

1.1 Overview

The lack of tissue and organs available for transplantation, as well as the problems associated with their transplantation such as donor site morbidity, immune rejection, and pathogen transfer, led to the emergence of the discipline of tissue engineering. The ultimate goal of tissue engineering as a treatment concept is to replace and even recover the anatomic structures and functions of the damaged, injured, or missing tissue and organs [1-3].

Tissue engineering science is the employ of physical, chemical, biological, and engineering treat to control and direct the various behaviours of cells. The interdisciplinary field of tissue engineering has been one of the most active and quickly expanding disciplines during the past two decades.

All tissue and organs in the body are three-dimensional structures. In order to repair and regenerate lost or damaged tissue and organs, three-dimensional scaffolds must be designed, fabricated, and utilized to regenerate the tissue similar in both anatomical structure and function to the original tissue or organ to be replaced or repaired. Therefore, certain principles of scaffold design must be established to ensure proper tissue regeneration.

A scaffold is an artificial three-dimensional frame structure that serves as a mimic of extracellular matrix for cellular adhesion, migration, proliferation, and tissue regeneration in three dimensions. Its architecture and microstructure define the ultimate shape and structure of the regenerated tissue and organs. An ideal scaffold for tissue engineering should possess the following characteristics [4-8] :

1. It is highly biocompatible and does not elicit an immunological or clinically detectable foreign body reaction.
2. It has a suitable surface chemistry allowing for cell attachment, migration, proliferation, and differentiation.
3. It is three-dimensional and capable of regenerating tissue and organs in their normal physiological shape.
4. It has controllable degradation and resorption rates that match the rate of tissue growth in vitro, ex vivo, and in vivo for biodegradable or resorbable materials.
5. It is highly porous with an interconnected pore network available for cell growth and nutrient and metabolic waste transport.
6. It possesses the appropriate mechanical properties which match those of the normal tissue and organs; and
7. It has a bioactive surface to encourage faster regeneration of the tissue.

The ultimate goal in scaffolding studies is to create the ideal scaffold, which would not only provide structural support, but also exchange physicochemical signals with the surrounding cells

and the host environment. For these reasons, biomaterials are the artificial materials utilized to repair, assist, or replace damaged or missing tissue or organs. Biomaterials are categorized in natural (collagen, elastin etc.) and synthetics. Like any other industrial material, biomaterials can be classified into four different categories: metals, ceramics, polymers, and composites. In order for any material to be considered a biomaterial, it must satisfy certain physical, mechanical, and chemical behavior requirements and also be biocompatible. For example, the material must be strong enough to bear physiological loads, be resistant to undesired degradation or corrosion, not be carcinogenic, immunogenic, antileukotactic, or mutagenic, and so on. Many factors, such as implant size, shape, material composition, surface wettability, roughness, and charge influence implant biocompatibility [2,9,10].

Currently, metals have been extensively used in orthopedic applications, especially for bone and dental replacements. However, there are very few uses of metals as tissue engineering scaffolds, due to their non-degradability and undesirable mechanical properties when compared with normal tissue [11,12].

Ceramics are inorganic materials primarily used in tissue engineering to serve as supporting scaffolds for cell culture and hard tissue formation and as carriers for bioactive molecule delivery [13-18].

Polymers are organic and the major compositional elements, which are similar to that of the human body, are carbon, hydrogen, oxygen, nitrogen, sulfur, and phosphorus. Due to differences in elemental arrangements and production methods, polymers are the most diverse type of materials with varying mechanical and physical properties and different levels of chemical reactivity and degradation. Owing to these differences, polymers are the most popular materials used for tissue engineering [11,16,19-22]. Specifically, biodegradable polymers show the most promising results for use as scaffolds and three categories of biodegradable polymers are the most frequently studied: (1) FDA-approved biodegradable and bioresorbable polymers, including natural and synthetic polymers, such as collagen, polyglycolide (PGA), polylactide (PLA), polycaprolactone (PCL), etc.; (2) non-approved polymers, such as polyorthoester (POE), polyanhydrides, etc. ; and (3) customized degradable polymers, which can selectively bind specific cell types and ward off unwanted cell types.

Composite materials are composed of at least two different categories of materials. The composites used for tissue engineering usually consist of polymers and ceramics. The typical composites are a mixture of hydroxy apatite or Bioglass with biodegradable polymers, such as polyesters [24]. The major application of these scaffolds is use for hard tissue engineering [11,23,24].

The artificial materials used for tissue engineering scaffolds can be polymers, ceramics, or composites and can be purely natural or fully synthetic. The trend in developing biomaterials for scaffolds includes the use of:

1. Temporary scaffolds, which gradually disappear after their intended use is completed.
2. Smart materials, which can respond to stimulation of the biological environment [25].
3. Scaffold chemistry patterning, using protein stamping [26,27], microfliudic patterning [28], or photochemical modification [29] to incorporate specific bioactive domains on the scaffold surface to promote cell adhesion, migration, and tissue ingrowth and repair.
4. Pulsatile delivery of drugs or bioactive molecules on demand [30]; and
5. Anti-nonspecific adsorption surfaces, which can block undesirable protein and cell adhesion [8,31].

A number of scaffold fabrication technologies have been developed or adopted from other disciplines for tissue engineering. There are three basic categories: three-dimensional polymeric scaffold fabrication, fiber and textile fabrication, and inorganic scaffold fabrication.

Techniques such us, stack method, solvent casting [32], spin casting [33], particulate leaching [34], supercritical-fluid gassing process [35], emulsion freeze drying [36], phase separation [37], fiber bonding [38], membrane lamination [39], melt molding [40], fused deposition modelling [39], three-dimensional printing [41] and so on have been proposed and utilized in fabricating three-dimensional scaffolds from polymeric materials.

In this thesis, a nonlinear lithography technique, two photon polymerization process was used for fabricating 3D complex tissue engineering porous scaffolds. Two photon polymerization is a highly promising technique for the fabrication of micron and submicron scale structures, which use an ultra–fast (femtosecond) laser. When the beam is tightly focusing into the volume of the photosensitive material, the pulses interact with the material through two photon absorption and two photon polymerization process starts. By moving the laser focus in three dimensions through the material, the polymerization process transferring liquid material into the solid state and the result is the fabrication of the 3D structure. After the illumination, the unmodified material is removed by an appropriate developer and the fabricated structure is revealed.

Firstly in this study, cells growth on 3D non-biodegradable scaffolds was investigated. As has already been mentioned, the materials that have been used, were Zirconium based and Titanium based materials. The hybrid Zirconium and Titanium based materials were prepared by a photosensitive sol-gel process which involved the sequential catalytic hydrolysis of sol-gel precursors and the heat-activated polycondensation of the hydrolyzed products, followed by the photopolymerization of the pendant organic moieties. The bioactivity of the materials was checked in previous work, by the cultivation of murine fibroblast cells (NIH / 3T3 fibroblasts) on

two dimensional thin films, which were prepared by spin-coating onto glass substrates. The cultivation of these films was for one, three, five and seven days. After the cultivation, cells viability, attachment of cells on the films and their cytoskeleton, were checked with a fluorescent microscope. The results show that cells were alive, with a well-spread morphology and good surface coverage. Besides that the attachment on films and their cytoskeleton arraignment were very good. Since the biocompatibility of materials was secured we proceeded to the cultivation on 3D scaffolds. The choice of scaffold for cell cultivation can greatly influence cell attachment, migration and differentiation. For that reason, we were fabricated firstly simple cubes and afterwards cross-hatched and woodpile structures, on which we cultivated again murine fibroblast cells. After the cultivation, the migration and the attachment of cells on the 3D scaffolds were investigated with a scanning electron microscope. The results show again a well-spread morphology and good surface coverage.

In the second part of this study, a new biodegradable polylactide-based material was used for fabricating tissue engineering scaffolds. As was already mentioned, except of the use of non-biodegradable materials in biomedicine, there is the need of temporary scaffolds, which gradually disappear after their intended use is completed. For that reason, this new material was synthesized in Kroto Research Institute and specifically the Department of Materials Science and Engineering of University of Sheffield, with which we cooperate in this study. At this part, cells viability and proliferation, was checked by the cultivation of neuronal cells (cell line PC12), as well as fibroblast cells (cell line3T3), on two dimensional thin films, which were prepared by spin-coating onto glass substrates. The cultivation time was again, for one, three, five and seven days and a fluorescent microscope was used for the treatment of samples. The results show that cells were alive, and SEM images demonstrated a well-spread morphology and good surface coverage and attachment on films. Then, 3D complex porous structures were fabricated, in different sketches and dimensions, for the investigation of cells migration and attachment on them. The results show a well-spread morphology and good surface coverage.

1.2 Chapter content

In **chapter 2** we will analyze the methods that were used and summarize their theory. In **chapter 3** we will describe the materials that we were used. **In chapter 4** we will analyze the experimental techniques, as well as the set-ups that were used for the experiments. In **chapter 5** we will present the results of cells cultivation on thin films and the cells cultivation on 3D non-biodegradable and biodegradable scaffold fabricated by two photon polymerization process.

References

1. Caplan, A. I. **Tissue engineering designs for the future: new logics, old molecules**. Tissue Eng. 6(1): 1-8(2000).

2. Ibarra, C., J. A. Koski, and R. F. Warren. **Tissue engineering meniscus: cells and matrix**. Orthop Clin North Am. 31(3): 411-418(2000).

3. Langer, R. & Vacanti, J. P. **Tissue engineering**. Science **260,** 920–926 (1993).

4. Atala, A. **Tissue engineering of artificial organs**. J Endourol. 14(1): 49-57.

5. Mayer, J., et al. **Matrices for tissue engineering-scaffold structure for a bioartificial liver support system**. J Controlled Release. 64(1-3): 81-90(2000).

6. Peter, S. J., et al. **Polymer concepts in tissue engineering**. J Biomed Mater Res. 43(4): 422-427(1998)

7. Cima, L. G., et al. **Tissue engineering by cell transplantation using degradable polymer substrates**. J Biomech Eng. 113(2): 143-151(1991).

8. Hubbell, J. A. **Biomaterials in tissue engineering**. Biotechnology (N Y). 13(6): 565-576(1995).

9. Boyan, B. D., et al. **Bone and cartilage tissue engineering**. Clin Plast Surg, 1999. 26(4): 629-645(1999).

10. Ratner, B. D. **Biomaterials science : an introduction to materials in medicine**. San Diego: Academic Press. 1-63(1996).

11. B. D. Ratner, A.s. Hoffman, **Biomaterials Science. An Introduction to Materials in Medicine**. Academic Press, 1996, Chapter 2.

12. J. B. Park, J. D. Bronzino, **Biomaterials. Principles and Applications**. CRC Press, 2003, Chapter 1.

13. Shinto, Y., et al. **Calcium hydroxyapatite ceramic used as a delivery system for antibiotics**. J Bone Joint Surg Br. 74(4): 600-604(1992).

14. Nolan, P. C., D. J. Wilson and R. A. Mollan. **Calcium hydroxyapatite ceramic delivery system.** J Bone Joint Surg Br. 75(2): 334 -335(1993).

15. De Diego, M. A., N. J. Coleman and L. L. Hench, **Tensile properties of bioactive fibers for tissue engineering applications**. J Biomed Mater Res. 53(3): 199 -203(2000).

16. K. C. Dee, D. A. Puleo, R. Bizios, **An Introduction To Tissue- Biomaterial Interactions**. Wiley-Liss, 2002, Chapter 1.

17. J. B. Park, J. D. Bronzino, **Biomaterials. Principles and Applications**. CRC Press, 2003, Chapter 2.

18. A. R. Boccaccini, J. E. Gough, **Tissue engineering using ceramics and polymers.** CRC Press, Woodhead Publishing Limited, 2007, Chapter 1.

19. J. B. Park, J. D. Bronzino, **Biomaterials. Principles and Applications**. CRC Press, 2003, Chapter 3.

20. Peter, S. J., et al. **Polymer concepts in tissue engineering**. J Biomed Mater Res. 43(4): 422-427(1998).

21. Cima, L. G., et al. **Tissue engineering by cell transplantation using degradable polymer substrates**. J Biomech Eng. 113(2): 143-151(1991).

22. A. R. Boccaccini, J. E. Gough, **Tissue engineering using ceramics and polymers.** CRC Press, Woodhead Publishing Limited, 2007, Chapter 2.

23. J. B. Park, J. D. Bronzino, **Biomaterials. Principles and Applications**. CRC Press, 2003, Chapter 4.

24. Ma, P. X., et al. **Engineering new bone tissue in vitro on highly porous poly(alpha-hydroxyl acids)/hydroxyapatite composite scaffolds**. J Biomed Mater Res. 54(2): 284-293 (2001).

25. Gan, D. and L. A. Lyon. **Tunable swelling kinetics in core — shell hydrogel nanoparticles**. JAmChemSoc. 123(31): 7511-7517(2001).

26. Patel, N. , et al. **Printing patterns of biospecifically - adsorbed protein**. J Biomater Sci PolymEd. 11(3): 319-331(2000).

27. Okabe, Y., et al. **Chemical force microscopy of microcontact-printed self-assembled monolayers by pulsed - force - mode atomic force microscopy**. Ultramicroscopy. 82(1-4): 203-212(2000).

28. Delamarche, E., et al. **Patterned delivery of immunoglobulins to surfaces using microfluidic networks.** Science. 276(5313): 779-781(1997).

29. Park, Y. J., et al. **Controlled release of platelet-derived growth factor from porous poly (L-lactide) membranes for guided tissue regeneration**. J Controlled Release. 51(2 -3): 201-211(1998).

30. Benghuzzi, H., R. Possley and B. England. **Pulsatile delivery of progesterone and estradiol to mimic the ovulatory surge in adult ewes by means of TCPL implants**. Biomed Sci lnstrum. 30: 187-195(1994).

31. Vert, M., et al. **Bioresorbability and biocompatibility of aliphatic polyesters**. J. Mater. Sci. 3: 432-446(1992).

32. Chun-Jen Liao, Chin-Fu Chen, et al. **Fabrication of porous biodegradable polymer scaffolds using a solvent merging/particulate leaching method**. Journal of Biomedical Materials ResearchVolume 59, Issue 4, (2001).

33. A. Khademhosseini, R. Langer, et al. **Microscale technologies for tissue engineering and biology**. 2480–2487, PNAS, (2006), vol. 103, no. 8.

34. Kang HG, Kim SY, Lee YM. **Novel porous gelatin scaffolds by overrun/particle leaching process for tissue engineering applications**. Journal of Biomedical Materials Research Part B: Applied Biomaterials, (2006) Nov; 79(2):388-97.

35. R. A. Quirk, R. M. France, et al. **Supercritical fluid technologies and tissue engineering scaffolds.** Current Opinion in Solid State and Materials Science 8 (2004) 313–321**.**

36. K. Whang, C. H. Thomas and K. E. Healy, **A novel method to fabricate bioabsorbable scaffolds**. Polymer, Volume 36, Issue 4, (1995), 837-842.

37. G. Wei, P. X. Ma, **Structure and properties of nano-hydroxyapatite/polymer composite scaffolds for bone tissue engineering.** Biomaterials 25 (2004) 4749–4757.

38. K. Tuzlakoglu, N. Bolgen et al. **Nano- and micro-fiber combined scaffolds: A new architecture for bone tissue engineering**. Journal of Materials Science: Materials in Medicine, Volume 16, Number 12, 1099-1104.

39. D. W. Hutmacher, **Scaffolds in tissue engineering bone and cartilage**. Biomaterials 21, (2000),2529-2543.

40. S. Oh, S. Kang et al. **Fabrication and characterization of hydrophilic poly(lactic-*co*-glycolic acid)/poly(vinyl alcohol) blend cell scaffolds by melt-molding particulate-leaching method**. Biomaterials, Volume 24, Issue 22, (2003), 4011-4021.

41. H. Seitz, W. Rieder, S. Irsen, B. Leukers, C. Tille, **Three-dimensional printing of porous ceramic scaffolds for bone tissue engineering**. Journal of Biomedical Materials Research Part B: Applied Biomaterials, Volume 74B, Issue 2, (2005), 782–788.

CHAPTER 2
METHODS

In this chapter are being explained the methods that were used in this study. In the first part are explained the meanings of tissue engineering and biocompatibility. The second part describe the two dimensional patterning method. Finally, in the third part is presented the three dimensional patterning method and more specifically is explained multi-photon polymerization.

2.1 Tissue engineering

A commonly applied definition of tissue engineering, as stated by Langer and Vacanti, is "an interdisciplinary field that applies the principles of engineering and life sciences toward the development of biological substitutes that restore, maintain, or improve tissues function or a whole organ". Tissue engineering has also been defined as "understanding the principles of tissue growth, and applying this to produce functional replacement tissue for clinical use." A further description goes on to say that an "underlying supposition of tissue engineering is that the employment of natural biology of the system will allow for greater success in developing therapeutic strategies aimed at the replacement, repair, maintenance, and/or enhancement of tissue function." In general, tissue engineering was categorised under biomaterials, but now it is big field so it can be considered as separate field, and is the use of a combination of cells, engineering and materials methods, and suitable biochemical and physio-chemical factors to improve or replace biological functions[2]. While most definitions of tissue engineering cover a broad range of applications, in practice the term is closely associated with applications that repair or replace portions of or whole tissues.

Biomaterials play a pivotal role in field of tissue engineering[1]. There can be no doubt that the most widely recognized applications of biomaterials involve those situations where a tissue or organ has suffered from some disease or condition that has resulted in pain, malfunction or structural degeneration, and which can only be alleviated by the replacement or augmentation of the affected part. The cause of the condition could be bacterial, viral or fungal, or could be related to an autoimmune, sclerotic, neoplastic or simply age-related process. They require that the pain is reduced or eliminated and that the offending tissue be circumvented by an alternative structure that is able to provide a degree of function compatible with the normal expectations of such a person. It may well be that this is best achieved by removal of the tissue and its replacement, but the objective may be better satisfied by introducing an additional functional component into the body that takes on the role of the affected tissue. It is, with a few exceptions, not necessary to make the prosthetic component look like or otherwise physically resemble the tissue that it is replacing, as long as it carries out the appropriate function. It follows on from this that it is a further, and indeed crucial, requirement that this prosthetic component is able to perform this function for as long as the patient is alive.

The main examples of this type of implantable device or prosthesis are joint replacements,

vascular grafts that replace blood vessels, prosthetic heart valves, venous valves soft tissue (e.g. breast tissue) reconstruction prostheses, dental implants and restorative materials, and intraocular lenses for the treatment of cataracts.,

A further type of application is the transient implantable system that is directed towards the temporary support of traumatised or deformed tissues. This includes sutures, clips, adhesives and staples for soft tissues, haemostatic and sealant materials and devices in the vascular system, plates, screws, pins and fixators for bone fracture repair and devices in orthodontics for tooth movement. Sometimes these devices are directed towards the regeneration of new tissue rather than assisting a natural repair process. The regeneration of skin in areas of chronic ulcers or burns, and the regeneration of tendons and ligaments after sporting injuries are good examples. The requirements in these cases will be varied depending upon the stress transfer system within the device-tissue complex and on the desire for biostability or biodegradation.

This review of the current clinical applications of biomaterials indicates the extensive range of functions and properties that are necessary.Biomimetic synthetic polymers have been created to elicit specific cellular functions and to direct cell-cell interactions both in implants that are initially cell-free, which may serve as matrices to conduct tissue regeneration, and in implants to support cell transplantation. These materials have been patterned in two-and three-dimensions to generate model multicellular tissue architectures, and this approach may be useful in future efforts to generate complex organizations of multiple cell types[15-24].

Figure 1: Tissue engineering approaches. Tissue engineering approaches are classified into three categories: (i) cells alone, (ii) cells with scaffolds, and (iii) scaffolds alone. Each one of these approaches can be enhanced by in vitro microenvironmental factors before application as a tissue substitute.

2.1.1 Biocompatibility

Biocompatibility is concerned with the interactions that take place between biomaterial and the tissue of the body. It is an enormously complex matter, involving a large number of mechanisms. It is intuitively obvious that since the human body does not normally contain foreign objects, such as large pieces of metal or plastic, and since evolution has determined that the body has exquisitely refined capabilities to defend itself against invasion, for example by bacteria, we should expect there to be a strong inherent capacity to respond aggressively to implanted medical devices. In the early stages of biomaterials development, there was only one major thought lying behind any decision to use a material on the basis of biocompatibility, which was that the material should do the patient no harm. This implied that the material should not interact with the body but merely reside in the body, carrying out its intended function without either being affected by the tissues or having any influence on those tissues. Early papers on the selection of biomaterials would set out the criteria in terms of a series of negatives such that the material should be inert and non-toxic, non-irritant, non-thrombogenic and so on[3-9]. At this time this was a sensible position and led, as we shall see, to the emergence of several materials that gave good performance in a range of devices, such as titanium, carbon and silicone elastomers.

It was, however, naïve to believe that anything could be placed in the human body without there being any interaction between the material and the tissue. Whilst it is certainly true that good performance has been achieved with a limited number of materials in a limited number of applications, there have been many other situations where success has been very hard to achieve on this basis. It is necessary therefore to consider the principles of these interactions in order to understand the rationale of the selection of biomaterials today, and the rationale of a somewhat different approach to reconstructive surgery. It is worth bearing in mind the currently accepted definition of biocompatibility, which is ‘the ability of a material to perform with an appropriate host response in a given situation’ . This definition emphasises the positive nature of the interactions. It allows for the act that the most appropriate situation may be inertness and non-recognition, but also implies that interactivity between the material and the host could be positively encouraged and directed in a way that is the most beneficial for the functionality and retention of the device.

Biocompatibility is not controlled by one process but is the sum of many different processes. There are two compartments in this system, the material and the host tissue, and it is usual to consider the reactions that occur within these separate parts. It is also important, however, that the phenomena within these two components are often mutually interdependent, and that there is an interface between them, which plays a crucial, of often subtle, role in the developing process.

2.2 2D Patterning Method

Two dimensional patterns with biomolecules (e.g., DNA and proteins), cells, and tissues immobilized on solid substrates are important tools for biological research, including genomics, proteomics, and cell analysis[15-17]. More specifically, cell microarrays offer tremendous versatility because several experimental parameters can be varied in combinatorial fashion to give a nearly endless variety of potential applications. Variables include the substance arrayed, the cell line, the cell culture conditions (including agents that can be added to the growth medium), external stimuli such as ultraviolet irradiation and the assaying method. Arrays representing particular categories of genes can be produced, such as all known transcription factors or transmembrane receptors. Alternatively, large collections of mutants of a particular gene could be expressed on a cell microarray to elucidate structure–function relationships. The size of cell microarrays would also allow the combinatorial expression of sets of genes products known to interact in biological processes of interest.

According to spot formation techniques, methods are categorized as “contact printing” and “non-contact printing.” [18] Contact printing is a widely used technology, comprising methods such as contact pin printing and microstamping. These methods have many advantages, including reproducibility of printed spots and facile maintenance, a well as drawbacks, including low-throughput fabrication of arrays. Non-contact printing techniques are newer and more varied, comprising photochemistrybased methods, laser writing, electrospray deposition, and inkjet technologies. These technologies emerged from other applications and have the potential to increase microarray fabrication throughput; however, there are several challenges in applying them to microarray fabrication, including interference from satellite drops and biomolecule denaturization. In this stady. non-contact printing techniques were used for the fabrication of 2D substrates.

2.2.1 Non-contact printing techniques

Contact printing methods include a variety of techniques, but all methods ultimately involve contact between the substrate surface and a stamp or pin. In contrast, non-contact printing techniques vary considerably from photochemistry-based methods to laser writing to fluid droplet dispensing.

There are two main advantages to non-contact printing: reduced contamination and higher throughput. By keeping the printing device and the substrate separated at all times, the likelihood of contamination is greatly reduced. Hence, the need to constantly clean the printing device between uses is eliminated. Furthermore, non-contact printing methods hold the greatest potential for

increasing microarray fabrication throughput. Many non-contact methods deposit solutions in parallel, allowing entire arrays to be produced simultaneously.

2.2.1.1 Photolithography

Photochemistry microarray printing is based on chemical treatment of the substrate and UV light exposure through photomasks. In photolithography, a negative photoresist layer is spin-coated onto the substrate, exposed to UV light through a photomask and then developed to remove the non exposed regions of photoresist.

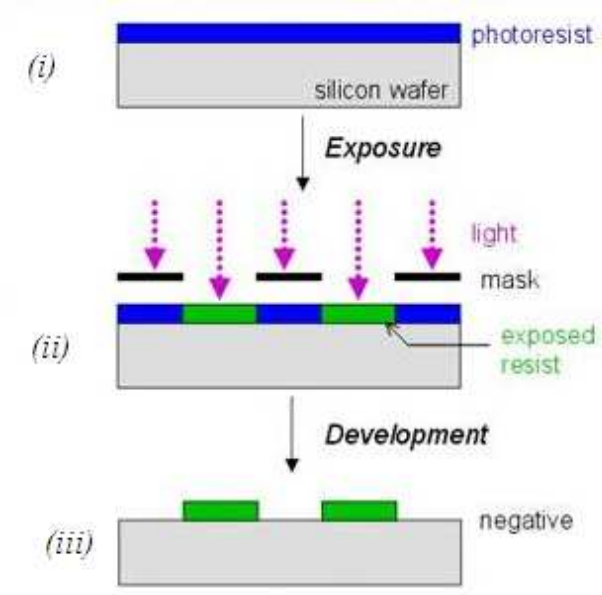

Figure 2: Negative tone photolithography. (i)a negative photoresist layer is spin-coated onto the substrate, (ii) exposure to UV light through a photomask, (iii) development to remove the non exposed regions of photoresist.

2.3 3D Patterning Method

Cell cultures are established in vitro models for studying cellular processes. For many decades cells have been cultivated in 2D. More recently the importance of the third dimension in cell biology has been better understood. The growing knowledge has attracted further attention to 3D culturing[19-24]. For this reason, 3D scaffolds must be fabricated.

The last years has rapid progress in computer-aided manufacturing (CAM) using UV curable resin, generally called laser rapid prototyping, is an expanding technology. It converts three dimensional (3D) objects of complex shape, designed via computer aided design (CAD). From designs into real products. The resin used for fabrication is photocured at the spot exposed to UV

laser, a single photon photopolymerization process. By scanning the laser beam, one slice of the 3D structure is first hardened according to the design patterns: and then a thin-layer liquid resin is added and a new patterned slice is polymerized. The entire structure is sequentially created the same way. This technology is suitable for manufacturing devices that are difficult or costly to prepare by conventional mechanical methods.

Commercial laser rapid prototyping machines have a fabrication precision greater than 10μm. This accuracy cannot fully satisfy the modern requirements for devices multifunctionalization and miniaturization that demand sub-micron feature size. The emergence of a new technology in 1997, two photon photopolymerization, has brought the light curable resin into the realm of nanofabrication. As indicated by the name, the resins are polymerized not by absorbing one UV photon, but by simultaneously absorbing two photons at longer wavelength, usually in the red-infrared (IR) spectral region.

Two photon process has at least two advantages compared to single photon absorption used in conventional rapid prototyping. First, common polymers have negligible linear absorption in the red near-infrared (NIR) region, so the laser penetrates deeply into materials and directly induced polymerization from inside without contaminating outside of focal volume. Secondly, the quadratic dependence of polymerization rate on the light intensity enables 3D spatial resolution, and the accuracy is better than that achieved in single photon process. Actually a near 100nm lateral spatial resolution has been reported. Two polymerization, as currently the only microprocessing approach that has intrinsic 3D fabrication capability, has been successfully applied to production of a variety of photonic and micromechanical devices. It accomplishes manufacturing that is otherwise not accessible and brings new scientific possibilities to nano-research.

Furthermore, in 2005 was experimental reported for the first time the three photon polymerization process (3PP), by M. Farsari, G. Filippidis and C. Fotakis, for fabrication microstructures with high resolution. 3PP is a process which allows the fabrication of components of very high resolution, by the absorption of three photos[35,36].

2.3.1 Two photon polymerization

Although two photon absorption was originally predicted by Maria Göppert-Mayer in 1931 in her doctoral dissertation, the first experimental verification by Isaac Abella, permitted thirty years later, after the invention of the laser[34]. By that experiment, two photon excited fluorescence was detected in a europium-doped crystal and then observed in a vapor (cesium). That season, the technology found limited application, for example, solely as a spectroscopic tool, due to the extremely small absorption cross-section of most materials. In 1965, two photon polymerization

was experimentally reported for the first time by Pao and Rentzepis, as the first example of multiphoton excitation-induced photochemical reactions. They focused 694nm laser from a pulsed Rudy laser into a sample of styrene that was cooled to 77K. After developing in methanol, solid precipitate was extracted and confirmed to be polystyrene through IR absorption. In the particular experiment, no photosensitizer was used and they tried to increase the two photon absorbance by using monomers with added functional groups, such as para-isopropylstyrene and chlorine-substituted derivatives of styrene. As a result, much enhanced two photon polymerization was observed. After this work, although there were some ensuing researchers that were scattered among the literature, no particular efforts were devoted to two photon photopolymerization until this technology found value as a microfabrication tool.

With the advent of convenient femtosecond lasers the utility of two photon excitation processes has undergone a rebirth in the past decade[25-29]. Fluorescent imaging of biological molecules is one of the most important uses. An other one is the stereolithography, in which femtosecond laser has found considerable use in optical memory, micron optical components, photonic crystals and complicated 3D patterning.

Two photon polymerization has unique advantages :

- It has intrinsic ability to produce 3D structures. In addition, the long wavelength chosen for TPA has less absorption and less scattering, which gives rise to the deep penetration of light; use of ultrashort pulses can start intense nonlinear processes at relatively low average power, without thermally damaging the samples.
- The two photon photopolymerization system resembles a laser scanning microscope, which does not need vacuum condition for operation. The system is easy to operate and maintain.
- No mask, mold, or stamp is needed for fabrication. It directly converts computer-designed patterns into matter structures. The rapid turnaround time for fabrication allows one to quickly iterate and modify design.

2.3.1.1 Nonlinear optical effects

Nonlinear processes , for example, multiphoton absorption including two-photon absorption (TPA) , has come to play a dominant role in nanofabrication[30,31]. In order to produce a lasting effect on a material, photons must first be absorbed. The energy and momentum are exchanged between the optical fields and molecules through absorption and emission. In such a process, the imaginary part of nonlinear susceptibility represents the energy transfer from the light field to a medium. The

lightmatter energy change per unit time and unit volume is:

$$\frac{dW}{dt} = \langle \vec{E} \cdot \dot{\vec{P}} \rangle$$

where $\vec{E}$, is the electric field vector and the brackets denote time average.
The value of material polarization P is:

$$P = x^{(1)}E + x^{(2)}E^2 + x^{(3)}E^3 + \ldots$$

where the quantities of $\chi^{(1)}$, $\chi^{(2)}$, $\chi^{(3)}$ are second-, third-, and fourth-rank tensors, representing linear, second-order and third-order optical susceptibilities. In resonant processes, there is no contribution from the even-order susceptibilities like $\chi^{(2)}$ and $\chi^{(4)}$. Therefore, the nonlinear absorption is described by the imaginary parts of $\chi^{(3)}$, $\chi^{(5)}$, of which typical effects are two photon and three-photon absorptions, respectively. Particularly, for degenerate TPA, that is, the process of photons of identical energy are simultaneously absorbed, the energy absorption rate is:

$$\frac{dW}{dt} = \frac{8\pi^2\omega}{c^2n^2} I^2 \,\mathrm{Im}\left[x^{(3)}\right]$$

It is seen that the TPA rate quadratically depends on the light intensity, which is an important mechanism to improve the spatial resolution in two photon fabrication.

2.3.1.2 Sequential and simultaneous TPA

Two photon absorption is a popular multiple photon excitation approach to the initiation of photochemical changes. There are two different mechanisms of TPA: sequential excitation and simultaneous two photon excitation. The former involves the excitation of the absorbing species to a real intermediate state. This first excited state becomes populated by the first absorbed photon and has a well-defined lifetime, typically 10^{-4} to 10^{-9} seconds; this state then absorbs a second photon, as illustrated in figure 3(a). The other mechanism is shown in figure 3(b) : there is no real intermediate state, but a virtual intermediate state is created by the interaction of the absorbing species with the first photon. Only if the second photon arrives within the virtual state lifetime, about 10^{-15} seconds, can it be absorbed. Therefore, it is apparent that higher intensities are required for the second approach, which usually requires a femtosecond laser. In figure 3(a) and 3(b), the energy of the incident photon is given by $\hbar\omega$, where $\hbar$ and ω are Planck's constant divided by 2π and the angular frequency of the incident light, respectively. The absorbing species

is raised to an excited state when it absorbs the energy of the single photon, which is equal to $\hbar\omega = E_1 - E_0$, where E_0 and E_1 are the energy levels ($E_0 < E_1$) of the absorbing species.

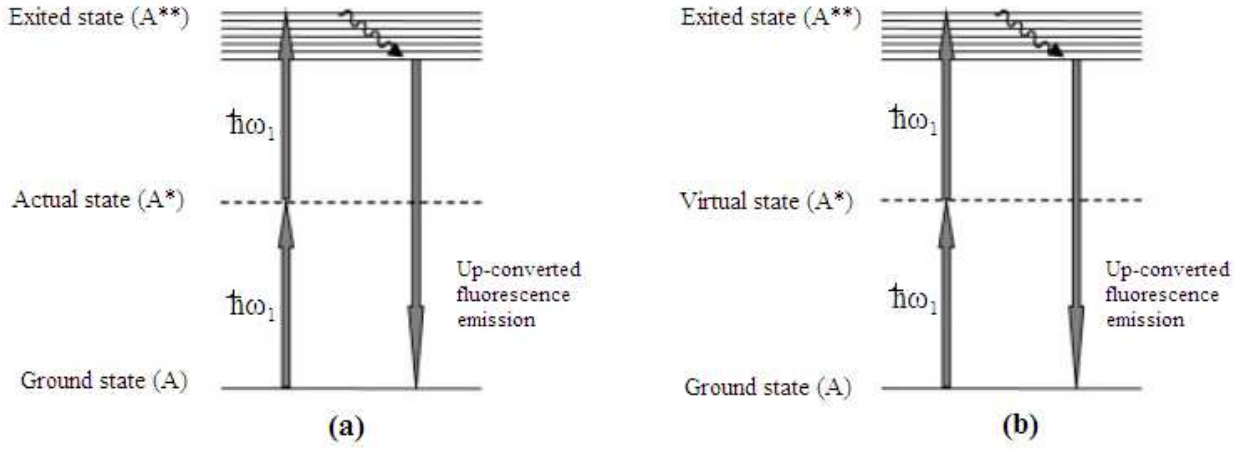

Figure 3: Two mechanisms of TPA: (a) sequential excitation and (b) simultaneous excitation.

In the case of TPA, two photons, each with half energy of the gap between the two energy levels, induce the electron transition. Ti: sapphire lasers are widely used for the inducing TPA because they produce ultrahigh peak power with a very short pulse width of approximately 100femtoseconds (fsec) or less. Furthermore, these lasers are very useful for TPP because of their central wavelength of approximately 800nm, which is close to half of the wavelength of the polymerization. This enables easy control of the polymerization threshold energy.

2.3.1.3 Cross-section in the focused spot

When a laser beam is closely focused with a high NA objective lens into a volume of photocurable resin, as shown in figure 4(a), photon-density-profiles are formed with a constant total number of photons at every cross-section in the focused spot. The constant number of photons at every cross-section precludes optical sectioning by exploiting the linear response of materials to the light intensity based on the single photon absorption. However, if the material response is proportional to the square of the photon density, the integrated material response is greatly enhanced at the focal point, as illustrated in figure 4(b) and 4(c). The two photon transition rate is extremely small in general, so a very high spatial resolution can be obtained,. ie. beneath the limit of diffraction of the light used in the TPP process.

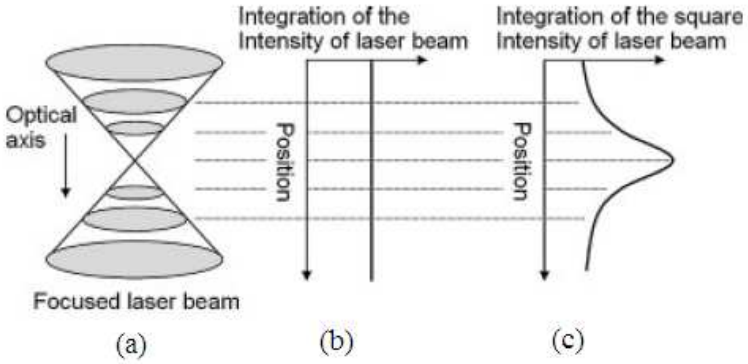

Figure 4: Comparison of TPA with single photon absorption generated by a tightly focused laser beam: (a) schematic diagram of focused laser beam; (b) total single photon absorption per transverse plane; © total two photon absorption per transverse plane, which is calculated by integrating the square intensity over the plane with respect to the optical axis.

2.3.1.4 Fundamentals of stereolithography using two photon photopolymerization

Photopolymerization is one of the most important types of photochemical reaction that have been used for laser fabrication. This is because the material resins undergo a significant phase transition after laser irradiation, from liquid to solid, and non-polymerized liquid is easily removed by a developing process so that solidified 3D structures stand out. The basic components of the starting liquid material are monomers and oligomers (or prepolymer). Upon light excitation, the monomers or oligomers may be solidified by two means: polymerization and crosslinking.

2.3.1.5 Description of polymerization based on radical initiators

An important feature of polymerization is the chain reaction by which macromolecules are created, while cross-linking is concerned more with the formation of crosslinks with chemical bonds. An important difference of these two kinds of reaction lies in their quantum yield, which is defined as the ratio of number of polymerized monomer units to the number of photons that are needed to cause this polymerization.

In the case of photocrosslinking, addition of each monomer unit requires absorption of a photon, leading to a quantum yield less than one.

In contrast, photopolymerization is realized via chain reactions as shown in the following equation, so the quantum yield can reach several thousands.

$$M \xrightarrow{M} M_2 \xrightarrow{M} M_3 ... M_{n-1} \xrightarrow{M} M_n$$

Here M is the monomer or oligomer unit, and M_n , the macromolecule containing n monomer

units. The quantum yield of general monomers and oligomers is low. In order to increase the initiating efficiency, one or several low-weight molecules that are more sensitive to light irradiation are added. They form initiating species of radicals or cautions by absorbing photons. Such small molecules are called photoinitiators:

$$I \xrightarrow{h\nu} I^* \rightarrow R\cdot$$

where symbols denote photoinitiator (I) , radical (R·) and I^* an intermediate state of the photoinitiator after absorbing a photon. Therefore the polymerization process is more precisely described by the following equation:

$$R\cdot + M \rightarrow RM\cdot \xrightarrow{M} RMM\cdots \rightarrow RM_n\cdot$$

The photoproduced radicals react with monomers or oligomers, producing monomer radicals, which combine with new monomers, and so on; so the monomer radicals expand in chain reaction, until two radicals meet with each other. This chain propagation stops in either of the following channels:

$$RM_n\cdot + RM_m\cdot \rightarrow RM_{m+n}R$$

$$RM_n\cdot + RM_m\cdot \rightarrow RM_n + RM_m$$

Therefore the polymerization process consists of several steps: (I) photonitiation, (ii) chain propagation, and (iii) termination.

A good photoinitiator should be (i) easily reduced to an initiating species upon light irradiation, and (ii) provide photoproduced radicals or cautions active enough to react with monomers or oligomers.

The nonlinear response of photopolymerization is caused by highly reactive oxygen molecules absorbed by resin. Oxygen molecules inhibit polymerization reaction at the beginning of polymerization, because oxygen molecules scavenge the radicals that generate the polymerization reaction. Accordingly, when the intensity of light is adequately low. polymerization reaction does not propagate, because almost all the photons are consumed by the oxygen molecules.

A photosensitizer is a molecule that absorbs light and then transfers the energy to a photoinitiator. With such a scheme, the photoinitiation process is expressed as:

$$S \xrightarrow{h\nu} S^* \ldots \xrightarrow{I} I^* \rightarrow R\cdot$$

where S is the photosensitizer. A co-initiator itself does not absorb light, but it is involved in the production of radical species. Reactions that are typically used for laser fabrication are double-bond addition of acrylates (radical-type)

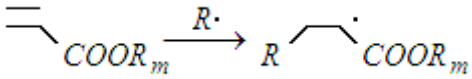

For a radical type initiator, benzoyl is the most widely used chromophore, which must have the initiator, since it exhibits good absorption in the UV region.

After polymerization, the oligomer constitutes the backbone of the polymer network. The physical, chemical and mechanical properties of the solidified resin in strictly depend on the nature and structure of the oligomer. Oligomers, generally contain at least two reactive groups, from which both cross-linking and polymerization could occur.

Monomers have a much smaller molecular weight and consist of one or several reactive groups. They polymerize similarly to oligomers and are an important factor in determining the efficiency of polymerization. In addition, monomers are also useful for diluting resins so that the polymer is easier to handle for a particular use.

For 3D micro-nanolithography, a suitable viscosity is of particular importance due to the opposite requirements in different steps of processing: a high viscosity is needed for keeping early produced volumes where they are created; while a low viscosity facilitates removal of unsolidified resin from intervals. For a successful fabrication the following behaviors are preferred: i) high polymerization efficiency upon light irradiation, (ii) lower shrinkage after polymerization, (iii) fast reaction time and low dark polymerization.

The difference between one photon and two photon induced photopolymerization lies in how the energy for activating initiators is provided. In the case of TPA photopolymerization, initiators are excited to triplet states by absorbing combined two photon energy, so correspondingly Equations …... and …. should be re-written as:

$$I \xrightarrow{2h\nu} I^* \rightarrow R\cdot$$

$$S \xrightarrow{2h\nu} S^* \ldots \xrightarrow{I} I^* \rightarrow R\cdot$$

2.3.2 Applications of TPP

Two photon polymerization as a micro – nanotechnology is used except from tissue engineering and medical applications, in photonics and optoelectronics devices as well for microelectromechanical systems.

References

1. D. F. Williams, **Biomaterials and tissue engineering in reconstructive surgery**. Sadhana, Vol. 28, pp. 563-574.
2. http://en.wikipedia.org/wiki/Tissue_engineering.
3. C. Morrison, R. Macnair, C. MacDonald, A. Wykmant, I. Goldie, M.H. Grant, **In vitro biocompatibility testing of polymers for orthopaedic implants using cultured fibroblasts and osteoblasts**. Biomoterials, 16**,** 987-992, (1995).
4. R. Albulescu, E. Codorean, L. Albulescu, G. Caraene, V. Vulturescu, C. Tanase, **In vitro biocompatibility testing of implantable biomaterials**. Roumanian Biotechnological Letters, Vol. 13, No. 4, , pp. 3863-3872, (2008).
5. S. K. Bhatia and A. B. Yetter, **Correlation of visual in vitro cytotoxicity ratings of biomaterials with quantitative in vitro cell viability measurements**. Cell Biol Toxicol 24, 315–319, (2008).
6. M. L.W. Knetsch, N. Olthof, L. H. Koole, **Polymers with tunable toxicity: A reference scale for cytotoxicity testing of biomaterial surfaces**. Journal of Biomedical Materials Research Part A 947- 957, (2007).
7. M. J. A. Van Luyn, P. B. Van Wachem, P. Nieuwenhuis, L. Olde Damink, H. Ten Hoopen, J. Feijen, **Methylcellulose cell culture as a new cytotoxicity test system for biomaterials**. Journal of Materials Science: Materials in Medicin 2, 142-148, (1991).
8. M. Theiszovα, S. Jantovα, J. Dragïňovα, P. Grznαrovα, M. Palou, **Comparison the Cytotoxicity of Hydroxyapatite Measured by Direct Cell Counting and MTT Test in Murine Fibroblast NIH-3T3 Cells**. Biomed Pap Med Fac Univ Palacky Olomouc Czech Repub., 149(2), 393–396, (2005).
9. T. A.G. Donato , L. H. de Almeida , R. A. Nogueira , T. C. Niemeyer , C. R. Grandini , R. Caram , S. G. Schneider , A. R. Santos Jr., **Cytotoxicity study of some Ti alloys used as biomaterial**. Materials Science and Engineering C 29, 1365–1369, (2009).
10. D. E. Ingber and J. Folkman, **Mechanochemical Switching between Growth and Differentiation during Fibroblast Growth Factor-stimulated Angiogenesis In Vitro: Role**

of Extracellular Matrix. The Journal of Cell Biology, Volume 109, 317-330, (1989).

11. L. N. Novikova, J. Pettersson, M. Brohlin, M. Wiberg, L. N. Novikov, **Biodegradable poly-b-hydroxybutyrate scaffold seeded with Schwann cells to promote spinal cord repair**. Biomaterials 29**,** 1198-1206, (2008).

12. A. Diener, B. Nebe, F. Luthen, P. Becker, U. Beck, H. G. Neumann, J. Rychly, **Control of focal adhesion dynamics by material surface characteristics**. Biomaterials 26, 383–392, (2005).

13. J. Wehland, M. Osborn, K. Weber, **Phalloidin-induced actin polymerization in the cytoplasm of cultured cells interferes with cell locomotion and growth**. Proc. Nati. Acad. Sci. USA, Vol. 74, No. 12, pp. 5613-5617, (1977).

14. M. A. Lana, C. A. Gersbacha, K. E. Michaelc, B. G. Keselowskyc, A. J. Garcıac, **Myoblast proliferation and differentiation on fibronectin-coated self assembled monolayers presenting different surface chemistries**. Biomaterials 26, 4523–4531, (2005).

15. S. Zhang, F. Gelain, X. Zhao, **Designer self-assembling peptide nanofiber scaffolds for 3D tissue cell cultures**. Seminars in Cancer Biology 15**,** 413-420, (2005).

16. D. Falconnet, G. Csucs, H. Grandin. M. textor, **Surface engineering approaches to micropattern surfaces for cell-based assays**. Biomaterials 27**,** 3044-3063, (2006).

17. C. Shen, J. Fu, C. Chen, **Petterning Cell and Tissue Function**. Cellural and Molecular Bioenginiring, Vol. 1, No. 1, 15-23, (2008).

18. I. Barbulovic-Nad, M. Lucente, Yu Sun, Yu Sun, A. R. Wheeler, M. Bussmann, **Bio-Microarray Fabrication Techniques—A Review**. Critical Reviews in Biotechnology, 26, 237–259, (2006).

19. W. Bonfield, **Designing porous scaffolds for tissue engineering**. Phil. Trans. R. Soc. A 364, 227–232, (2006).

20. T.B.F. Woodfield, J. Malda , J. de Wijn, F. P!eters, J. Riesle, C.A. van Blitterswijk, **Design of porous scaffolds for cartilage tissue engineering using a three-dimensional fiber-deposition technique**. Biomaterials 25, 4149–4161, (2004).

21. C. M. Nelson and J. Tien, **Microstructured extracellular matrices in tissue engineering and development**. Current Opinion in Biotechnology 17, 518–523, (2006).

22. S. J. Hollister, **Porous scaffold design for tissue engineering**. Nature Materials , Vol. 4, 518-524, (2005).

23. C. Sandino, J.A. Planell, D. Lacroix, **A finite element study of mechanical stimuli in scaffolds for bone tissue engineering**. Journal of Biomechanics (2008).

24. Yi Lu, G. Mapili, G. Suhali, S. Chen, K. Roy, **A digital micro-mirror device-based system for the microfabrication of complex, spatially patterned tissue engineering scaffolds**. Wiley InterScience, 396-405, (2006).

25. N. H. Rizvi, **Femtosecond laser micromachining: Current status and applications**. Riken Review No. 50, 107-112, (2003).

26. A. Daskalova, **Femtosecond lasers: powerful tools for biological hard tissue investigations**. SPIE (2007).

27. S. Nolte, G. Kamlage, F. Korte, T. Bauer, T. Wagner, A. Ostendorf, C. Fallnich, H. Welling, **Microstructuringwith Femtosecond Lasers**. Advanced Engineering Materials 2, No. 1-2, 23-27, (2000).

28. M. Miwa, S. Juodkazis, T. Kawakami, S. Matsuo, H. Misawa, **Femtosecond two-photon stereo-lithography**. Appl. Phys. A 73, 561–566 (2001).

29. T. Baldacchini, C. N. LaFratta, R. A. Farrer, M. C. Teich, B. E. A. Saleh, M. J. Naughton, J. T. Fourkas, **Acrylic-based resin with favorable properties for three-dimensional two-photon polymerization**. Journal of Applied Physics Vol. 95, No. 11, 6072-6076, (2004).

30. H. Sun, S. Kawata, **Two-photon Phoyopolymerization and 3D Lithographic Microfabrication**. APS 170, 169-273, (2004).

31. H. Misawa, S. Juodkazi, **3D Laser Microfabrication**. WILEY-VCH.

32. K. Lee, D. Yang, S. Park, R. Kim, **Recent developments in the use of two-photon polymerization in precise 2D and 3D microfabrications**. Polymers for advanced Technologies 17, 72-82, (2006).

33. A. Ovsianikov and B. N . Chichkov, **Two - Photon Polymerization – High Resolution 3D Laser Technology and Its Applications**. Nanoelectronics and Photonics 427-446, (2008).

34. http://en.wikipedia.org/wiki/Two-photon_absorption.

35. G. Filippidis, M. Farsari, C. Fotakis, **Construction of sub-micron three-dimensional structures employing multi-photon polymerization**.

36. T. S. Drakakis, G. Papadakis, K. Sambani, G. Filippidis, S. Georgiou, E. Gizeli, C. Fotakis, M. Farsaria, **Construction of three-dimensional biomolecule structures employing femtosecond lasers**. Applied Physics Letters 89, 144108, (2006).

37. A Ostendorf, B. N. Chichkov, **Two photon Polymerization: A New approach to Micromachining**. Photonics Spectra, (2008).

38. L. Li and J. T. Fourkas, **Multiphoton polymerization**. Materials today Vol. 10, No. 6, 30-37, (2007).

39. J. Serbin, A. Egbert, A. Ostendorf, and B. N. Chichkov, R. Houbertz, G. Domann, J. Schulz, C. Cronauer, L. Fröhlich, and M. Popall, **Femtosecond laser-induced two-photon polymerization of inorganic–organic hybrid materials for applications in photonics**. Optics Letters Vol. 28, No. 5, 301-303, (2003).

40. A. Ovsianikov, B. Chichkov, P. Mente, N. A. Monteiro-Riviere, A. Doraiswamy, R. J. Narayan, **Two Photon Polymerization of Polymer–Ceramic Hybrid Materials for Transdermal Drug Delivery**. Int. J. Appl. Ceram. Technol., 4 [1] 22–29, (2007).

41. H. K. Tonshoff, A. Ostendorf, K. Korber, C. Kulik, G. Kamlage, **Micro Material Processing Using UV Laser and Femtosecond Laser**.

42. R. Narayan, C. Jin, A. Doraiswamy, I. Mihailescu, M. Jelinek, A. Ovsianikov, B. N. Chichkov, D. Chrisey, **Laser Processing of Advanced Bioceramics**. Advanced Engineering Materials 7, No. 12, 1083-1098, (2005).

43. A Doraiswamy, C. Jin, R. Narayan, P. Mageswaran, P. Mente, R. Modi, R. Auyeung, D. Chrisey, A. Ovsianikov, B. N. Chichkov, **Two photon indused polymerization of organic-inorganic hybrid biomaterials for microstructured medical devices**. Acta Biomaterialia 2, 267-275, (2006).

44. A. Ovsianikov, S. Schlie, A. Ngezahayo, A. Haverich, B. N. Chichkov, **Two-photon polymerization technique for microfabrication of CAD-designed 3D scaffolds from commercially available photosensitive materials**. J Tissue Eng Regen Med. 1, 443–449, (2007).

45. A. Ovsianikov , A. Ostendorf, B.N. Chichkov, **Three-dimensional photofabrication with femtosecond lasers for applications in photonics and biomedicine**. Applied Surface Science 253, 6599–6602, (2007).

46. J. Stampfl, S. Baudis, C. Heller, R. Liska, A. Neumeister, R. Kling, A. Ostendorf, M. Spitzbart, **Photopolymers with tunable mechanical properties processed by laser-based high-resolution stereolithography**. J. Micromech. Microeng. 18**,** 125014, 1-9, (2008).

CHAPTER 3
MATERIALS

In this chapter the materials that were used in this study are being described. This chapter is separated in two parts. In the first part, we present the non-biodegradable and biodegradable materials, that were used for the films and the 3D structures. In the second part are presented the materials that were used for cells cultivation, viability assay and immuneostaining assays.

A. Materials that were used for thin films and 3D structures

I. Non-biodegradable materials

Biocomposites are excellent organic-inorganic hybrid materials produced by natural biomineralization. Bones, teeth, and shells are typical biocomposites, which consist of an organic polymer matrix reinforced by an inorganic deposit[11]. In biocomposites, the inorganic phase is regularly and highly organized in a polymer matrix.

Over the last decade, new types of copolymers using monomers which form inorganic network polymers (glass-like) and organic networks have been developed and can be described as inorganic-organic copolymers. The inorganic-organic hybrid polymers have attracted interest because of the physical and chemical properties resulting from their hybrid nature. They are prepared by the sol-gel process starting from liquid precursors.

3.1 Sol-gel process

Interest in the sol-gel processing of inorganic ceramic and glass materials began as early as the mid-1900s with Ebelmanl, and Graham's studies on silica gels. These early investigators observed that the hydrolysis of tetraethyl orthosilicate (TEOS), $Si(OC_2H_5)_4$, under acidic conditions yielded SiO_2 in the form of a "glass-like material". Fibers could be drawn from the viscous gel, and even monolithic optical lenses or composites formed. However, extremely long drying times of one year or more were necessary to avoid the silica gels fracturing into a fine powder, and consequently there was little technological interest. Roy and co-workers recognized the potential for achieving very high levels of chemical homogeneity in colloidal gels and used the sol-gel method in the 1950s and 1960s to synthesize a large number of novel ceramic oxide compositions, involving Al, Si, Ti, Zr, etc., that could not be made using traditional ceramic powder methods.

Sol-gel technology is a powerful tool for the fabrication of organic and inorganic-organic hybrid materials[1,7,8]. The advantages of the ease of preparation, modification and processing of the materials along with their high optical quality, photochemical and electrochemical inertness and good mechanical and chemical stability have established this method among other available techniques. The process is based on the phase transformation of a sol obtained from metallic

alkoxides or organomettalic precursors. This sol, which is a solution containing particles in suspension, is polymerized at low temperature to form a wet gel. This one is going to be densified through a thermal annealing to give an inorganic product like glass, polycrystals or a dry gel. By using this method inorganic-organic hybrid materials offer properties better than those prepared alone. Many configurations such as monoliths, fibers, thin and thick films can be achieved in the process of fabrication. Sol-gel materials have been applied in many fields, such as membranes, chemical sensors and catalysis[2-6].

The material is generally formed through a 4-step process.

1. The first step is the hydrolysis and condensation in which precursors or monomers such as metal oxides or metal alkoxides are mixed with water and then undergo hydrolysis and condensation to form a porous interconnected cluster structure. Either an acid such as HCl or a base like NH3 can be employed as a catalyst.
2. The second step includes gelation, where the solvent is removed and a gel is formed by heating at low temperature. Hydrolysis and condensation do not stop with gelation; it is at this stage that solvents are removed and any significant volume loss occurs.
3. Thirdly, the process moves to photopolymerization. Because of the presence of the double bonds and provided that a photoinitiator has been added to the gel, the photoinduced radicals will cause polymerization only in the area in which they are present. At this step, there is no material removal and no volume loss; the reaction that occurs is the cleavage of the pendant carbon-carbon double bonds by a free-radical process to form the organic polymer backbone.
4. Finally comes the development step; the sol-gel is immersed in an appropriate solvent and the area of the sol-gel that is not photopolymerized is removed.

In this work, the sol-gel process has been used to prepare two different photosensitive composites, a zirconium containing hybrid and a titanium containing hybrid. The synthesis of these materials is described below.

3.2 Zirconium sol-gel material

Recently this organic-inorganic hybrid sol-gel material, which is a zirconium-silicon composite, was produced by M. Farsari and M. Vamvakaki for photonic applications by multiphoton polymerization technique. The characteristic of this material is the minimal shrinkage during photopolymerization[12-16]. Furthermore, it is observed that by changing the zirconium-silicon ration, the refractive index of the material is tuned.

3.2.1 Synthesis of Zirconium sol-gel material

The material was fabricated from methacryloxypropyltrimethoxysilane (MAPTMS, Polysciences Inc.) and methacrylic acid (MAA, Sigma-Aldrich), both of which possess photopolymerizable methacrylate moieties. Zirconium n-propoxide ($Zr(OCH_2CH_2CH_3)_4$, (ZPO, 70% solution in 1-propanol, Sigma-Aldrich) was used as an inorganic network former. The molar ratio of MAPTMS to ZPO was 8:2. The inorganic propoxide were chelated by adding MAA. We were investigated four different molar ratios of ZPO to MAA, 1:3, 1:4, 1:8, 1:12. The synthesis of these materials is described below.

Firstly, MAPTMS was hydrolyzed by the addition of 0.1M HCl and the mixture was stirred for 30 minutes. In a separate flask, ZPO was clelated by adding MAA in the presence of an equal volume of Dimethyl Sulfoxide and the sol was stirred for 30 minutes. Next, the MAPTMS sol was added drop-wise to the stirred ZPO sol and it was stirred for 1 hour. Then, the photoinitiator Irgacure 369 (Ciba Speciality Chemicals) , 1.4wt% to MAPTMS was added to the final product. After stirring for 6 hours, the materials were filtered using 0.22μm filters. In figure 9 are presented the chemical structures of the reagents and sol-gel process leading to the formation of the inorganic matrix.

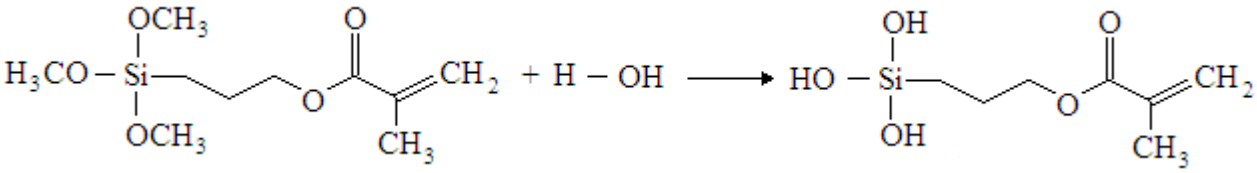

(a) MAPTMS hydrolysis

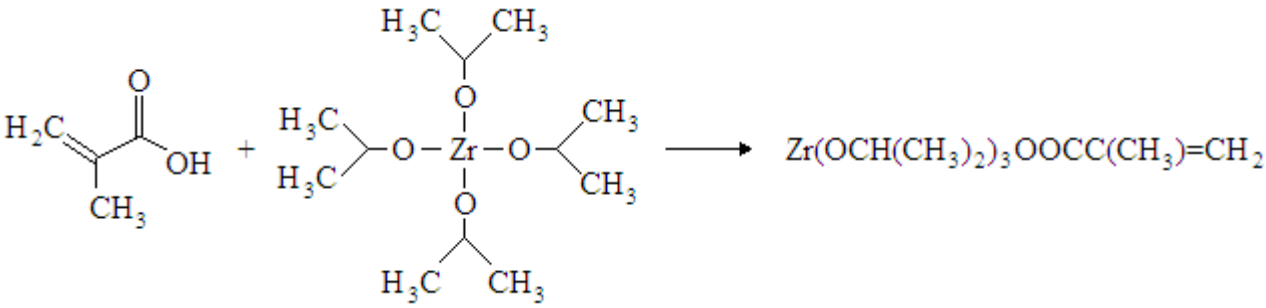

(b) MAA-ZPO complexation

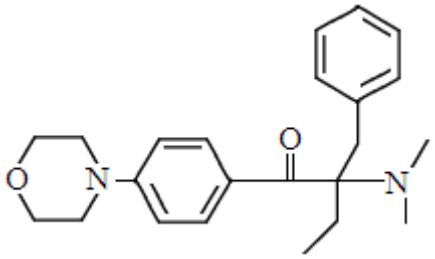

(c) Irgacure 369

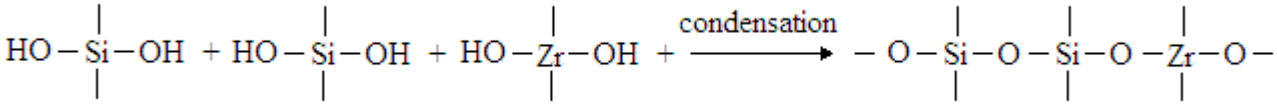

(d) Condensation

Figure 9: Chemical structures of the reagents and sol-gel process leading to the formation of the inorganic matrix.

3.2.2 Preparation before polymerization

Thin films were prepared by spin-coating and the samples for 3D structuring by drop-casting onto glass substrates. The thin films dried over night under vacuum conditions before photopolymerization, in addition to the samples for 3D structuring which dried at 100^{o}C and under vacuum conditions for 1 hour. The vacuum and heating processes resulted in the condensation of the hydroxyl-mineral moieties and the formation of the inorganic matrix. In a subsequent processing step, the material which was not exposed to the laser radiation, was removed by developing in a 1:1 mixture of isopropanol and 4-methyl-2-pentanone and then in isopropanol.

3.2.3 Transmission of Zirconium

The transmission spectras of thin films of these materials were measured using a UV-Vis spectrometer. Figure 10 shows the absorption spectra of the materials.

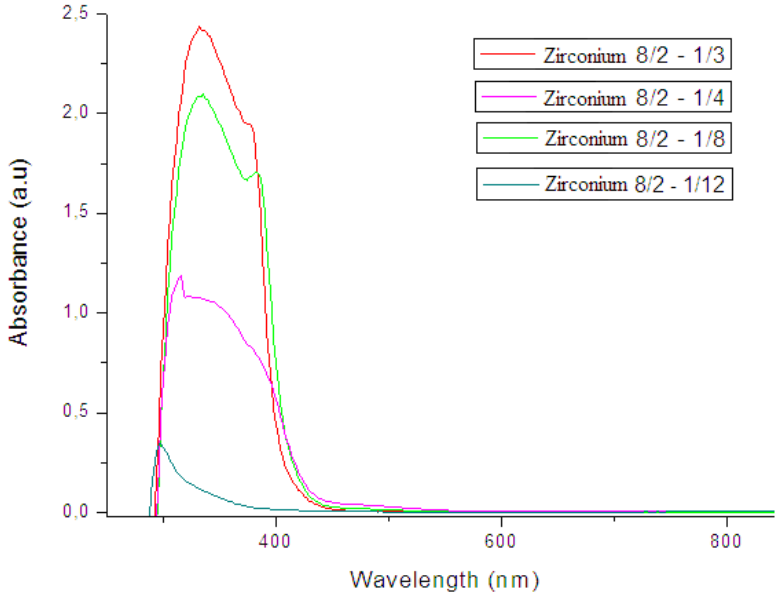

Figure 10: Absorption spectrum of Zirconium

3.2.4 Optical properties

It is proved that by varying the molar ratio of MAPTMS and ZPO, the refractive index of the composite could be modified as shown in figure 11.

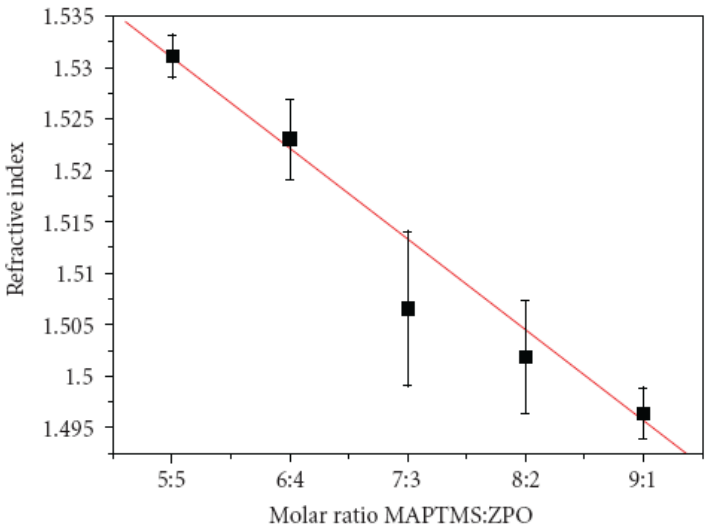

Figure 11: Refractive index variation of the MAPTMS : ZPO complex.

It can be seen that as the ZPO content increases, so does the material's refractive index. The fact that this increase is linear greatly simplifies the material design criteria, as typically such increases are saturating so that the doping concentration becomes very critical. However, in this concentration range, no such limitation is apparent.

3.2.5 Applications of Zirconium

Zirconium finds a lot of applications in photonics. It is used for the fabrication of spliters and bends for optical elements and for photonic crystals.

3.3 Titanium sol-gel material

Recently this organic-inorganic hybrid sol-gel material, which is a titanium-silicon composite, was produced by M. Farsari and M. Vamvakaki for photonic and medical applications by multiphoton polymerization technique. It is observed that the refractive index increases linearly with the titanium isopropoxide [17]. Furthermore, results show that it has minimal shrinkage during photopolymerization.

3.3.1 Synthesis of Titanium sol-gel material

The material was fabricated from methacryloxypropyltrimethoxysilane (MAPTMS, Polysciences Inc.) and methacrylic acid (MAA, Sigma-Aldrich), both of which possess photopolymerizable methacrylate moieties. Titanium isoproxide ($Ti[OCH(CH_3)_2]_4$), (Ti(iPO), 97% Sigma-Aldrich) was used as an inorganic network forming material. The molar ratio of MAPTMS to Ti(iPO) was 8:2. The inorganic propoxide were chelated by adding MAA. We were investigated four different molar ratios of Ti(iPO) to MAA, 1:3, 1:4, 1:8, 1:12. The synthesis of these materials is described below.

Firstly, Ti(iPO) was clelated by adding MAA in the presence of an equal volume of Dimethyl Sulfoxide and the sol was stirred over night. In a separate flask MAPTMS was hydrolyzed by the addition of 0.1M HCl and the mixture was stirred for 30 minutes. Next, the MAPTMS sol was added drop-wise to the stirred Ti(iPO) sol and it was stirred for 1 hour. Then, the photoinitiator Irgacure 369 (Ciba Speciality Chemicals) , 1.4wt% to MAPTMS was added to the final product. After stirring for 6 hours, the materials were filtered using 0.22μm filters.

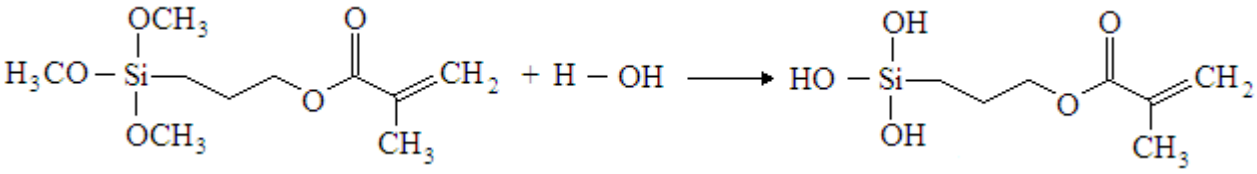

(a) MAPTMS hydrolysis

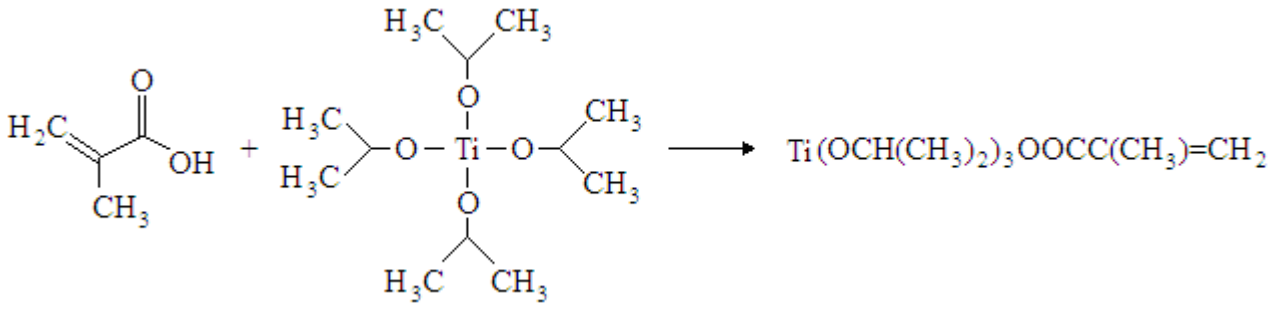

(b) MAA- Ti(iPO) complexation

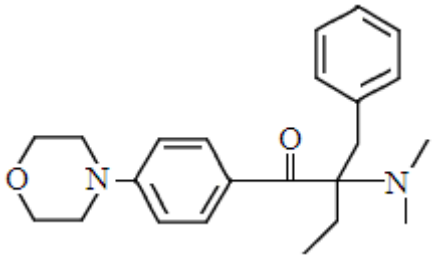

(c) Irgacure 369

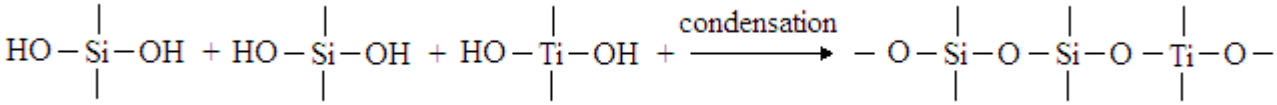

(d) Condensation

3.3.2 Preparation before polymerization

Thin films were prepared by spin-coating and the samples for 3D structuring by drop-casting onto glass substrates. The thin films dried over night under vacuum conditions before photopolymerization, in addition to the samples for 3D structuring which dried at 100°C and under vacuum conditions for 30 minutes. The vacuum and heating processes resulted in the condensation of the hydroxyl-mineral moieties and the formation of the inorganic matrix. In a subsequent processing step, the material which was not exposed to the laser radiation, was removed by developing in a 1:1 mixture of isopropanol and 4-methyl-2-pentanone and then in isopropanol.

3.3.3 Transmission of Titanium

The transmission spectras of thin films of these materials were measured using a UV-Vis spectrometer. Figure 12 shows the absorption spectra of the materials.

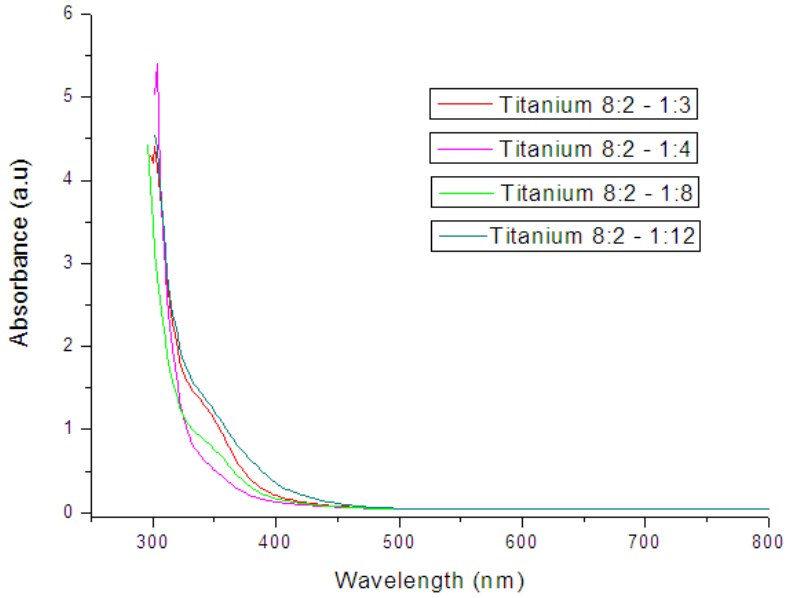

Figure 12: Absorption spectrum of Titanium

3.3.4 Optical properties

It is proved that while the refractive index increases linearly with titanium isopropoxide, the increase of the methacrylic acid does not affect the refractive index of the material, as it is shown in figure 13.

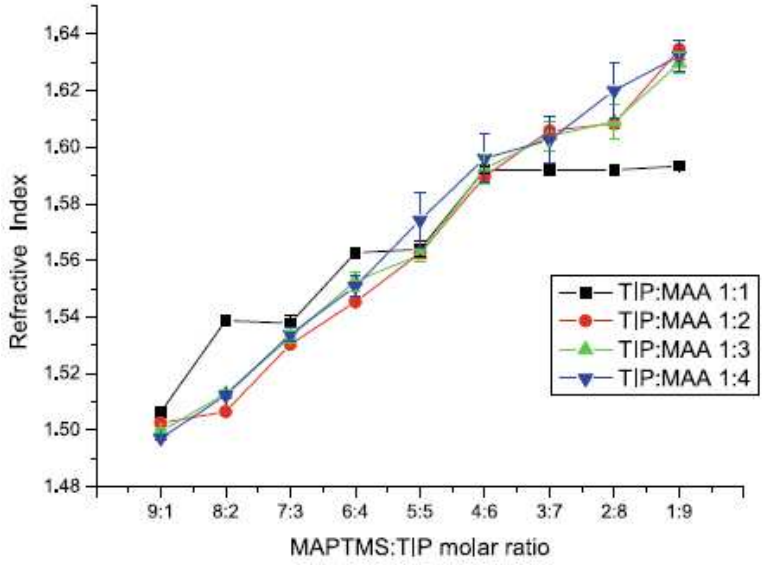

Figure 13: Refractive index dependence on the titanium content of the composite for four different Titanium:MAA mole ratios.

The effect of Titanium on the refractive index overcomes the influence of the organic component of the material and allows one to the organic-inorganic content of the composite without changing its refractive index.

3.3.5 Applications of Titanium

In this time titanium is used for experiments in photonics, in tissue engineering and in medical applications.

II. Biodegradable material

Synthetic biocompatible, biodegradable polymers (e.g. based on polylactide, polyglycolide or polycaprolactone) are attractive materials to produce porous tissue engineering scaffolds, given their ease of synthesis as (co)polymers and the associated flexibility this provides for tuning their physical properties, such as degradation rate and mechanical properties.

The use of implantable guides to repair lacerated peripheral nerves following traumatic injury is one strategy for clinical repair. However, regeneration distance is often limited to just a few millimetres. Nerve guides are usually made from either natural materials (collagen) or synthetic polymers (PLGA), but are typically fabricated in to a simple entubulating device. An important improvement in guide design is the incorporation of an internal structure for physically directing regenerating axons, which can comprise of channels or fibres[18]. However, versatile fabrication methods for constructing feature sizes at length-scales appropriate for neural regeneration (tens to hundreds and micrometers) for materials used as nerve guides are presently limited. Here, we describe the synthesis of a polylactide-based (PLA) photopolymer.

3.4 Polylactide-based material

This material is a liquid polylactide-based resin and was synthesised by Frederick Claeyssens in the Kroto Research Center, for tissue engineering applications. It is observed that the 3D scaffolds, which produsedby multiphoton polymerization technique, exhibit high resolution.

3.4.1 Synthesis of Polylactide-based material

Pentaerythritol (Sigma-Aldrich, > 98%), (3S)-cis-3,6-dimethyl-1,4-dioxane-2,5-dione (Sigma-Aldrich, 98%), Stannous 2-ethylhexanoate (Sigma-Aldrich, 95%), Triethylamine (Sigma-Aldrich, >99%), Methacrylic anhydride (Sigma-Aldrich, 94%), Toluene (Sigma-Aldrich, Anhydrous, 99.8%), Poly(L-lactide) (Sigma-Aldrich, M_w 152000 g/mol, decyl ester end group)

and Dichloromethane (Sigma-Aldrich, Anhydrous, >99.8%, 50ppm Amylene stabiliser) were used as supplied without further purification. The synthetic route followed for the synthesis of the low molecular weight four-arm PLA star polymer is outlined below and is schematically shown in figure 14.

In a typical synthesis (3S)-cis-3,6-dimethyl-1,4-dioxane-2,5-dione (25.5g, 0.177 moles, 8 molar equivalents) and pentaerythritol (3g, 0.022 moles, 1 molar equivalent) were refluxed in toluene under a nitrogen atmosphere at 160°C for 8h in dry glassware in the presence of 1 drop of stannous octoate initiator. Upon cooling the product formed a lower viscous layer which was decanted and purified by vacuum distillation to yield 25g of the desired oligomer as a clear viscous oil.

This four armed PLA star oligomerwas further acrylated by following protocol:glassware was dried at 120°C overnight and flushed with nitrogen prior to use. Triethylamine (22.30ml, 0.16 moles, 16 molar equivalents) and 12.5g of the four-arm PLA (0.01 moles, 1 molar equivalent) were dissolved in dry dichloromethane in a three necked round bottom flask under nitrogen. The solution was cooled to 0°C in an ice bath and methacrylic anhydride (11.92ml, 0.08 moles, 8 molar equivalents) was added slowly with an addition funnel. The reaction mixture was allowed to react at room temperature for 24 hours. The product was isolated by vacuum distillation and purified by precipitation in isopropanol at -20°C to give 15g of the desired acrylated oligomer as a clear, viscous oil.

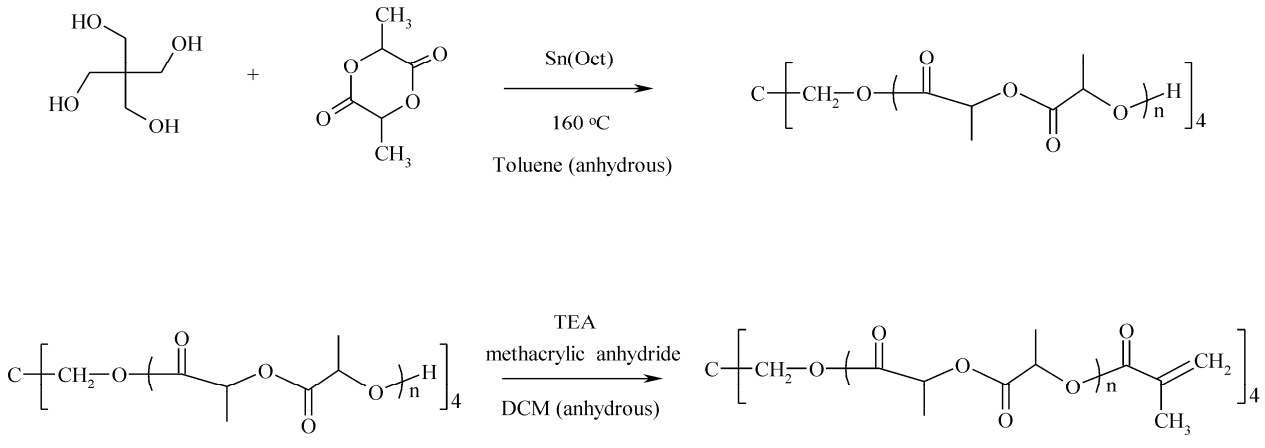

Figure 14: Synthesis and acrylation of the 4-arm PLA star oligomer.

3.4.2 Preparation before polymerization

In order to make the material photosensitive, 20mg of 4,4'-bis(diethylamino)benzophenone photoinitiator was mixed with 1gr of polymer in 250µl of 4-methyl-2-pentanone and stirred for 15 minutes with a magnetic stirrer bar. The mixture was then passed through a 0.4µm pore size polycarbonate filter prior to spin coating. The coverslips were prepared by bathing in a solution of 250µl MAPTMS in 20ml $CHCl_3$ prior to use. This allows the polymer to chemically bind to the surface upon curing, preventing the film peeling off during cell culture.

Thin films were prepared by spin-coating at 4000rpm for 1 minute before being dried overnight under vacuum to remove the solvent. Thin films were polymerised with an excimer laser (Lambda-Physik, LPX 210, 248 nm, 30 ns) by using 50 shots at 58 mJ/cm^2 and were further developed for 5 minutes in 4-methyl-2-pentanone.

The samples for 3D structuring, prepared by drop-casting and dried overnight in room temperature. In a subsequent processing step, the material which was not exposed to the laser radiation, was removed by developing in 4-methyl-2-pentanone and rinsed with isopropanol.

3.4.3 Properties of polylactide-based material

Thin films of the in-house synthesized PLA were prepared via spin-coating/UV curing and compared with spin coated thin films of commercially available PLA. The chemical composition and purity of the photocurable PLA resin was determined by NMR. Additionally, IR spectrometry was used to confirm the success of the acrylation reaction. The surface properties of the photocurable PLA thin films were assessed via XPS and sessile drop water contact angle measurements. The water contact angle measurements were compared to those of a commercially available PLA.

The ^1H NMR spectra, showed that the 4-arm star polymer consists of ~8 PLA monomer repeat units and thus ~2 lactide monomeric units per side arm. The number average molecular weight of the prepolymer was calculated ~1200 g/mol. NMR after acrylation also shows that the prepolymer is fully acrylated (4 acrylate groups per oligomer). The acrylation of the polymer was also confirmed by IR spectrometry. The appearance of a sharp peak around 1600 cm^{-1} was attributed to the acrylate group and was accompanied by a noted decrease in absorption at ~3500 cm^{-1} due to the loss of free terminal OH groups.

The surface properties of cured thin films of 4-arm star PLA were determined by X-Ray Photoelectron Spectroscopy (XPS) and water contact angle measurements. The contact angle measurements were compared with measurements on thin films prepared from a commercially available linear PLA. The XPS data were in good accordance with the NMR results. The survey

scan revealed a C/O ratio of 1.83, which is close to the theoretical value of 1.73 for our 4-arm star PLA. The C1s high resolution, scan reveals 42% of C-C bonding, 24.5% of O-C=O bonding 25% of C-O bonding and 6.5% of C-COOH bonding, this is in good agreement with the theoretical values from the structure derived from the MNR spectrum (36% C-C, 29% O-C=O and C-O and 6% C-COOH bonding).

A detailed investigation for the surface properties was conducted via surface contact angle measurements and the results are given in table 1. Surface contact angle measurements were performed at different pH values (from pH 7.0 to pH 2.0). The pH measurements at pH 2.2 provide an insight on the influence of the surface acidic (mainly carboxylate) groups on the water contact angle values. The surface contact angle of the commercially available linear PLA is 69º at pH 7.0 and pH 2.2 (see table 1), while the 4-arm PLA after UV irradiation has a surface contact angle of 67º at pH 7.0 and 69º at pH 2.2. However, the surface contact angle at pH 7.0 of the commercially available PLA decreased to 65º after 5 minutes of UV irradiation, while it remained unchanged at pH 2.2. This indicates that there is a small but discernable effect of surface oxidation of the commercially available PLA (as also previously reported [21]). The effect of surface oxidation due to UV irradiation is far less pronounced in our *in-house* 4-arm star PLA and thus variation in cell adhesion due to UV curing.

Contact Angle	**Non-acrylated PLA**	**Non-acrylated PLA: 9 W/cm^2 UV light**	**Acrylated PLA: 9 W/cm^2 UV light**
pH 7.0	69.4 º ± 0.9º	65.4º ± 0.5º	67.2º ± 1.3º
pH 2.2	69.0 º ± 0.9 º	69.0º ± 1.2º	69.4º ± 2.3º

Table 1: Contact angle values on different PLA surfaces. The contact angles reported are an average of 5 separate measurements. In comparison the contact angles measured for borosilicate glass were 38.3º at both pH 2.2 and 7.0 in good accordance with values reported in the literature.

3.4.4 Applications of polylactide-based material

This is a novel material, which is used for tissue engineering scaffolds. It is proved that it is a biocompatible material and in future it will be used for biomedical applications.

B. Materials that were used for cells cultivation, viability assay and immuneostaining assays

In the first part of this thesis, fibroblast cells were cultivated on the non-biodegradable scaffolds, while in the second part, neuronal cells and fibroblast cells were cultivated on the biodegradable scaffolds.

3.5 Cell lines

Tissue engineering utilizes living cells as engineering materials. Examples include using living fibroblasts in skin replacement or repair, cartilage repaired with living chondrocytes, or other types of cells used in other ways.

In this study, murine fibroblast cells (NIH/3T3) and neuronal cell line (PC12) were used for the first and second part respectively.

3.5.1 Fibroblast cells

A fibroblast is a type of cell that synthesizes the extracellular matrix and collagen (and fibrin), the structural framework (stroma) for animal tissues, and play a critical role in wound healing. They are the most common cells of connective tissue in animals[19]. Fibroblasts and fibrocytes are two states of the same cells, the former being the activated state, the latter the less active state, concerned with maintenance. Currently, there is a tendency to call both forms fibroblasts. The suffix "blast" is used in cellular biology to denote a stem cell or a cell in an activated state of metabolism. The main function of fibroblasts is to maintain the structural integrity of connective tissues by continuously secreting precursors of the extracellular matrix[20]. Fibroblasts secrete the precursors of all the components of the extracellular matrix, primarily the ground substance and a variety of fibres. The composition of the extracellular matrix determines the physical properties of connective tissues.

Fibroblasts are morphologically heterogeneous with diverse appearances depending on their location and activity. Though morphologically inconspicuous, ectopically transplanted fibroblasts can often retain positional memory of the location and tissue context where they had previously resided, at least over a few generations. Unlike the epithelial cells lining the body structures, fibroblasts do not form flat monolayers and are not restricted by a polarizing attachment to a basal lamina on one side, although they may contribute to basal lamina components in some situations. Fibroblasts can also migrate slowly over substratum as individual cells, again in contrast to epithelial cells. While epithelial cells form the lining of body structures, it is fibroblasts and related connective tissues which sculpt the "bulk" of an organism.

Like other cells of connective tissue, fibroblasts are derived from primitive mesenchyme. Thus they express the intermediate filament protein vimentin, a feature used as a marker to distinguish their mesodermal origin. However, this test is not specific as epithelial cells cultured in vitro on adherent substratum may also express vimentin after some time. In certain situations epithelial cells can give rise to fibroblasts, a process called epithelial-mesenchymal transition (EMT). Conversely, fibroblasts in some situations may give rise to epithelia by undergoing a mesenchymal to epithelial transition (MET) and organizing into a condensed, polarized, laterally connected true epithelial sheet. This process is seen in many developmental situations (eg. nephron and notocord development).

Fibroblasts have a branched cytoplasm surrounding an elliptical, speckled nucleus having one or two nucleoli. Active fibroblasts can be recognized by their abundant rough endoplasmic reticulum. Inactive fibroblasts, which are also called fibrocytes, are smaller and spindle shaped. They have a reduced rough endoplasmic reticulum. Although disjointed and scattered when they have to cover a large space, fibroblasts when crowded often locally align in parallel clusters. Fibroblasts make collagens, glycosaminoglycans, reticular and elastic fibers, and glycoproteins found in the extracellular matrix. Growing individuals' fibroblasts are dividing and synthesizing ground substance. Tissue damage stimulates fibrocytes and induces the mitosis of fibroblasts.

Mouse embryonic fibroblasts (MEFs) are often used as "feeder cells" in human embryonic stem cell research. However, many researchers are gradually phasing out MEFs in favor of culture media with precisely defined ingredients of exclusively human derivation. Further, the difficulty of exclusively using human derivation for media supplements is most often solved by the use of "defined media" where the supplements are synthetic and achieve the primary goal of eliminating the chance of contamination from derivative sources.

3.5.2 Murine fibroblast cells (NIH/3T3)

3T3 cells come from a cell line established in 1962 by two scientists then at the Department of Pathology in the New York University School of Medicine, George Todaro and Howard Green. The 3T3 cell line has become the standard fibroblast cell line. Todaro and Green originally obtained their 3T3 cells from Swiss mouse embryo tissue.

Figure 15: NIH/3T3 Mouse Embryo Fibroblast

The '3T3' designation refers to the abbreviation of "3-day transfer, inoculum 3 x 10^5 cells." This cell line was originally established from the primary mouse embryonic fibroblast cells that were cultured by the designated protocol, so-called '3T3 protocol'. The primary mouse embryonic fibroblast cells were transferred (the "T") every 3 days (the first "3"), and inoculated at the rigid density of 3 x 10^5 cells per 20-cm² dish (the second "3") continuously. The spontaneously immortalized cells with stable growth rate were established after 20-30 generations in culture, and then named '3T3' cells.

3.5.3 Neuronal cells

A neuron is an electrically excitable cell that processes and transmits information by electrical and chemical signaling[21]. Chemical signaling occurs via synapses, specialized connections with other cells. Neurons connect to each other to form networks. Neurons are the core components of the nervous system, which includes the brain, spinal cord, and peripheral ganglia. A number of specialized types of neurons exist: sensory neurons respond to touch, sound, light and numerous other stimuli affecting cells of the sensory organs that then send signals to the spinal cord and brain. Motor neurons receive signals from the brain and spinal cord, cause muscle contractions, and affect glands. Interneurons connect neurons to other neurons within the same region of the brain or spinal cord.

A typical neuron possesses a cell body (often called the soma), dendrites, and an axon. Dendrites are filaments that arise from the cell body, often extending for hundreds of micrometres and branching multiple times, giving rise to a complex "dendritic tree". An axon is a special cellular filament that arises from the cell body at a site called the axon hillock and travels for a distance, as far as 1 m in humans or even more in other species. The cell body of a neuron frequently gives rise to multiple dendrites, but never to more than one axon, although the axon may branch hundreds of times before it terminates. At the majority of synapses, signals are sent from the axon of one neuron to a dendrite of another. There are, however, many exceptions to these rules: neurons that lack dendrites, neurons that have no axon, synapses that connect an axon

to another axon or a dendrite to another dendrite, etc.

All neurons are electrically excitable, maintaining voltage gradients across their membranes by means of metabolically driven ion pumps, which combine with ion channels embedded in the membrane to generate intracellular-versus-extracellular concentration differences of ions such as sodium, potassium, chloride, and calcium. Changes in the cross-membrane voltage can alter the function of voltage-dependent ion channels. If the voltage changes by a large enough amount, an all-or-none electrochemical pulse called an action potential is generated, which travels rapidly along the cell's axon, and activates synaptic connections with other cells when it arrives.

3.5.3 PC12 neuronal cells

PC12 is a cell line derived from a pheochromocytoma of the rat adrenal medulla[22]. A pheochromocytoma or phaeochromocytoma (PCC) is a neuroendocrine tumor of the medulla of the adrenal glands (originating in the chromaffin cells), or extra-adrenal chromaffin tissue that failed to involute after birth and secretes excessive amounts of catecholamines, usually noradrenaline (norepinephrine), and adrenaline (epinephrine) to a lesser extent. PC12 cells stop dividing and terminally differentiate when treated with nerve growth factor. This makes PC12 cells useful as a model system for neuronal differentiation.

At the end of 2000 more than 5.500 peer-reviewed papers listed on Medline, in which these cells were used for a various purposes, such as models for neuronal differentiation, neuroendocrine secretion, neurotoxicoligy, signal transduction and apoptosis[23,24]. Many of the results initially obtained in PC12 cells have been faithfully validated in nontransformed cells of neuronal/neuro- endocrine origin.

3.6 Cell culture

Prior to cell culture the structured surfaces were irradiate with a UV lamp for 2 hours and then transferred onto sterile 12 well plates.

The NIH/3T3 cells were suspended to a concentration of 10^5 cells/mL in Dulbecco's modified Eagle's medium (DMEM) with 10% fetal bovine serum (FBS), and 1% antibiotic solution (GIBCO, Invitrogen, Kalsruhe, Germany) and 2ml of cell suspension was added in the 12 well plate and cultured at 37^{o}C, 5% CO_2 . Before seeding the cells on the different surfaces, cells were grown to confluency, detached with 0.05% trypsin/EDTA (GIBCO, Invitrogen, Kalsruhe, Germany) and diluted in complete medium at an appropriate density.

The neuronal cell line (PC12) was obtained from the American Type Culture Collection (ATCC) and maintained in DMEM supplemented with 10% horse serum and 5% FBS and 1% antibiotic solution (GIBCO, Invitrogen, Karlsruhe, Germany). Culture plates were kept at 37ºC in

a humidified atmosphere containing 5% CO_2 in air following standard procedures. Before seeding the cells on the different surfaces, cells were grown to confluency, detached with 0.05% trypsin/EDTA (GIBCO, Invitrogen, Karlsruhe, Germany) and diluted in complete medium at an appropriate density.

3.7 Cells viability assay

For the convenient discrimination between live and dead cells the *Live-Dead Cell Staining Kit* (BioVision) was used. The kit utilizes Live-Dye, a cell-permeable green fluorescent dye (Ex/Em = 488/518 nm), to stain live cells. Dead cells can be easily stained by propidium iodide (PI), a cell non-permeable red fluorescent dye (Ex/Em = 488/615). At the end of the incubation time (24, 72,120 or 168 hours), structured surfaces with the cells were covered with the staining solution and incubated for 15 min at 37^{o} C. Cells were observed immediately under a fluorescence microscope. Stained live and dead cells can be visualized by fluorescence microscopy using a band-pass filter (detects FITC and rhodamine). Healthy cells stain only the cell-permeable Live-Dye, fluorescing green. Dead cells can stain both the cell-permeable Live-Dye and the cell non-permeable PI (red), the overlay of green and red appears to be yellow-red. The staining procedure was the same for both cell lines.

3.8 Immunostaining assays

For the double staining of F-actin and Vinculin, of the NIH/3T3 cells, the focal adhesion staining kit (Chemicon International Inc., Temecula, CA, USA) was used. The cells were fixed with 4% paraformaldehyde for 15 min and permeabilized with 0.1% Triton X-100 (Merck KGaA, Darmstadt,Germany) in PBS for 3-5 min on ice. The non-specific binding sites were blocked with 1% BSA in PBS for 30 min. Actin and Focal adhesion complexes were stained by incubating cells in diluted primary antibody (anti-vinculin) in blocking solution (1:200) for 1 h and subsequently labeling them with diluted secondary antibody (1:200) (mouse–anti-mouse FITC conjugate) (Sigma-Aldrich Chemie GmbH, Munich, Germany) for 45 min, with simultaneous incubation with diluted tetramethyl rhodamine isothiocyanate-conjugated phalloidin. The samples were then washed with PBS and stored 10% glycerol in PBS in dark. Confocal microscopy was performed on ‘Zeiss AxiosKop 2 plus’ laser scanning confocal microscope.

In order to verify the neuronal differentiation of PC12 on 3D scaffolds, the presence of class III b-tubulin isotype, a neuronal cytoskeletal antigens, have been studied by immunoflourence experiments. Following the culture period, cells were fixed and permeabilized as described above. The non-specific binding sites were blocked also with 1% BSA in PBS for 30 min and primary

antibody solution (anti-tubulin in blocking solution 1:200) was added, followed by 1h incubation at room temperature. Finally secondary antibody (Goat Antimouse IgG) was addied in the dark for 45 min at room temperature. The cells were rinsed and with PBS and stored in 10% glycerol in PBS in the dark. For cells imaging the 'Zeiss AxiosKop 2 plus' laser scanning confocal microscope was used.

3.9 Scanning electron microscopy

The morphologies of NIH/3T3 fibroblasts seeded on thin films surfaces or on 3D structures were observed by SEM. After incubation cells were washed with 0.1M of sodium cacodylate buffer (SCB) and then were incubated with the SCB for 15 minutes. This step was repeated twice and followed by the fixation of the cells using a fixative buffer (2% glutaraldehyde , 2% formaldehyde in 1% SCB) for 1 hour at 4^0C. Subsequently, the surfaces were washed twice (from 15 minutes each time) with 1% SCB at 4^0C. After that, cells were dehydrated through a graded aceton series (10%, 30%, 50%, 70%, 80%, 90% and 100%) for 15 minutes at 4^oC and incubated for 15 minutes on dry 100% aceton. Prior to electron microscopy examination the samples were passed from a critical point dryer and then were sputter coated with a 15nm gold layer. SEM was performed on a JEOL 7000 field emission scanning electron microscope with an acceleration voltage of 15kV.

References

1. C.J. Brinker, G.W. Scherer, **Sol–Gel science**. Boston, MA: Academic Press, (1990).
2. D. Sangeeta, J. R. LaGraff, **Inorganic Materials Chemistry, Desk Reference**. Second Edition, ed, (CRC Press)
3. L. C. Klein, **Sol-Gel Optical Materials**. Annual Review Materials ScienceVol. 23, 437-452, (1993).
4. S. Sakka, **Sol-Gel Science and Technology**. Volume 3, Sol-gel prepared Organic-inorganic hybrids and nanocomposites.
5. L. C. Klein, **Sol-Gel Optics, Processing and applications**.
6. L. C. Klein, **Sol-Gel Technology for Thin Films, Fibers, Preforms, Electronics and Specialty Shapes**. Noyes Publications.
7. H. Schmidt, **Inorganic-Organic Composites by Sol-Gel Techniques**. Journal of Sol-Gel Science and Technology **1**, 217-231, (1994).

8. J. P. Boiloty, J. Biteauy, F. Chaputy, T. Gacoiny, A. Brunz, B. Darracqz, P. Georgesz, Y. Levyz, **Organic–inorganic solids by sol–gel processing: optical Applications**. Pure Appl. Opt. **7,** 169–177, (1998).

9. J. M. Nedelec, **Sol-Gel Processing of Nanostructured Inorganic Scintillating Materials**. Journal of Nanomaterials Vol. 2007, Article ID 36392, 8 pages.

10. A Klukowska, U. Posset, G. Schottner, A. Jankowska-Frydel, V. Malatesta, **Photochromic sol-gel derived hybrid polymer coatings: the influence of matrix properties on kinetics and photodegradation**. Materials Science-Poland, Vol. 22, No. 3, 187-199, (2004).

11. J. Stampfl, M. Schuster, S. Baudis, H. Lichtenegger, R. Liska, C. Turecek, F. Varga, **Biodegradable stereolithography resins with defined mechanical properties**. Virtual and Rapid Manufacturing), 283-288, (2007).

12. I. Sakellari, A. Giakoumaki, D. Gray, M. Vamvakaki, M. Farsari, C. Fotakis, **Two-Photon Polymerization of Hybrid Sol-GelMaterials for Photonics Applications**. Laser Chemistry, Vol. 2008, Article ID 493059, 7 pages.

13. A. Ovsianikov, J. Viertl, B. N. Chichkov, M. Oubaha, B. MacCraith, I. Sakellari, A. Giakoumaki, D. Gray, M. Vamvakaki, M. Farsari, C. Fotakis, **Ultra-Low Shrinkage Hybrid Photosensitive Materials for Two-Photon polymerization Microfabrication**. American Chemical Society, Vol. 2, No. 11, 2257-2262, (2008).

14. A. Ovsianikov, X. Shizhou, M. Farsari, M. Vamvakaki, C. Fotakis, B. N. Chichkov, **Shrinkage of microstructures produced by two-photon polymerization of Zr-Based hybrid photosensitive materials**. Optics Express, Vol. 17, No. 4, 2143-2148, (2009).

15. B. Bhuian, R.J. Winfield, S. O'Brien, G.M. Crean, **Investigation of the two-photon polymerisation of a Zr-based inorganic–organic hybrid material system**. Applied Surface Science 252, 4845–4849, (2006).

16. M. Farsari, C. Reinhardt, I. Sakellari, A. Giakoumaki, A. Ovsianikov, M. Vamvakaki, D. Gray, B.N. Chichkov, C. Fotakis, **Three-Dimensional Direct Writing of Novel Sol-Gel Composites for Photonics Applications**.

17. I. Sakellari, A. Gaidukeviciute, A. Giakoumaki, D. Gray, C. Fotakis, M. Farsari, M. Vamvakaki, C. Reinhardt, A. Ovsianikov, B.N. Chichkov, **Two-photon polymerization of titanium-containing sol–gel composites for three-dimensional structure fabrication**. Appl Phys A (2010) 100: 359–364

18. Murray-Dunning C, McArthur SL, Sun T, McKean R, Ryan AJ, Haycock JW: **Three-dimensional alignment of schwann cells using hydrolysable microfiber scaffolds: strategies for peripheral nerve repair.** *Methods in molecular biology (Clifton, NJ),* **695:**155-166.

19. www.fibroblast.org

20. T. Wong, J.A. McGrath and H. Navsaria, **The role of fibroblasts in tissue engineering and Regeneration**. Journal Compilation, British Association of Dermatologists, British Journal of Dermatology (2007) 156, pp1149–1155.

21. C. Hammond, **Cellural and Molecular Neurophysiology**. Third Edition, (2008) Academic Press.

22. G. Banker and K. Goslin, **Culturing Nerve Cells**. Second Edition, Massachusetts Institute of Technology, Chapter 6.

23. K. Fujita, P. Lazarovici, G. Guroff, **Regulation of the differentiation of PC12 Pheochromocytoma cells**. (1989) Environ Health Perspect 80, 127-142.

24. T. J. Shafer, W. D. Atchison, **Transmitter ion channel and receptor properties of pheochromocytoma PC12 cells. A model for neurotoxicological studies**. Neurotoxicology 12, 473-492.

CHAPTER 4
EXPERIMENTAL

In this chapter are been described, firstly the experimental set-up of two photon polymerization that was used for the 3D structures and secondly the experimental techniques that were used for the characterization of samples.

4.1 Two photon polymerization set-up

The set-up for the fabrication of three dimensional microstructures by two photon micro stereolithography is shown in figure 16.

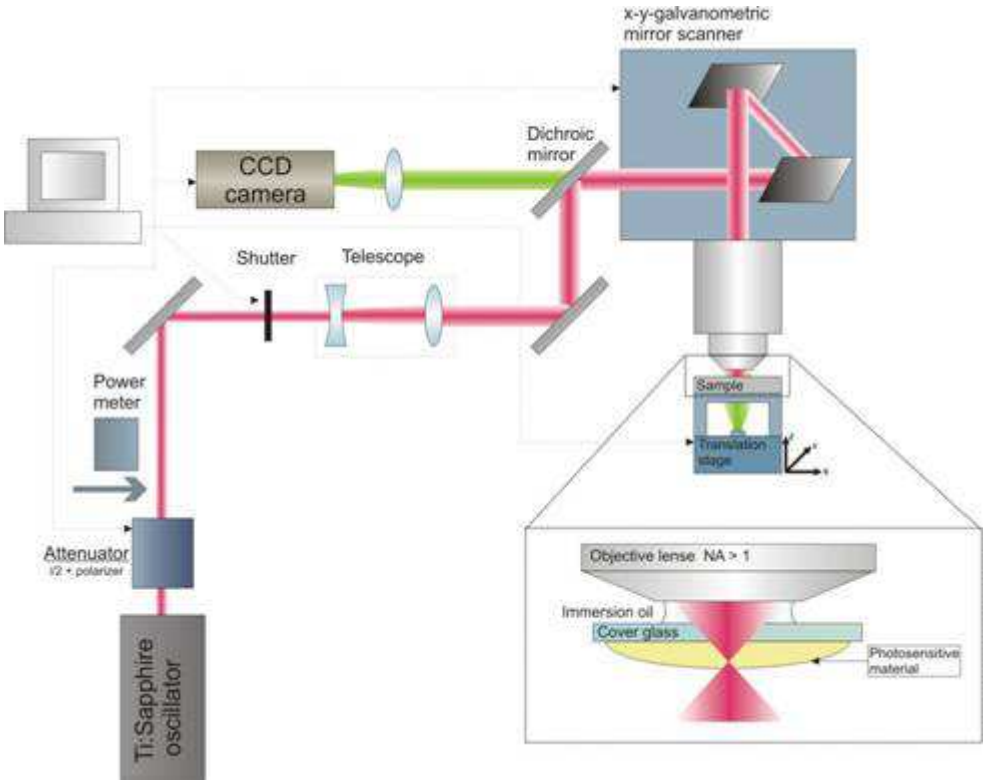

Figure 16: Experimental set-up for TPP

The laser source that was used is a Ti:Sapphire femtosecond oscillator operating at 800nm. The laser has a pulse length of less than 200fs and a repetition rate of 50-80MHz. The energy required for the polymerization process will depend on the material, the photoinitiator and the focusing, but is usually in the order of a few nanojules per pulse.

By moving the laser focus in a three-dimensional manner through the liquid, three-dimensional structures can be fabricated. The photopolymerized structure is usually generated in a layer by layer format. Each layer either using an x-y galvanometric mirror scanner or x-y piezoelectric stages. The main difference between the two cases is that in the former case, the structure remains immobile and the structure is generated by the laser beam moving, while in the latter case the x-y stages move the structure and the laser beam remains immobile. Movement on the z-axis can be achieved using a piezoelectric or a high resolution linear stage. So the

photopolymerized structure can be generated using an x-y-z galvanometric minor digital scanner (Scanlabs Hurryscan II). controlled by SAMLight (SCAPS) software. SAMlight software allowed the drawing of varius stuctures built layer by layer. To achieve the tight focusing conditions required for multi-photon polymerization to occur, a microscope objective needs to be used: when the numerical aperture (N.A.) of the objective is higher than 1. immersion oil is used for index matching. Galvo scanners have to be adapted to accommodate microscope objectives, as usually they are designed to take lenses with long focal lengths. The beam waist of the focused laser beam is given by r= 0.61X/N.A.

Beam control can be achieved by either using a fast mechanical shutter or an acousto-optic modulator, while beam intensity control can be achieved using neutral density filters, a variable attenuator or a combination of a polarizer and a waveplate. For the online monitoring of the Photopolymerization process, a CCD camera can be mounted behind a dichroic mirror, as shown in figure 14 above. This is possible as the refractive index of most photopolymers changes during polymerization, so that the illuminated structures become visible during the building process.

After the completion of the photopolymerization process and in order to remove the non-photopolymerized resin, the samples need to be developed like in any lithographic process. The developer used and the time for development will depend on the material.

4.2 Excimer

The set-up for the polymerization of thin films, after spin coating, is shown in figure 17.The laser source that was used is a KrF Excimer laser (Lambda-Physik, LPX 210), operating at 248nm. The laser has pulse duration of 30nsec.

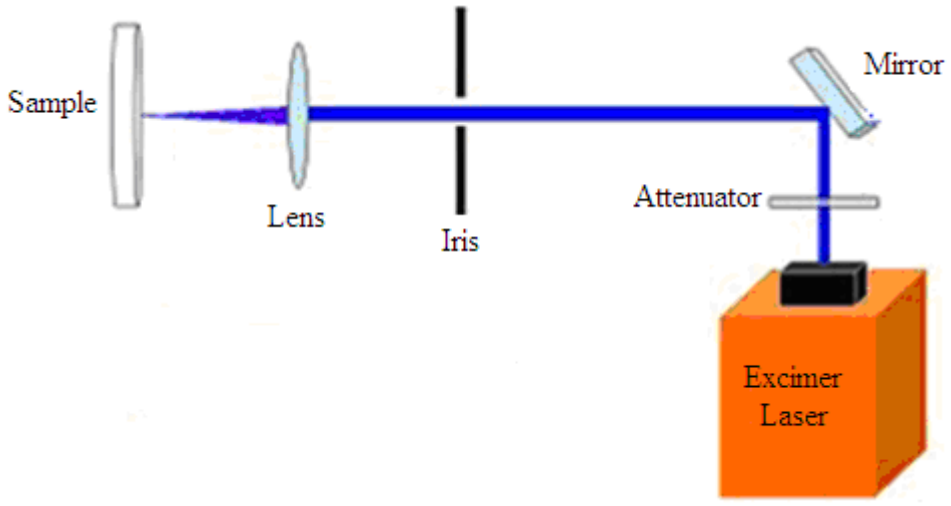

Figure 17: Experimental set-up of Excimer Laser.

4.3 Scanning electron microscopy

A traditional light microscope uses visible light to resolve an image. The wavelength of visible light ranges from about 400-700 nanometers. These wavelengths give the light microscope physical limitations of 500-1000 times magnification and 200 nanometer resolution. Electrons have both particle and wave-like properties. When accelerated through a voltage, electrons can have a wavelength on the order of 0.1 nanometers. This allows much higher resolution, and magnification of the surface and morphology of the sample.

A SEM functions in a similar way to a traditional light microscope. An electron gun generates electrons, which are then accelerated by an electric potential. There are then condensing lens that collimate the electrons into small beam. While lenses in an optical system are made of curved pieces of plastic or glass, in a SEM a lens is made by a coil of current-carrying wire. This coil makes a magnetic field which exerts a force on the moving electrons.

After the condensing lens is another coil which scans the beam of electrons over the sample. There is a final objective lens that focuses the beam to a small spot on the sample. The electron beam hits the sample and causes secondary electrons to leave the sample. The secondary electrons hit a detector which generates an electrical signal. This electrical signal is processed by a computer into an image. All the SEM components are contained inside a vaccum chamber to minimize electron-gas interactions.

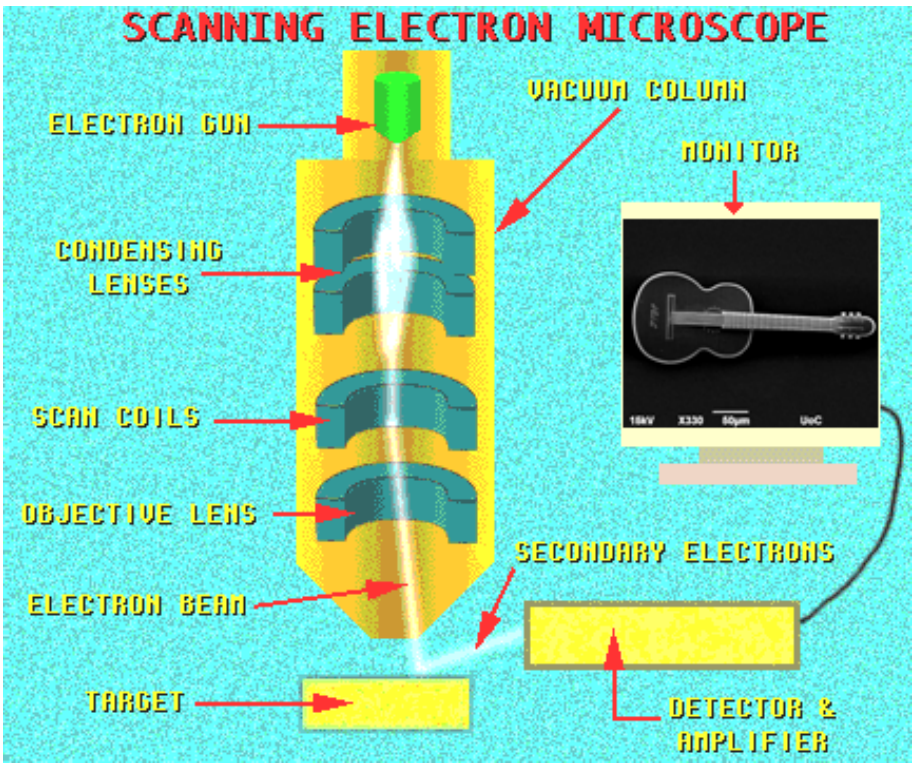

Figure 18: Schematic drawing of a SEM

The sample preparation is very crucial and requires different approach for various types of materials. As a rule the material should be conductive otherwise we have charging effect. The metal samples require only trimming or sectioning to the appropriate size. Nonconductive samples require coating of a very thin layer of metal using an instrument named as sputter coater. This instrument has a target of a metal, which can be gold, gold/palladium, platinum, tungsten or graphite, and using plasma sputtering we deposit the desired layer of the metal. Apart from the conductivity this process increases the contrast and reveals the details of our sample. The biological samples, as like cells, firstly must be dehydrated.

References

1. E. Hecht, **Optics**. Addison Wesley Longman, Third Edition, (1998).

2. M. Straub, L.H. Nguyen, A. Fazlic, M. Gu, Optical Materials 27, 359-364, (2004).

3. W. Haske, V.W. Chen, J.M. Hales, W. Dong, S. Barlow, S.R. Marder, J.W. Perry, Optic. Express 15, 3426-3436, (2007).

CHAPTER 5
RESULTS

This chapter is separated in two parts. In the first part are been presented the results of cells cultivation on the non-biodegradable scaffolds, while in the second part, are been presented the results of cells cultivation on the biodegradable scaffolds. The results are presented in the same way for both parts. Firstly are been presented the results of the cultivation on thin films for the investigation of cytotoxicity of the materials. The parameters that were investigated were the time of cultivation and in the first part the mechanical properties (differences in stiffness or elasticity) of the materials. Then, the results of cultivation on 3D scaffolds are presented. The parameters that have been investigated were the size of 3D scaffolds, the different shapes of them and how the cells were developed on them, according to the time of cultivation.

A. Cells cultivation on non-biodegradable scaffolds

5.1 Cultivation on thin films

After the thin films fabrication on coverslips as it is described in chapter 3, (Zirconium based thin films in paragraph 3.2.2 and Titanium based thin films in paragraph 3.3.2), they were transferred onto sterile 12 well plates and 2ml of cell suspension was added and cultured at 37^{o}C, 5% CO_2. Also were transferred in plates control surfaces (glass surfaces), for the comparison of cells' attachment, migration and differentiation on control surfaces to films surfaces. The incubation time of cells was 1day, 3 days, 5 days, and 7 days. For every day of cultivation was used another plate and after the proper incubation time we checked cells viability assay (paragraph 3.7), the distribution of F-actin and Vinculin (paragraph 3.8.1) and finally the morphology of cells seeded on films surfaces (paragraph 3.8.2). Below are presented the results firstly for the morphology of cells seeded on films surfaces and cells viability assay and then the distribution of F-actin and Vinculin.

5.1.1 Results for the morphology of cells seeded and cells viability assay on films

In figure 19 are presented the results for cells seeded (Lines I, III, V, VII) and viability assay (Lines II, IV, VI, VIII) , for the first, third ,fifth, and seventh day of cultivation on control surfaces (a) and on Zirconium-based thin films (b-e). The corresponding results are presented in figure 20 for cells cultivation on control surfaces (a) and Titanium-based thin films (b-e).

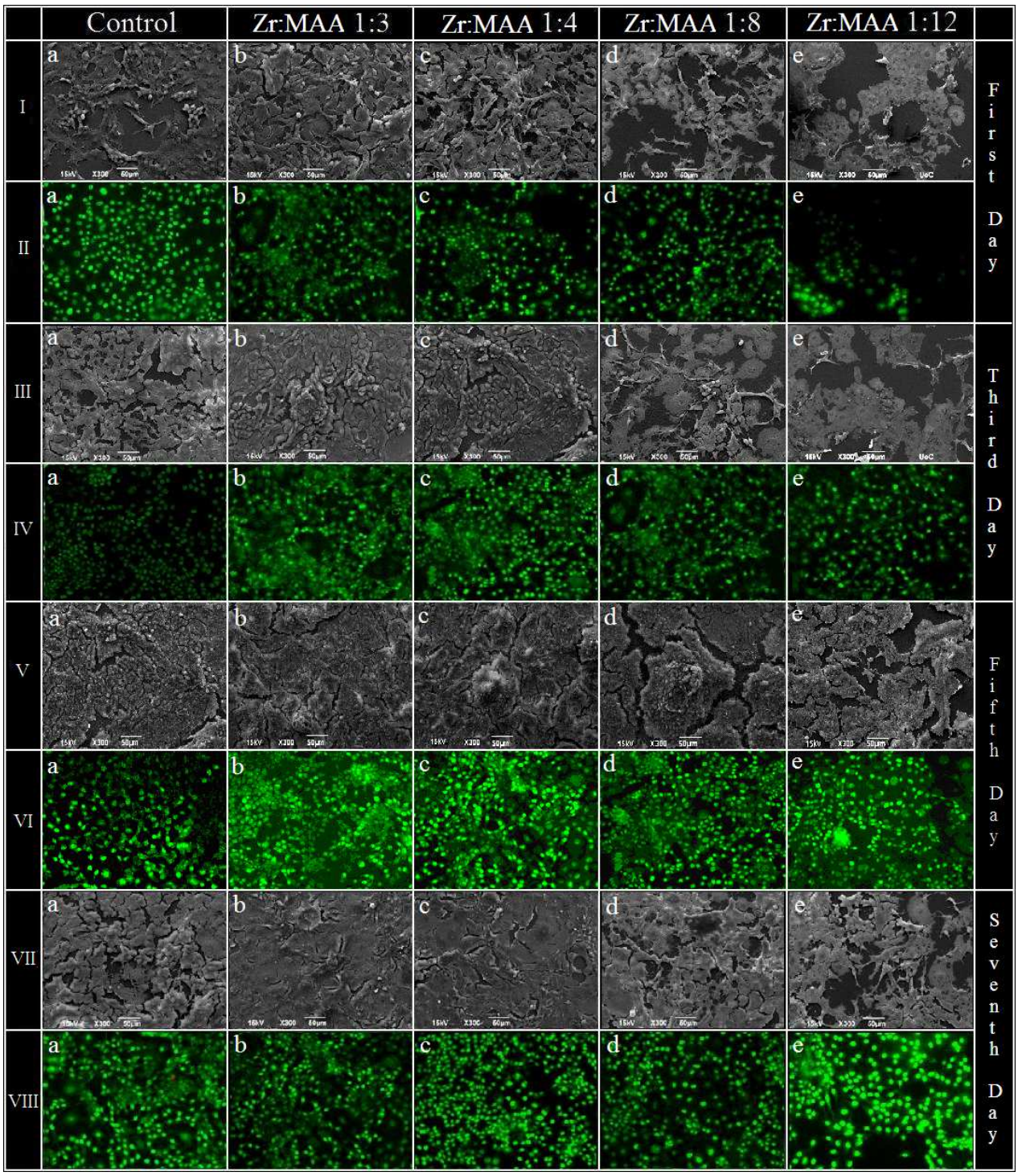

Figure 19 : SEM images of cells seeded (Lines I, III, V, VII) and Fluorescence microscopy images of live (green) and dead (orange–red) cells (Lines II, IV, VI, VIII) , for the first, third ,fifth, and seventh day of cultivation on control surfaces (a) and on Zirconium-based thin films (b-e). The magnification for all the SEM images are 50μm.

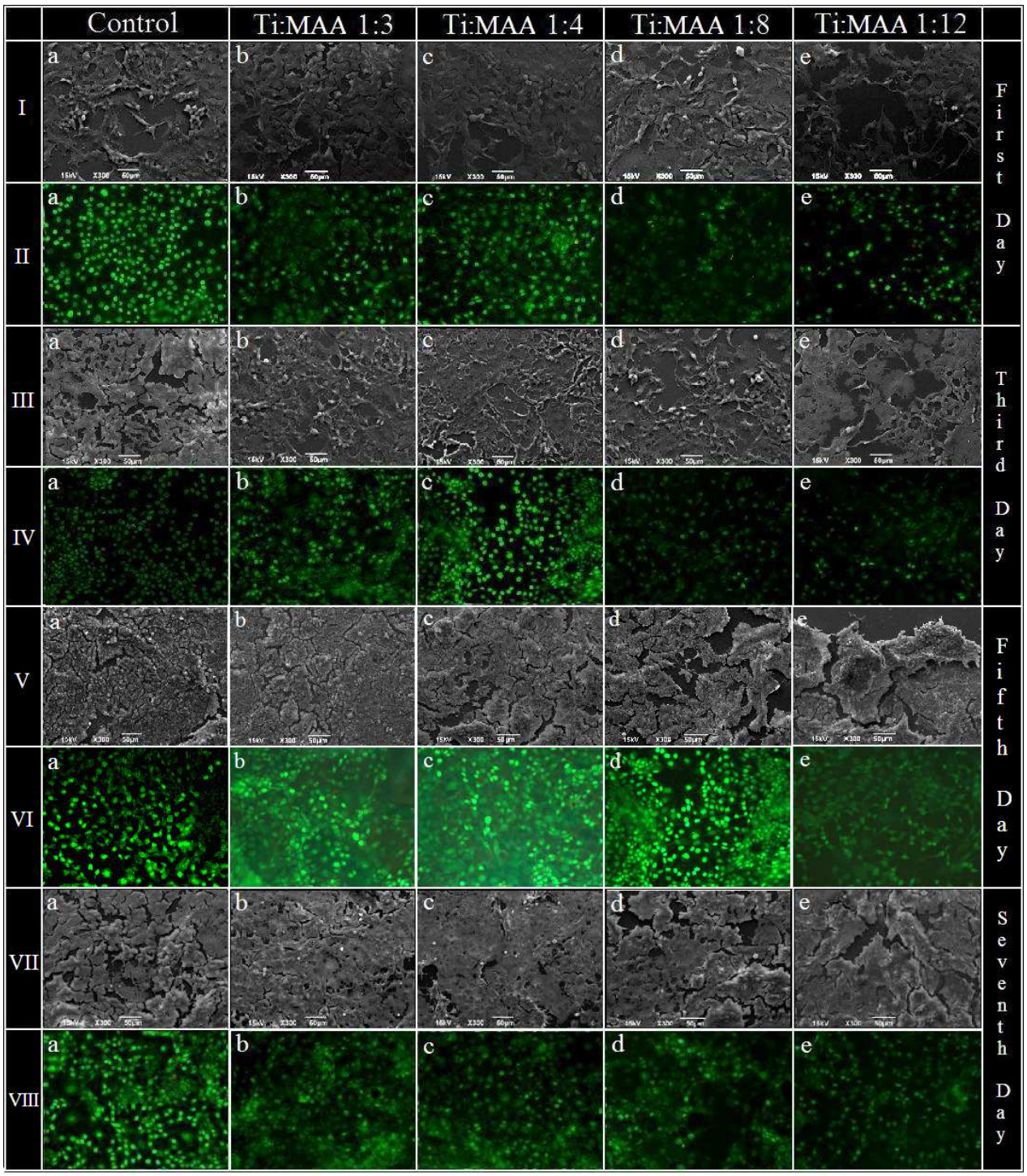

Figure 20: SEM images of cells seeded (Lines I, III, V, VII) and Fluorescence microscopy images of live (green) and dead (orange–red) cells (Lines II, IV, VI, VIII) , for the first, third ,fifth, and seventh day of cultivation on control surfaces (a) and on Titanium-based thin films (b-e). The magnification for all the SEM images are 50μm.

Cells that fluorescing green are healthy cells, in addition to cells that fluorescing red which are dead cells. In our photographs dead cells seems to be red or orange because of the mixture of red with the green colour. From the previous photographs we can observe that even from the first

day of cultivation fibroblasts have been developed enough on the surfaces and remain healthy until the seventh day of cultivation.

Furthermore, results show that the composition (organic/inorganic ratio) of the material significantly affected cells growth (Figure 21). The calculated cell densities (number of cells per surface area) on the hybrid films and on control glass surfaces showed that although both the zirconium and the titanium-based materials exhibited a similar behaviour, cell growth was inversely proportional to the MAA content of the film. For all the time intervals tested, higher cell densities could be detected in the Zr:MAA, Ti:MAA 1:3 and 1:4 films, suggesting that these substrates provide a favourable environment for cell proliferation. However, because of the easier preparation process of the metal:MAA 1:3 film, this structure was selected for application in the subsequent experiments and the 3D scaffold fabrication.

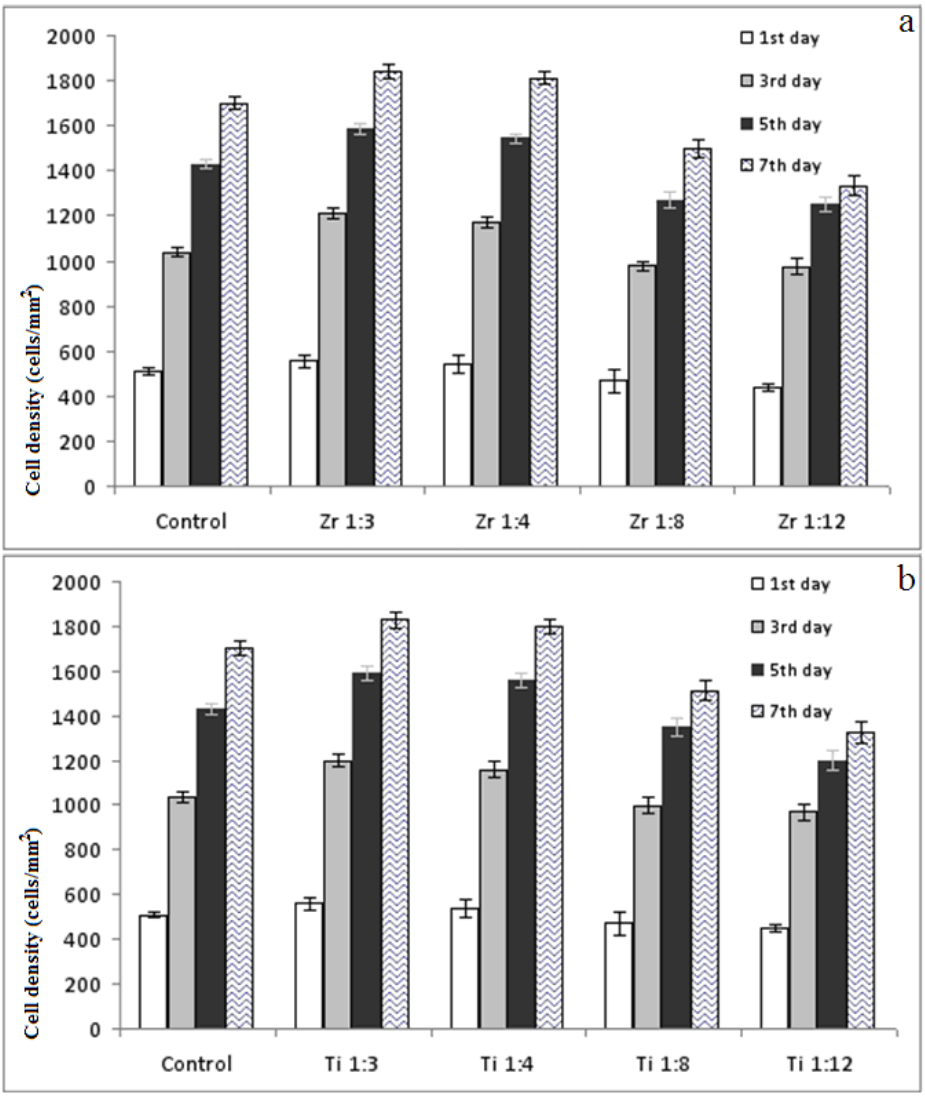

Figure 21: Cells densities (number of cells per mm^2) of (a) the different Zirconium-based surfaces and (b) the different Titanium-based surfaces on the first, third, fifth and seventh day of culture. Cells densities of control surface are shown too.

5.1.2 Results for the distribution of F-actin and Vinculin

Cytoskeleton morphology was studied by analysing actin distribution in the cultured cells. Actin filaments, composed of two intertwined chains, are mostly concentrated just beneath the cell membrane and are responsible for tension resistance, maintenance of cellular shape and formation of cytoplasmatic protuberances like pseudopodia and microvilli. In the experiments presented here, the use of phalloidin toxin allowed staining of actin and following up of cell growth and interaction with surfaces. The detection of F-actin distribution in the cytoplasm allowed to precisely studying the morphology of each individual cell and appreciating the quality of cell communication and cell-surface adhesion on the Zirconium and Titanium-based films (Figures 22a and 22b). The formation of a complete cytoskeleton showed that fibroblasts fully interact with the underlying hybrid film. Confocal microscopy analysis demonstrated the development of a complete microfilament network indicating that the fibroblasts interacted strongly with the hybrid surfaces (Figure 22). Here are presented the results of the staining for three days cells cultivation.

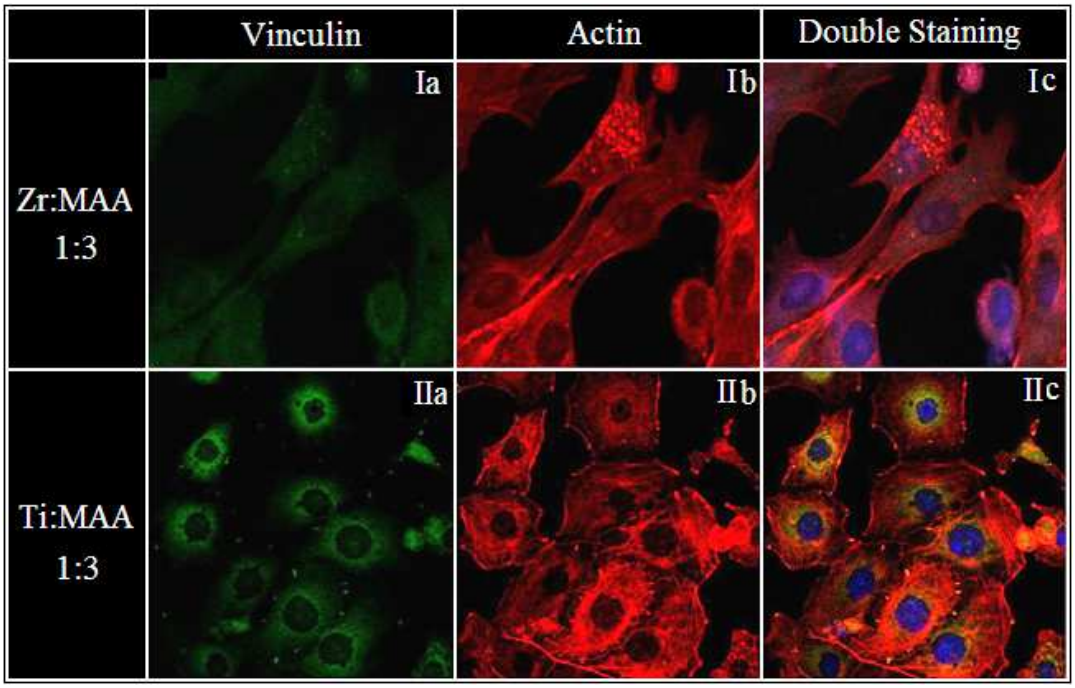

Figure 22: Detection of vinculin and actin in fibroblasts cultured on bioactive materials using confocal microscopy analysis. Confocal microscopy images show the distribution of vinculin (green) and actin (red) in fibroblasts cultured for 3 days on the Zirconium-based (I) and Titanium-based films (II). Double stained images are also shown (Ic, IIc). Nuclei were stained (blue) with TO-PRO-3 dye.

5.1.3 Conclusions for the cultivation on non-biodegradable thin films

After the repetition of experiments for three times so that we are sure for repetition of our results, we led to the conclusion that our materials are not cytotoxic. We observed that cells growth was inversely proportional to the MAA content of the film. For all the time intervals tested, higher cell densities could be detected in the Zr:MAA, Ti:MAA 1:3 and 1:4 films, suggesting that these substrates provide a favourable environment for cell proliferation. However, because of the easier preparation process of the metal:MAA 1:3 film, this ratio was selected for application in the subsequent experiments for the 3D scaffold fabrication.

5.2 Cultivation on 3D structures

After cultivation of cells on thin films and the confirmation that our materials are not cytotoxic, we advanced in the fabrication of 3D structures. As demonstrated above, the optimal organic/inorganic composition of the hybrid materials in terms of cells viability was the Zr:MAA = 1:3 and Ti:MAA = 1:3, which were thereafter used for the construction of all 3D scaffolds. Three differed sketches of 3D scaffolds were fabricated by using two photon polymerization technique.

Firstly, 3D cubes were chosen as a simple arbitrary model to increase the culture surface. Their size and spacing was varied systematically to investigate the effect of spatial distribution on cell proliferation. The fabricated structures were placed next to each other, in order to maintain the culture conditions constant and minimize the variations cell density or other environmental factors.

Secondly, since porosity is a common feature of most tissues, the construction of 3D porous scaffolds is an intriguing and promising technology. Such scaffolds, could comfortably accommodate a cell culture. Three different sizes were used for the fabrication of the cross-hatched scaffolds.

Finally, woodpile-shaped structures, consisting of layers of crossed rods, with a stacking sequence that repeated itself every four layers, were constructed.

Below are presented the parameters of the manufacturing of scaffolds and the results after the cultivation.

5.2.1 Parameters of cubes fabrication and the results of cells cultivation

The pattern of 3D cubes that were fabricated is presented in Figure 23. There are four areas of cubes differs on the size of cubes and the space between cubes. The sizes of cubes and the spaces between them are presented next to each area in the figure.

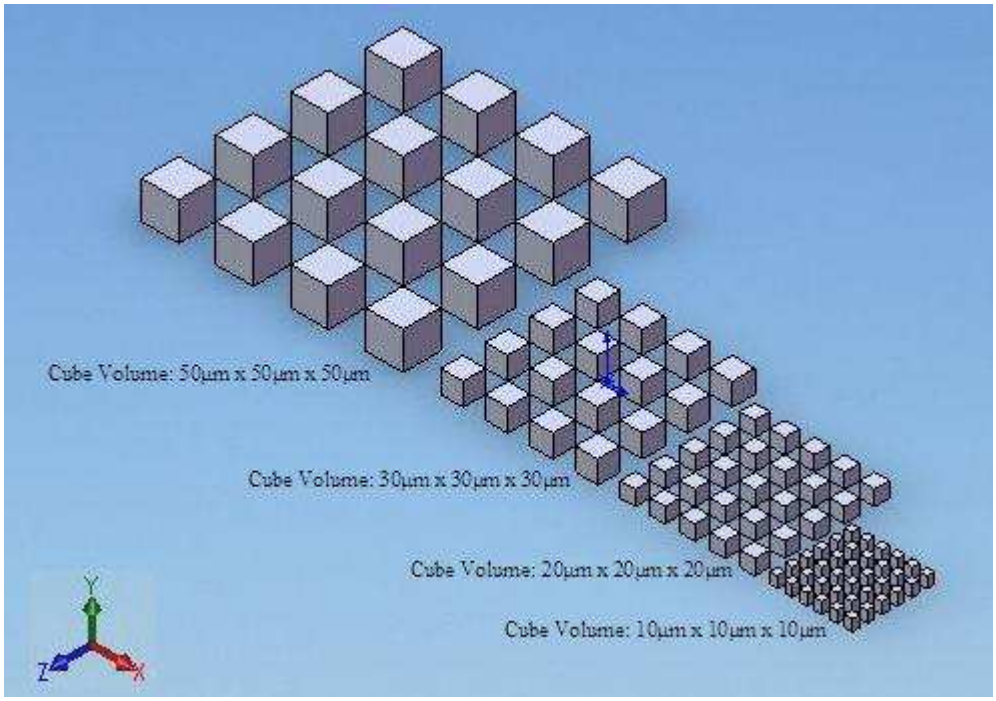

Figure 23: Computer Aided Design (CAD) model of cubes area.

5.2.1a Parameters and results for Zirconium-based cubes

For the fabrication of cubes with 50μm edge, we had to slice them in 28 layers, for 30μm edge in 18 layers and for 20μm edge in 13 layers. Each layer has a thickness of 2μm. The laser scanning sequence for each slice including layer initial border solidification and subsequent, internal area, hatching at a step of 0.2μm. The laser scanning speed was 5000μm/s and the laser power was 31mW.

For the fabrication of cubes with 10μm edge, we had to slice them in 8 layers, each layer of a thickness of 2μm. The hatching step was also 0.2μm, the laser scanning speed was 1500μm/s and the laser power was 27mW.

After the fabrication, we continued with the cultivation of cells on the scaffold (paragraph 3.6). After 3 days of cultivation, the cells were fixed, dehydrated and visualized using scanning electron microscopy technique (paragraph 3.9). In figure 24 are presented the results.

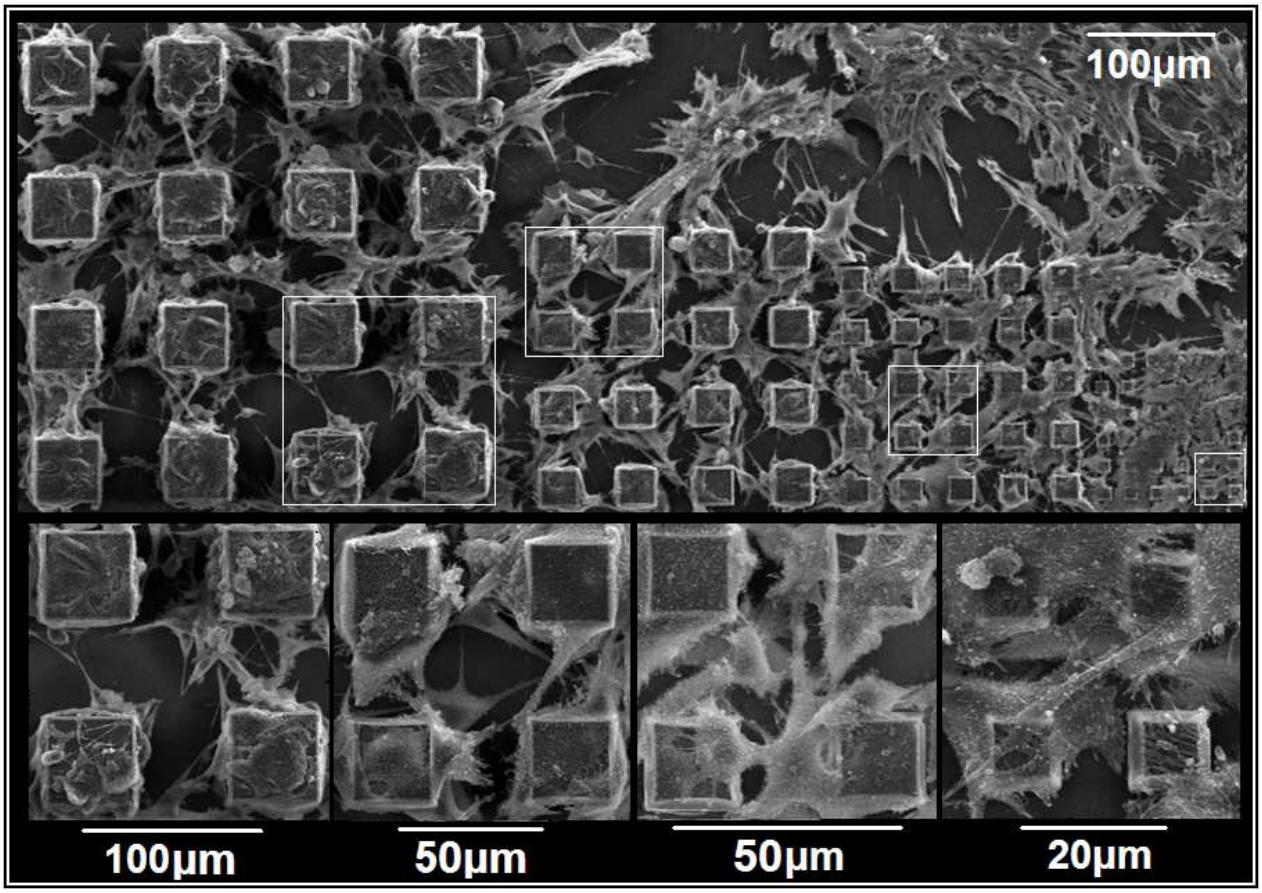

Figure 24: High magnification SEM images of fibroblast cells cultured on Zirconium-based microcubes after 3 days of cultivation.

Thus, it was shown that microcubes increased the culture surface without obstructing cell proliferation and adherence. At higher magnification, it can be seen that fibroblasts use their filopodia to tightly attach to the side surfaces of the cubes and form communication bridges between neighbouring structures, taking thus full advantage of the increased culture surface.

5.2.1b Parameters and results for Titanium-based cubes

For the fabrication of cubes with 50μm edge, we had to slice them in 17 layers of 4μm thickness, for 30μm edge in 12 layers of 4μm thickness too and for 20μm edge in 11 layers of 3μm thickness. The hatching step was 0.2μm. The laser scanning speed was 9000μm/s and the laser power was 37mW, 31mW and 27mW respectively.

For the fabrication of cubes with 10μm edge, we had to slice them in 8 layers, each layer of a thickness of 3μm. The hatching step was also 0.2μm, the laser scanning speed was 5000μm/s and the laser power was 27mW.

In figure 25 are presented the results of cells cultivation, which shows also, that microcubes can be used to increase culture surface without obstructing cell proliferation.

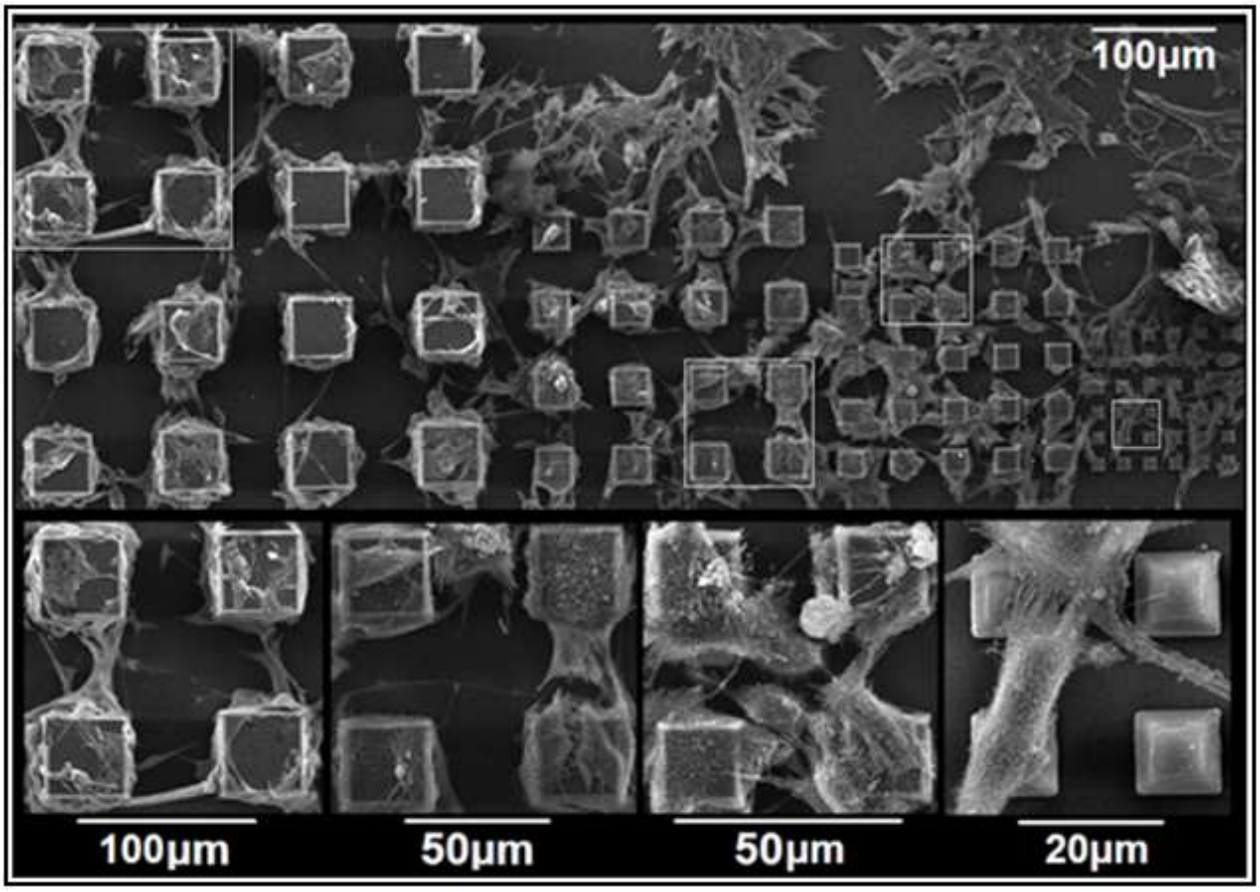

Figure 25: High magnification SEM images of fibroblast cells cultured on Titanium-based microcubes after 3 days of cultivation.

5.2.2 Parameters of cross-hatched scaffolds fabrication and the results of cells cultivation

The pattern of the cross-hatched porous scaffolds that were fabricated is presented in Figure 26. The dimensions of the scaffolds are presented in the figure. The wall thickness for all the scaffolds is 10µm. The porosity of each construction is 0.625, 0.755 and 0.873 respectively.

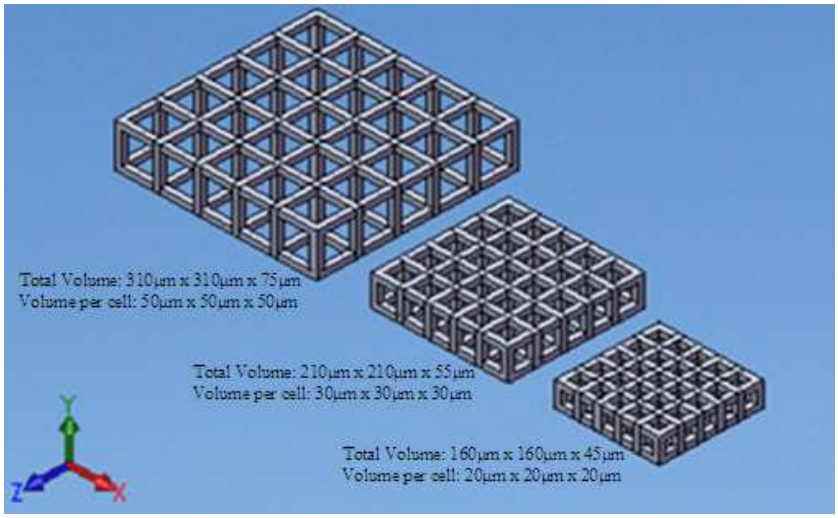

Figure 26: Computer Aided Design (CAD) model of cross-hatched porous scaffolds.

5.2.2a Parameters and results for Zirconium-based cross-hatched scaffolds

For the fabrication of the cross-hatched scaffolds we had to slice them in layers of 2μm thickness, so the bigger structure was sliced in 40 layers, the middle one in 30 layers and the smaller one in 25 layers. For the fabrication of the scaffolds, the hatching step was 0.2μm. The laser scanning speed for the fabrication of the top and the bottom layer of each scaffold was 3000μm/s while for the pillars was 800μm/s. The laser power was 23mW.

After the fabrication, we continued with the cultivation of cells on the scaffolds (paragraph 3.6). After 3 days of cultivation, the cells were fixed, dehydrated and visualized using scanning electron microscopy technique (paragraph 3.9). In figure 27 are presented the results.

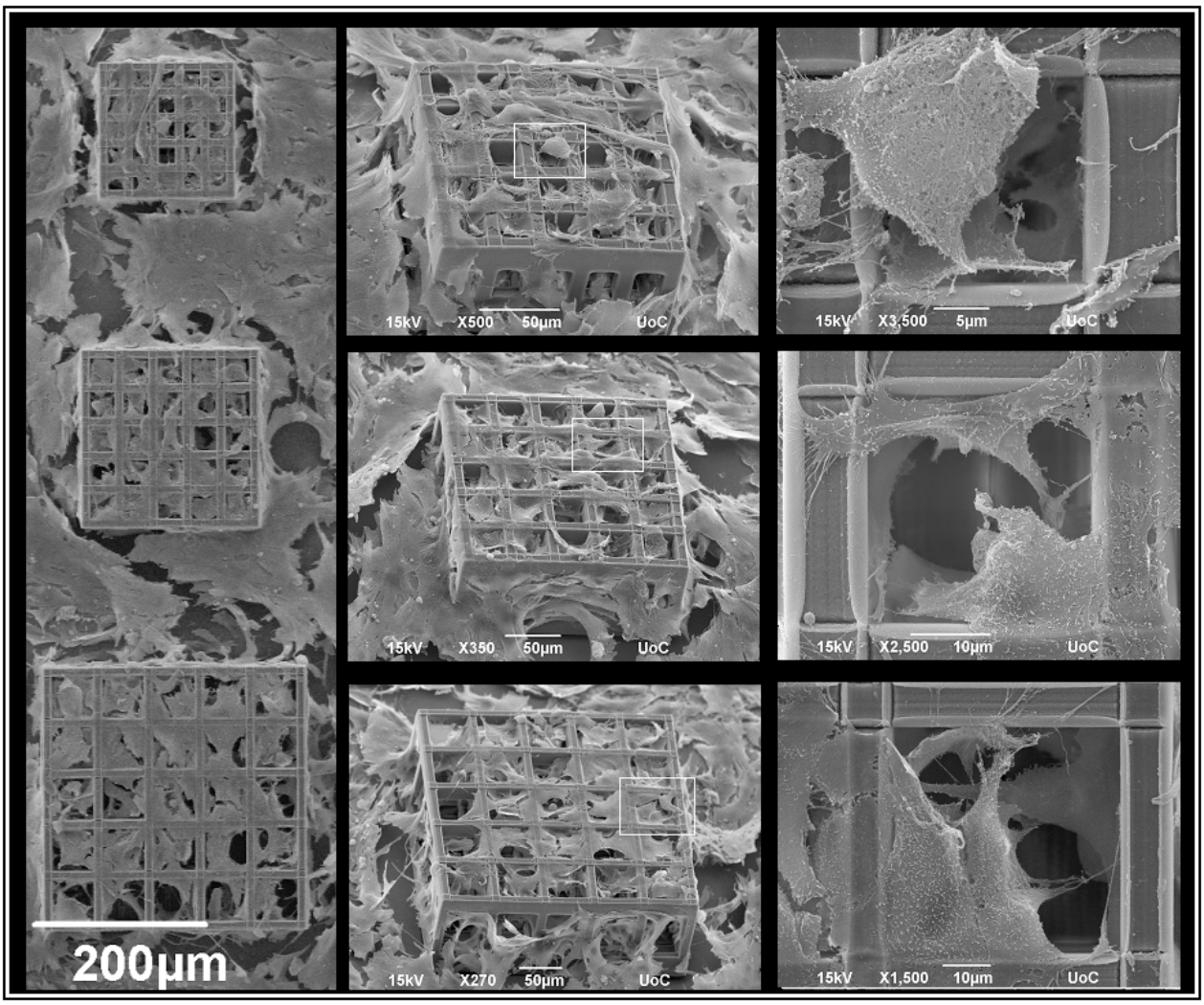

Figure 27: SEM images of 3D fibroblast cell cultured on Zirconium-based cross-hatched porous scaffolds after 3 days of cultivation.

In this case, fibroblasts migrated successfully on the three dimensional scaffolds, independently of their size. Bigger pores facilitated the formation of 3D cultures in the inner part of the structure, which can be very useful for culturing more than one type of cells. A complete

cell spreading with cells developing filopodia and lamelipodia facilitating cell-substrate and cell-cell interactions could be observed.

5.2.2b Parameters and results for Titanium-based cross-hatched scaffolds

For the fabrication of the cross-hatched scaffolds with the Titanium-based material, we used the same parameters like these for the fabrication with Zirconium-based material.

The results of the cultivation are presented in figure 28 and shows also complete cell spreading. In some cases, we can observe that cells spread creating a layer on the scaffold.

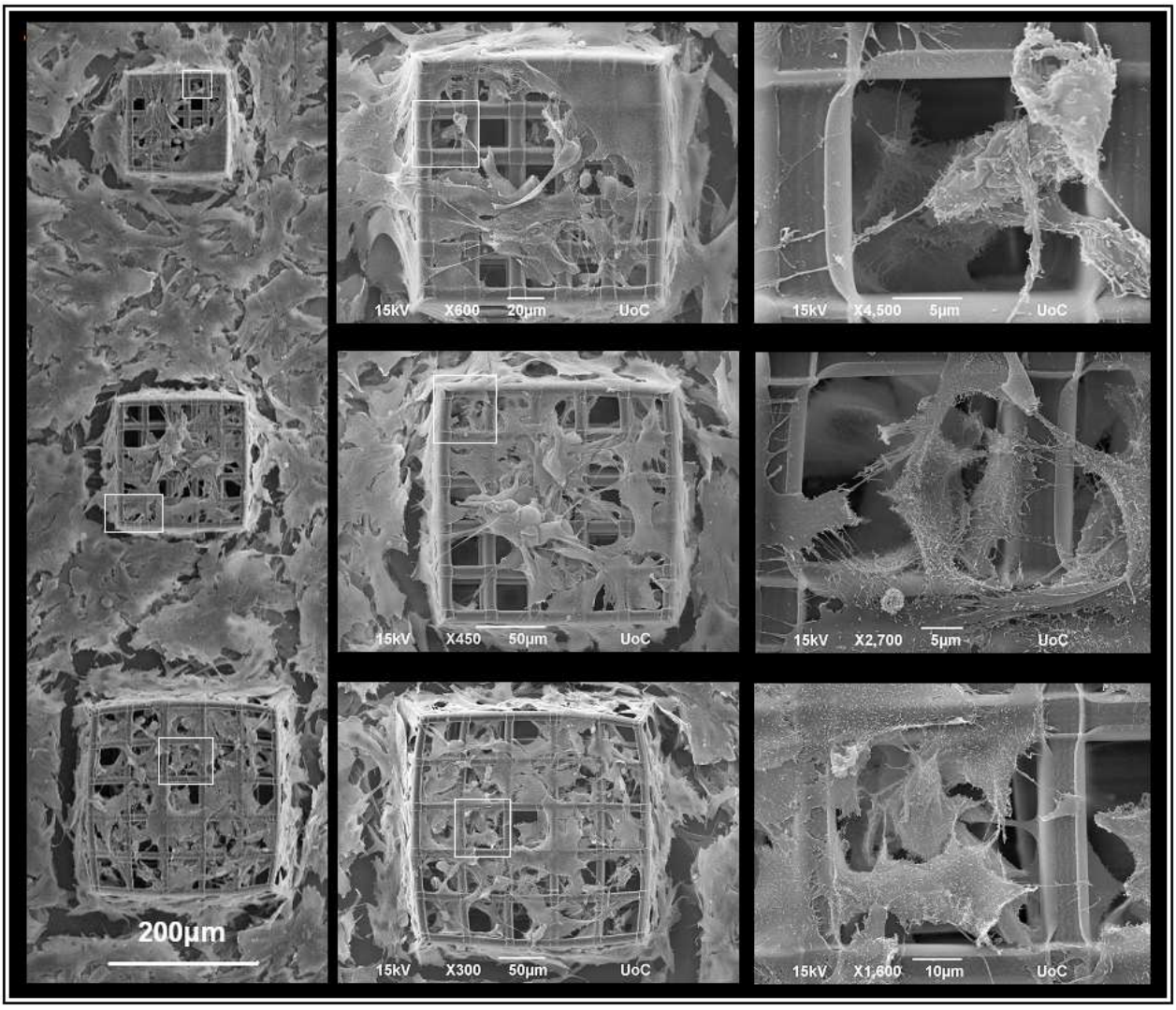

Figure 28: SEM images of 3D fibroblast cell cultured on Titanium-based cross-hatched porous scaffolds after 3 days of cultivation.

5.2.3 Parameters of woodpile-shaped scaffolds fabrication and the results of cells cultivation

The pattern of the woodpile-shaped scaffolds that were fabricated is presented in Figure 29. The structure, consisting of layers of crossed rods with thickness of 10µm, with a stacking

sequence that repeated itself every four layers. In every layer, the distance between two lines is 50μm. The porosity of this type of structures is 0.895.

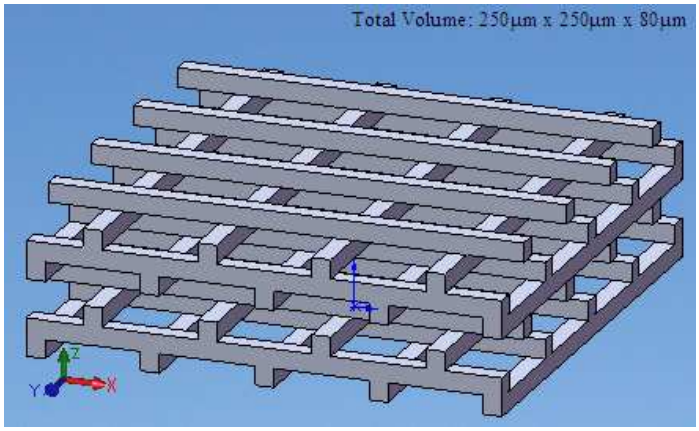

Figure 29: Computer Aided Design (CAD) model of woodpile-shaped scaffolds.

5.2.3a Parameters and results for Zirconium-based woodpile-shaped scaffolds

For the fabrication of the woodpile-shaped scaffolds we had to slice them in 44 layers of 2μm thickness. For the fabrication of the scaffolds, the hatching step was 0.2μm. The laser scanning speed was 3000μm/s and the laser power was 22mW.

After the fabrication, we continued with the cultivation of cells on the scaffolds (paragraph 3.6). After 3 days of cultivation, the cells were fixed, dehydrated and visualized using scanning electron microscopy technique (paragraph 3.9). In figure 30 are presented the results.

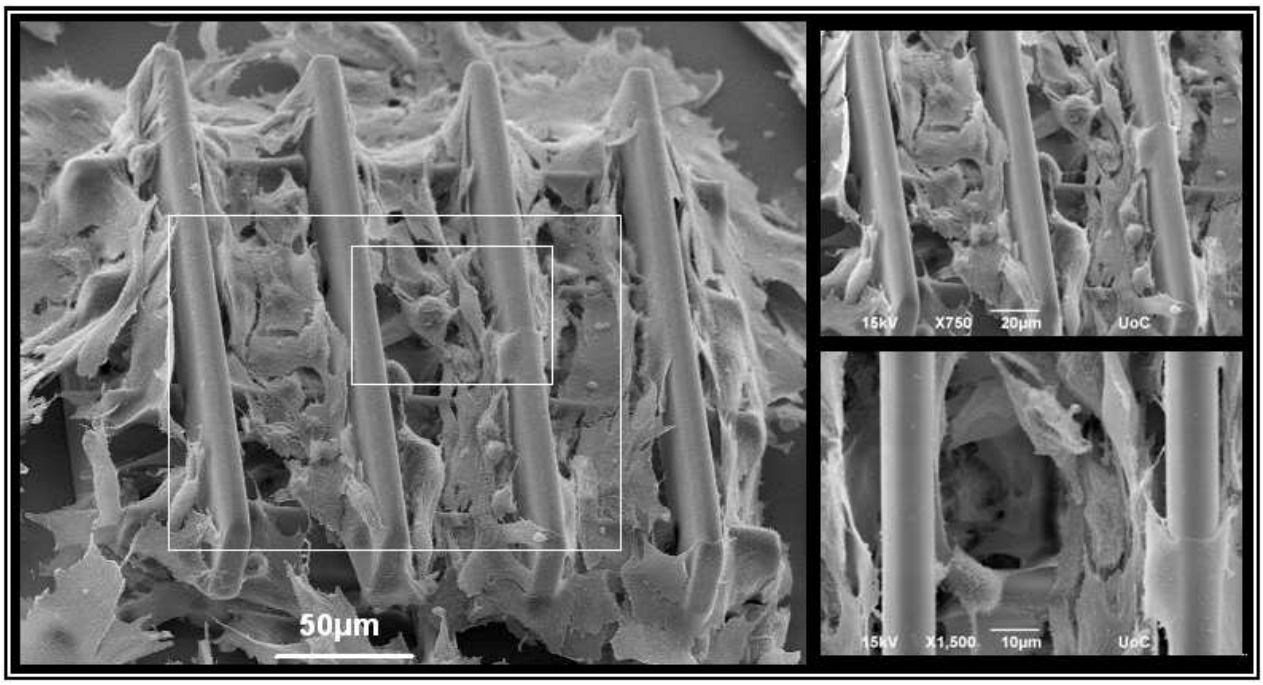

Figure 30: SEM images of 3D fibroblast cell cultured on Zirconium-based woodpile-shaped scaffolds after 3 days of cultivation.

In this case, fibroblasts were bound to the free edges of the scaffold, which were used as anchors for migration in the adhesion points of the 3D structures. Similar to the results discussed above, cells were fully developed inside the structures, forming filopodia to facilitate adherence on the hybrid surfaces and sense the environmental morphology for expansion.

5.2.3b Parameters and results for Titanium-based woodpile-shaped scaffolds

For the fabrication of the woodpile-shaped scaffolds with the Titanium-based material, we used the same parameters like these for the fabrication with Zirconium-based material.

The results of the cultivation are presented in figure 31 and shows also complete cell spreading.

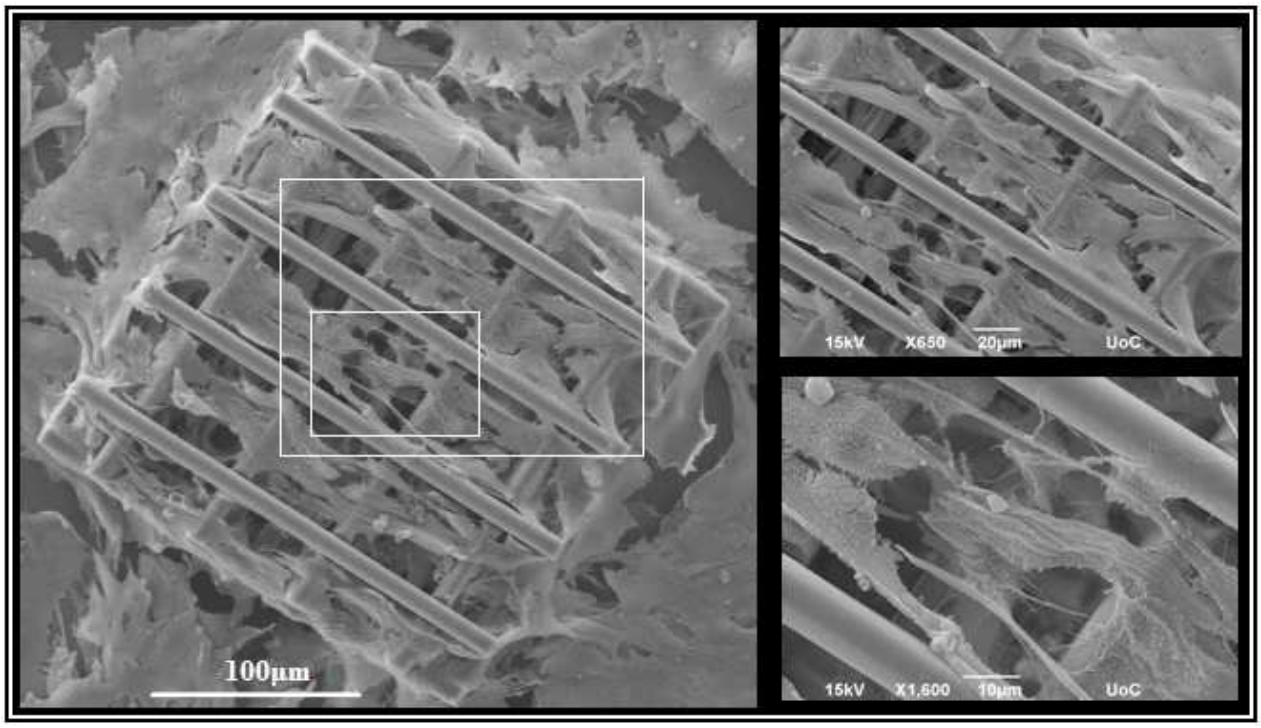

Figure 31: SEM images of 3D fibroblast cell cultured on Titanium-based woodpile-shaped scaffolds after 3 days of cultivation.

5.2.4 Conclusions for the cultivation on non-biodegradable 3D Scaffolds

Cell attachment was shown to be further enhanced and facilitated by the proper choice of the shape and size of 3D scaffolds. Thus, in cubic structures the smaller cube volume facilitated cell proliferation as it was easier for the cells to explore the whole surface of the scaffolds, while smaller spacing allowed better cell communication with neighbouring cubes. In the cross-hatched scaffolds, cells preferred the larger structures that allowed cell migration inside the pores. Finally, woodpile-shaped scaffolds were offering more cell adhesion points on the free extremities, facilitated cell migration within the scaffold.

B . Cells cultivation on biodegradable scaffolds

5.3 Cultivation on thin films

After the thin films fabrication on coverslips as it is described in chapter 3, (paragraph 3.4.2), they were transferred onto sterile 12 well plates and 2ml of cell suspension was added and cultured at 37^{o}C, 5% CO_2. Glass surfaces have also been used as control surfaces. The incubation time of cells was 1 day, 3 days, 5 days, and 7 days. After the proper incubation time we checked cells viability assay (paragraph 3.7) and the morphology of cells seeded on films surfaces (paragraph 3.8.2). Below are presented the results for the morphology of cells seeded on films surfaces and cells viability assay.

5.3.1 Results for the morphology of cells seeded and cells viability assay on films

In figure 32 presented the results for neuronal cells growth, after one, three, five and seven days of cultivation on control surfaces (a,b) as well as on PLA-based thin films (c,d). Columns I and III illustrate the morphology of PC12 cells (SEM images), while the proliferation rate (viability assays) presented on columns II and IV.

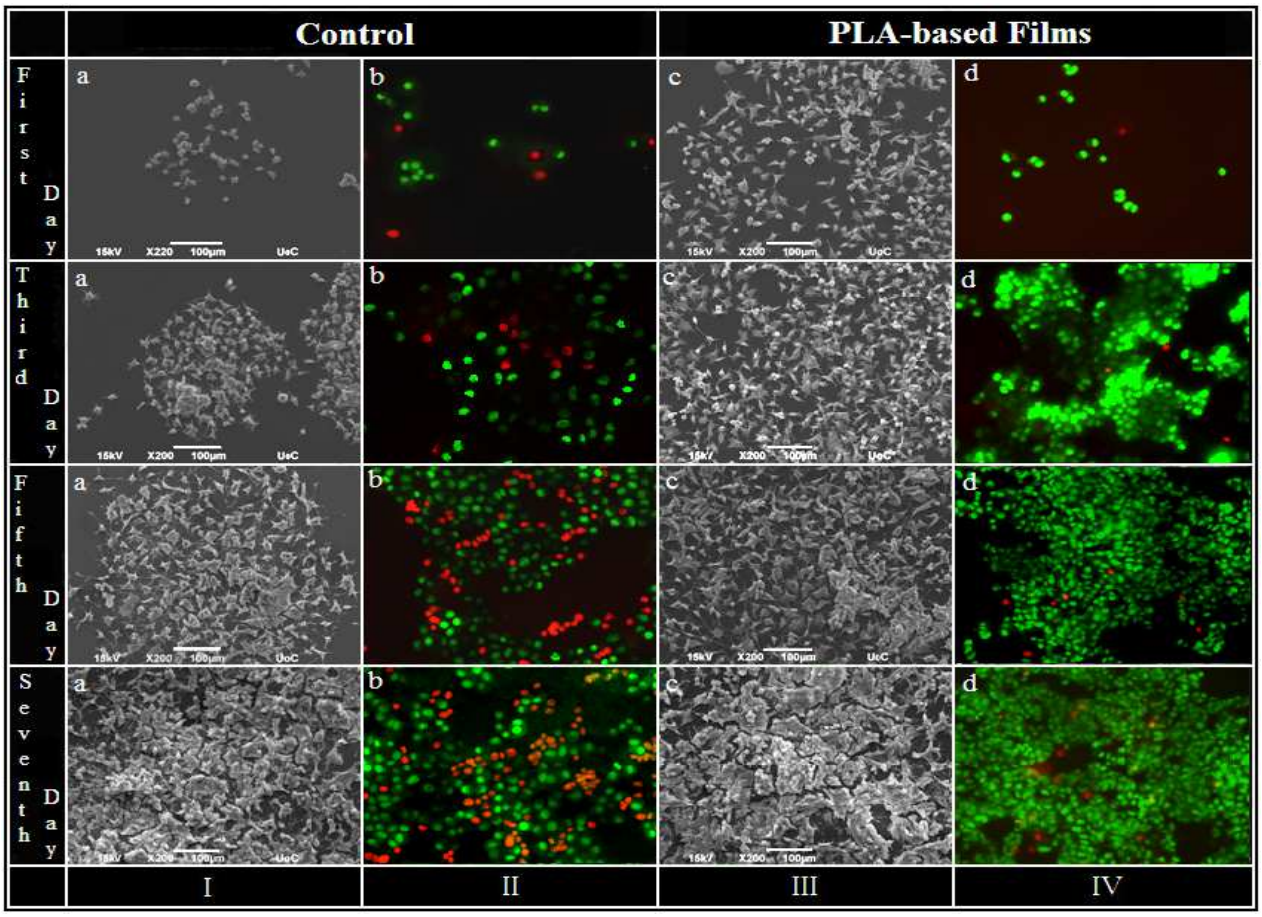

Figure 32: SEM images of PC12 cells growth (Columns I, III) and Fluorescence microscopy

images of live (green) and dead (orange–red) cells (Columns II,VI) , for the first, third ,fifth, and seventh day of cultivation on control surfaces (a,b) and on PLA-based thin films (c,d). The magnification for all the SEM images are 100μm.

The results for fibroblast cells cultivation are presented in Figure 33.

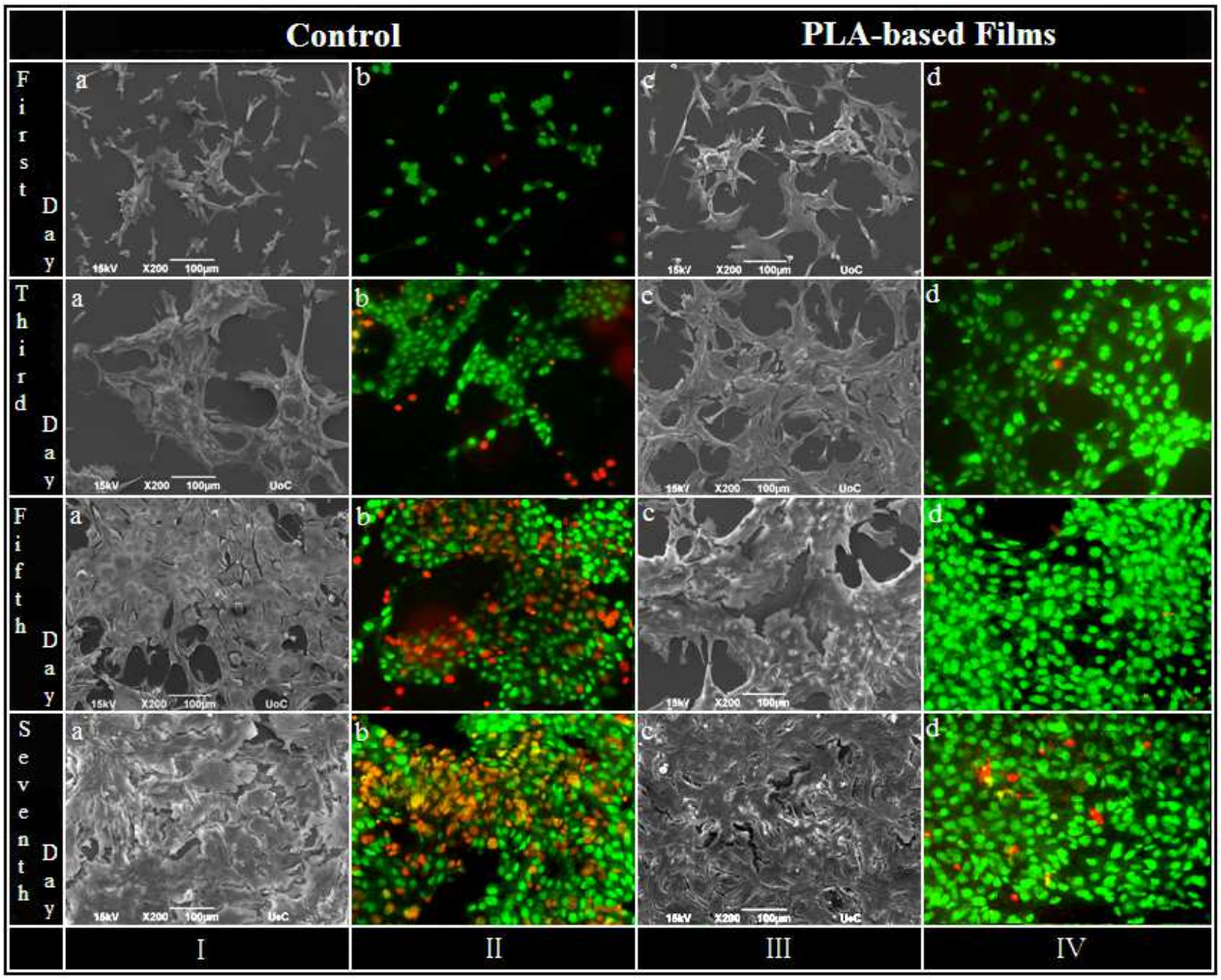

Figure 33: SEM images of 3T3 cells growth (Columns I, III) and Fluorescence microscopy images of live (green) and dead (orange–red) cells (Columns II,VI) , for the first, third ,fifth, and seventh day of cultivation on control surfaces (a,b) and on PLA-based thin films (c,d). The magnification for all the SEM images are 100μm.

As already mentioned, cells that fluorescing green are healthy cells, in addition to cells that fluorescing red which are dead cells. In our photographs dead cells seems to be red or orange because of the mixture of red with the green colour. From the previous photographs we can observe that even from the first day of cultivation neuronal cells as well as fibroblasts have been attached enough on PLA films surfaces and remained healthy until the seventh day of cultivation, in comparison to cells that were cultivated on glass surfaces.

In Figure 34 presented the results of the calculated cell densities (number of cells per surface area) on PLA-based films and on control glass surfaces for PC12 cells as well as for 3T3.

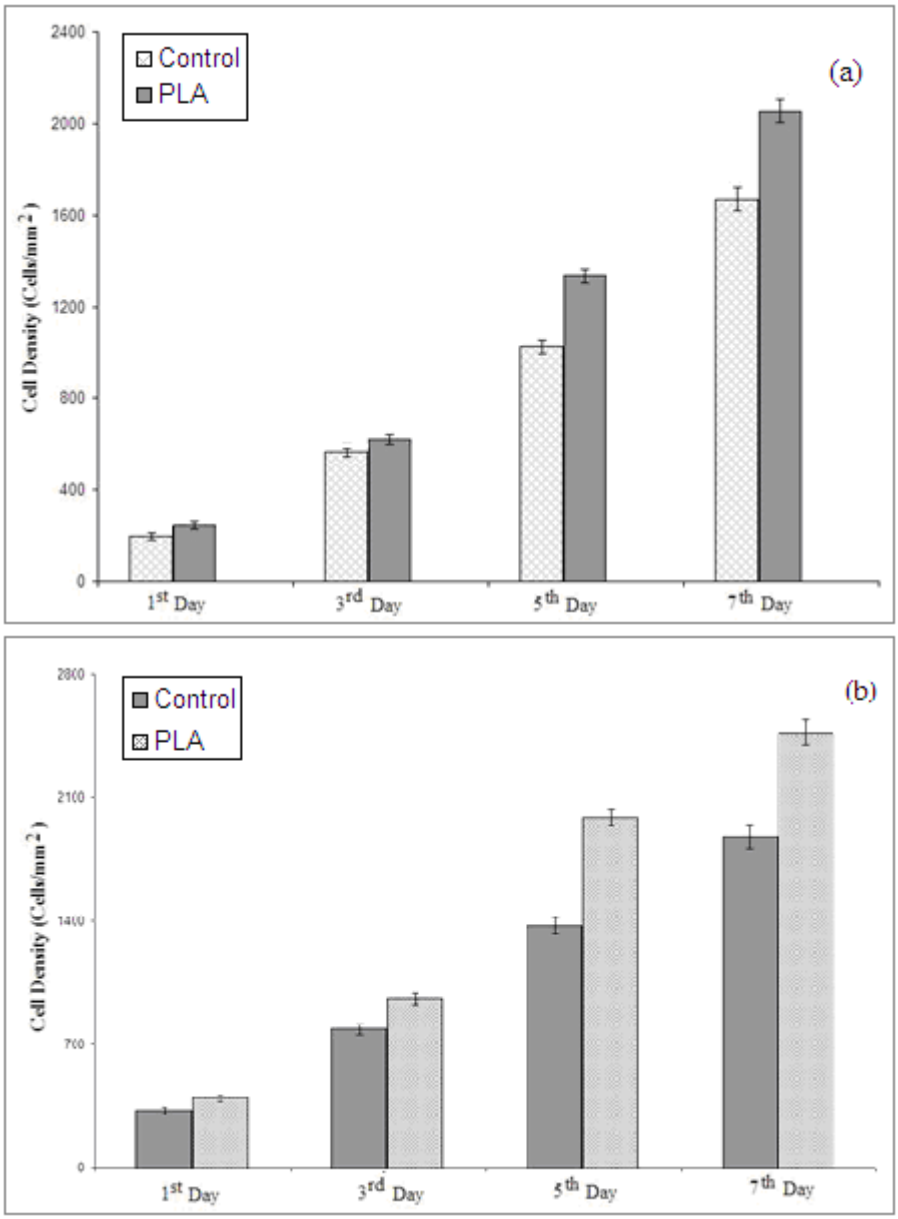

Figure 34: Cells densities (number of cells per mm^2) on glass surfaces and on PLA-based films for the first, third, fifth and seventh day of a) neuron cells cultivation and b)fibroblast cells cultivation..

Bellow are presented the results for cells morphology. We can observe that cells interact with the film, by developing neurons in case of PC12 (Figure 35) and filopodia in case of 3T3 (Figure 36). Furthermore, it is obvious that there is interaction between cells in both cases.

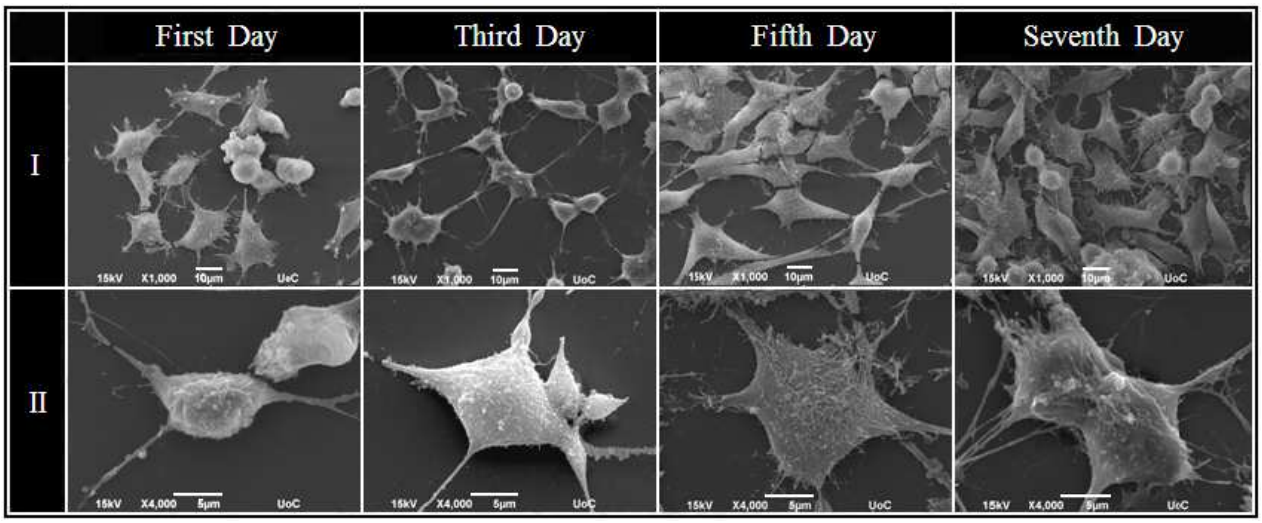

Figure 35: SEM images of PC12 cells seeded for the first, third , fifth, and seventh day of cultivation on PLA-based thin films.. The magnification for the SEM images in line I is 10μm, while in line II is 5μm.

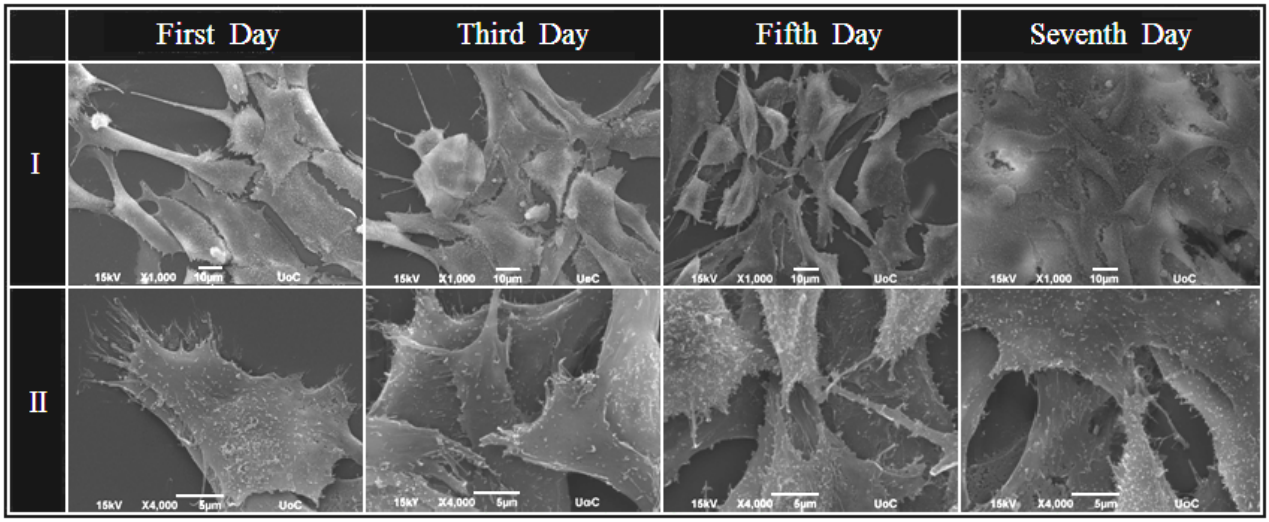

Figure 36: SEM images of 3T3 cells seeded for the first, third ,fifth, and seventh day of cultivation on PLA-based thin films.. The magnification for the SEM images in line I is 10μm, while in line II is 5μm.

5.3.2 Conclusions for the cultivation on biodegradable thin films

After the repetition of experiments for three times so that we are sure for repetition of our results, we led to the conclusion that our material is not cytotoxic. Neuronal cells as well as fibroblasts remained healthy until the seventh day of cultivation.

5.4 Cultivation on 3D structures

After cultivation of cells on thin films and the confirmation that our material is not cytotoxic, we advanced in the fabrication of 3D structures. Six differed sketches of 3D scaffolds were fabricated by using two photon polymerization technique.

Firstly, 3D cubes were chosen again as a simple arbitrary model to increase the culture surface. Then, cross-hatched scaffolds and woodpile-shaped structures were fabricatet again, with purpose to check the use of these microstructures as cell delivery vehicle. For the same reason 3D sea-shell type structures and pyramid type structures were fabricated. Finally, suspended guidelines, which were constructed between 2 parallel rectangular blocks, were fabricated to study cell alignment and directed growth.

Below are presented the parameters of the manufacturing of scaffolds and the results after the cultivation.

5.4.1 Parameters of cubes fabrication and the results of cells cultivation

The pattern of 3D cubes that were fabricated is illustrated in Figure 23. For the fabrication of cubes with 50μm edge, we had to slice them in 13 layers, for 30μm edge in 9 layers and for 20μm edge in 7 layers. Each layer has a thickness of 5μm. The laser scanning sequence for each slice including layer initial border solidification and subsequent, internal area, hatching at a step of 0.2μm. The laser scanning speed was 3000μm/s and the laser power was 31mW.

For the fabrication of cubes with 10μm edge, we had to slice them in 6 layers, each layer of a thickness of 3μm. The hatching step was also 0.2μm, the laser scanning speed was 1500μm/s and the laser power was 27mW.

After the fabrication, we continued with the cultivation of cells on the scaffolds (paragraph 3.6). After 3 days of cultivation, the cells were fixed, dehydrated and visualized using scanning electron microscopy technique (paragraph 3.9). In figure 36 and 38 are presented the results for PC12 and 3T3 cells respectively.

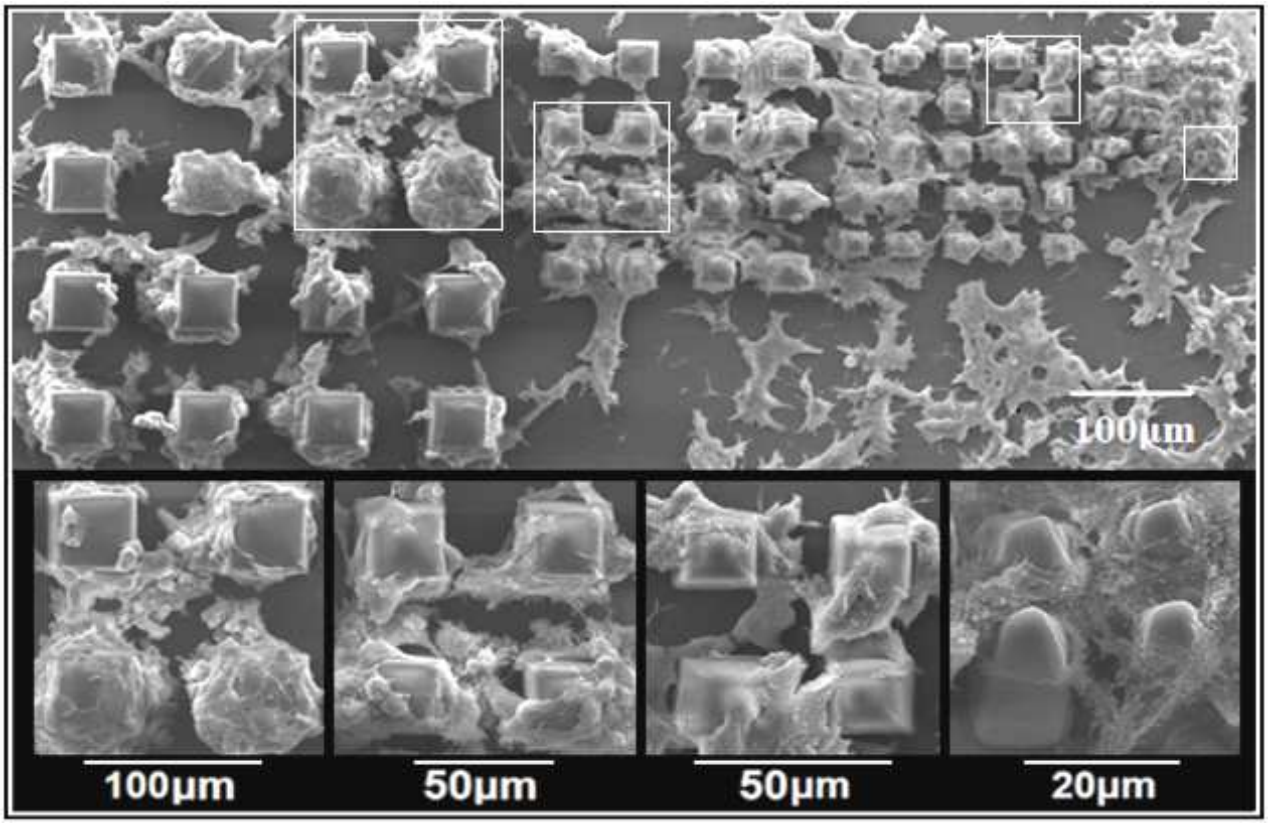

Figure 37: High magnification SEM images of neural cells cultured on PLA-based microcubes after 3 days of cultivation.

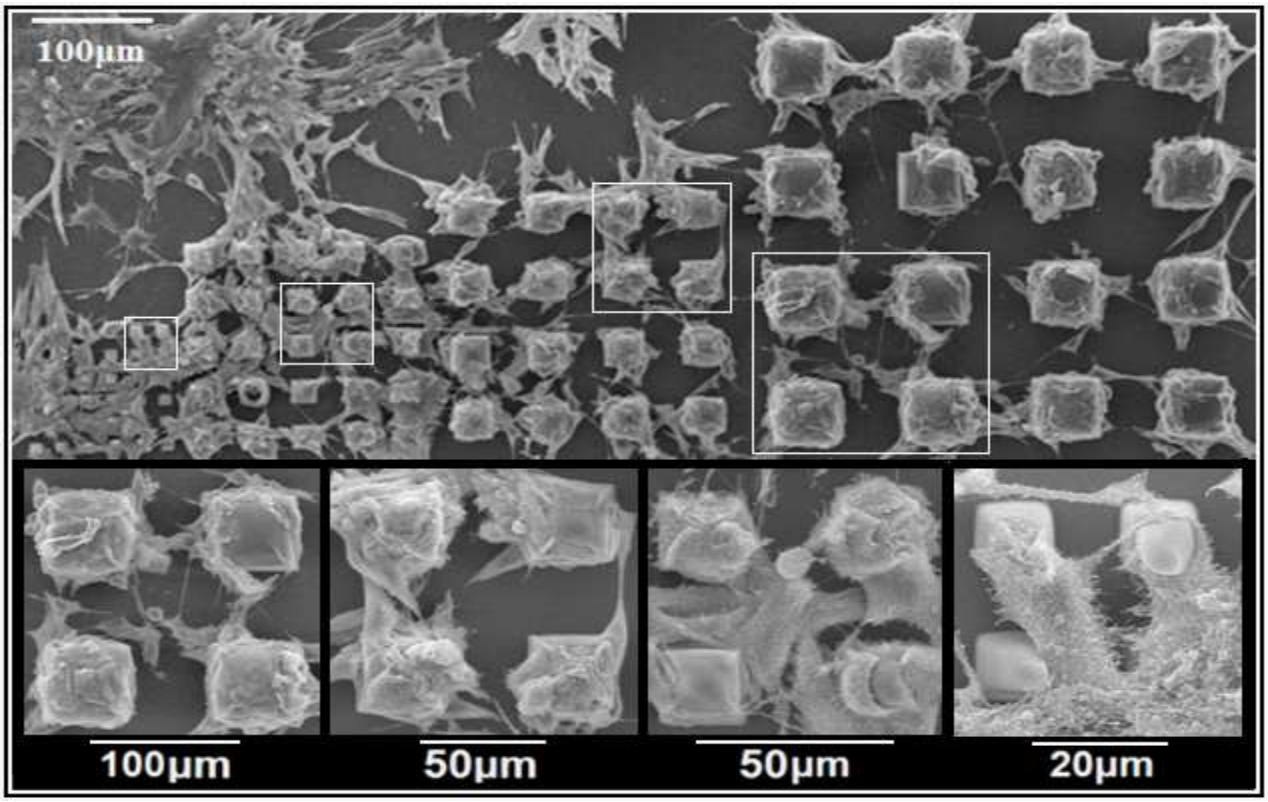

Figure 38: High magnification SEM images of fibroblast cells cultured on PLA-based microcubes after 3 days of cultivation.

As it is obvious, microcubes increased the culture surface without obstructing cell proliferation and adherence. At higher magnification, it can be seen that neural cells use their neurons (figure 37), while fibroblasts use their filopodia (figure 38), to tightly attach to the side surfaces of the cubes and form communication bridges between neighbouring structures, taking thus full advantage of the increased culture surface.

5.4.2 Parameters of cross-hatched scaffolds fabrication and the results of cells cultivation

The pattern of the cross-hatched porous scaffolds that were fabricated is presented in Figure 26. For the fabrication of the cross-hatched scaffolds we had to slice them in layers of 5μm thickness, so the bigger structure was sliced in 17 layers, the middle one in 13 layers and the smaller one in 11 layers. For the fabrication of the scaffolds, the hatching step was 0.2μm. The laser scanning speed for the fabrication of the top and the bottom layers of each scaffold was 3000μm/s while for the pillars was 1000μm/s. The laser power was 31mW.

The time of cultivation was 5 days and the results are presented in figure 39 for neural cells and in figure 40 for fibroblast cells.

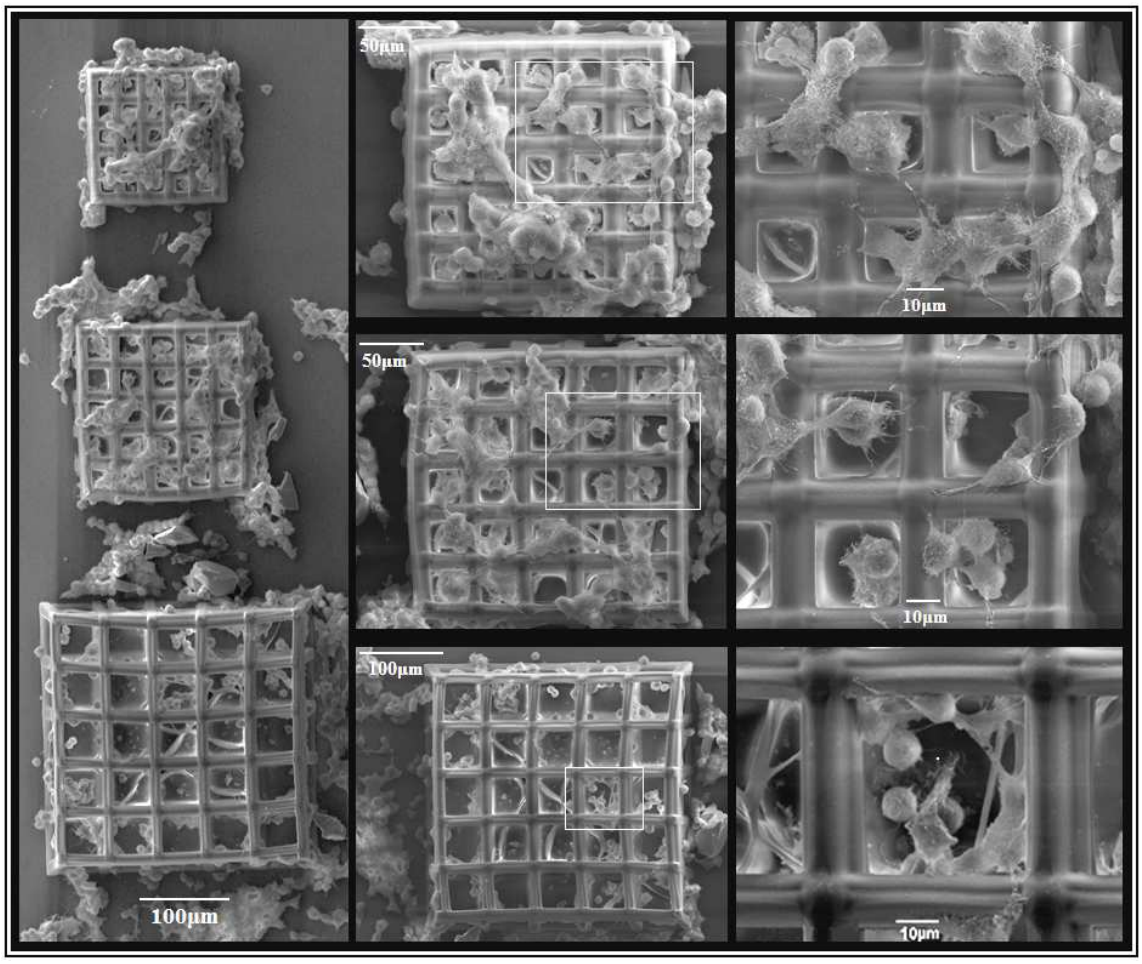

Figure 39: SEM images of neural cells cultured on PLA-based cross-hatched porous scaffolds after 5 days of cultivation.

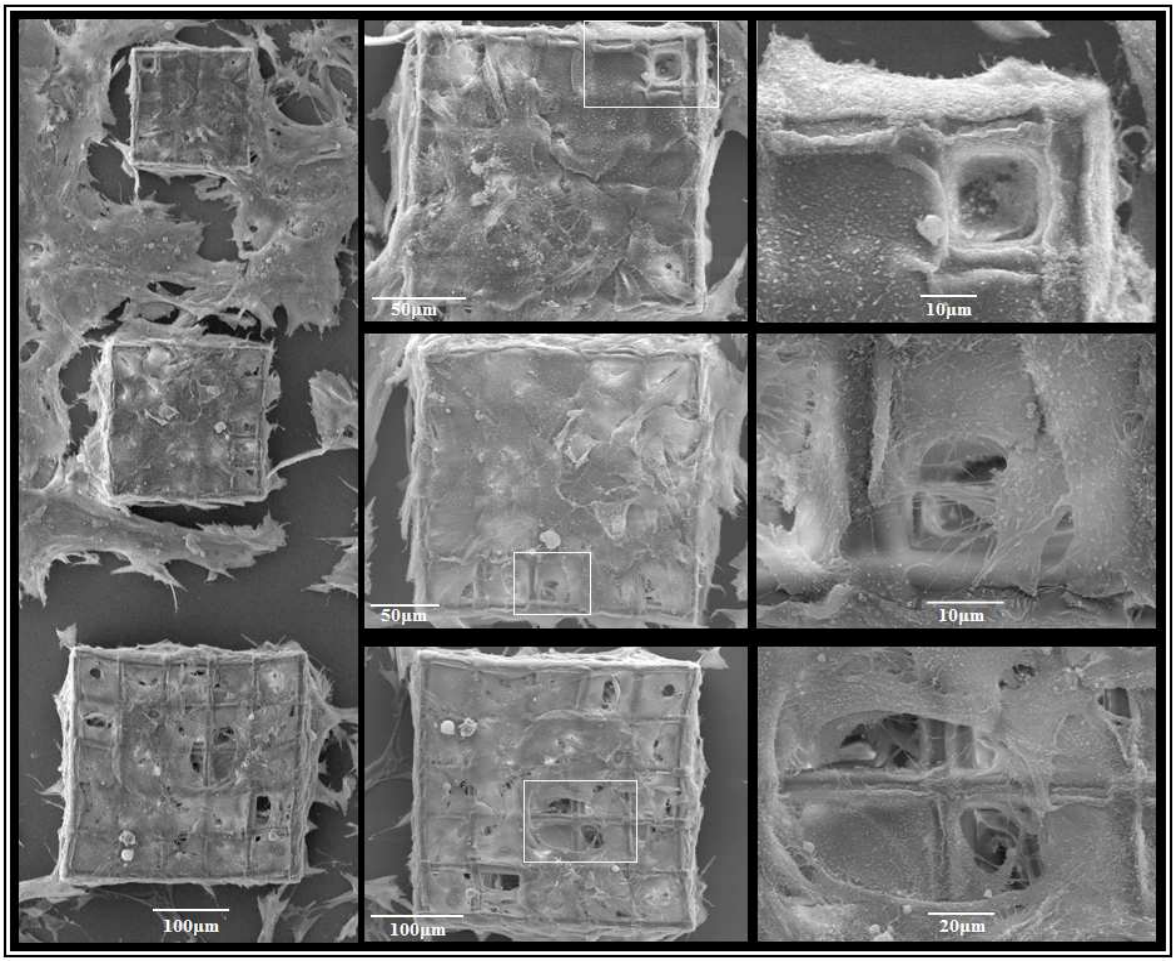

Figure 40: SEM images of fibroblast cells cultured on PLA-based cross-hatched porous scaffolds after 5 days of cultivation.

In this case, cells migrated successfully on the three dimensional scaffolds, independently of their size. In case of neural cells (Figure 39), pores scaffolds facilitated the formation of 3D cultures in the inner part of the structure, while cultivation of fibroblasts (Figure 40) gave a complete cell spreading, creating a layer of cells on the surface of the structures. In both cases it can be observed that cells developing neurons in case of PC12 and filopodia and lamelipodia in case of 3T3, facilitating cell-substrate and cell-cell interactions.

5.4.3 Parameters of woodpile-shaped scaffolds fabrication and the results of cells cultivation

The pattern of the woodpile-shaped scaffolds that were fabricated is presented in Figure 29. For the fabrication of the woodpile-shaped scaffolds we had to slice them in 19 layers of 5μm thickness. For the fabrication of the scaffolds, the hatching step was 0.2μm. The laser scanning speed was 3000μm/s and the laser power was 31mW.

After the fabrication, we continued with the cultivation of cells on the scaffolds (paragraph 3.6). After 5 days of cultivation, the cells were fixed, dehydrated and visualized using scanning

electron microscopy technique (paragraph 3.9). In figures 34 and 35 are presented the results for PC12 and 3T3 cells respectively.

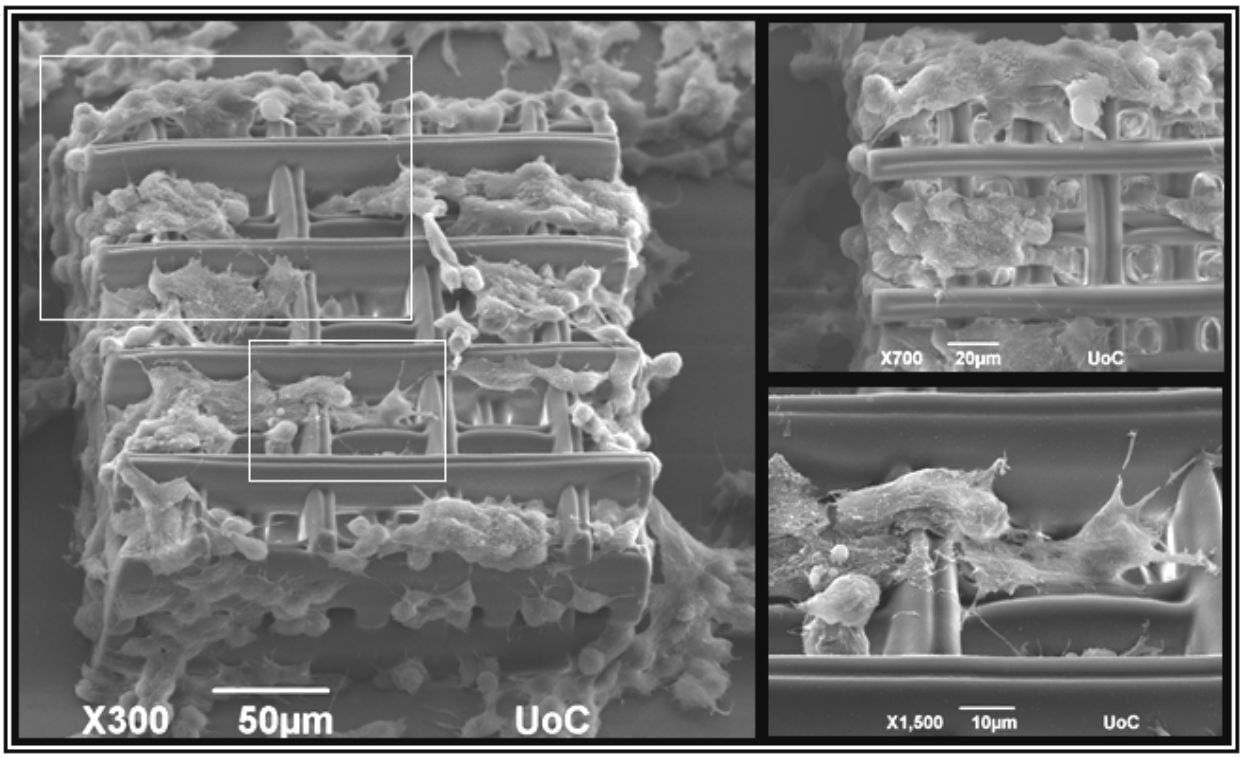

Figure 41: SEM images of neural cells cultured on PLA-based woodpile-shaped scaffolds after 5 days of cultivation.

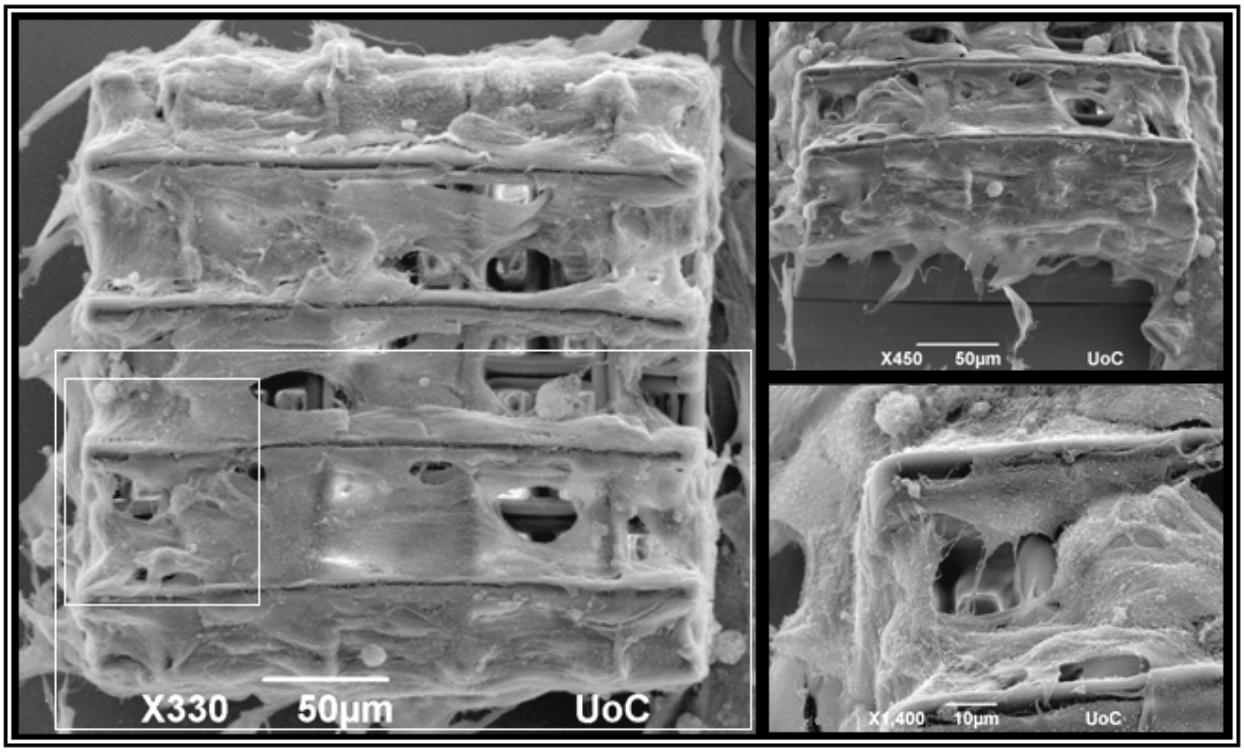

Figure 42: SEM images of fibroblast cells cultured on PLA-based woodpile-shaped scaffolds after 5 days of cultivation.

In this case, cells were bound to the free edges of the scaffold, which were used as anchors for migration in the adhesion points of the 3D structures. As it is obvious, cells were developed inside the structures, forming neurons (Figure 41) and filopodia (Figure 42) while gave a complete cell spreading especially in case of fibroblasts.

5.4.4 Parameters of sea-shell type scaffolds fabrication and the results of cells cultivation

The pattern of the sea-shell type scaffolds that were fabricated is presented in Figure 43. There is an area of 5x5 sea-shell sketches witch sizes are been presented in figure 36. The space between the top of two neighbour structures is 80μm.

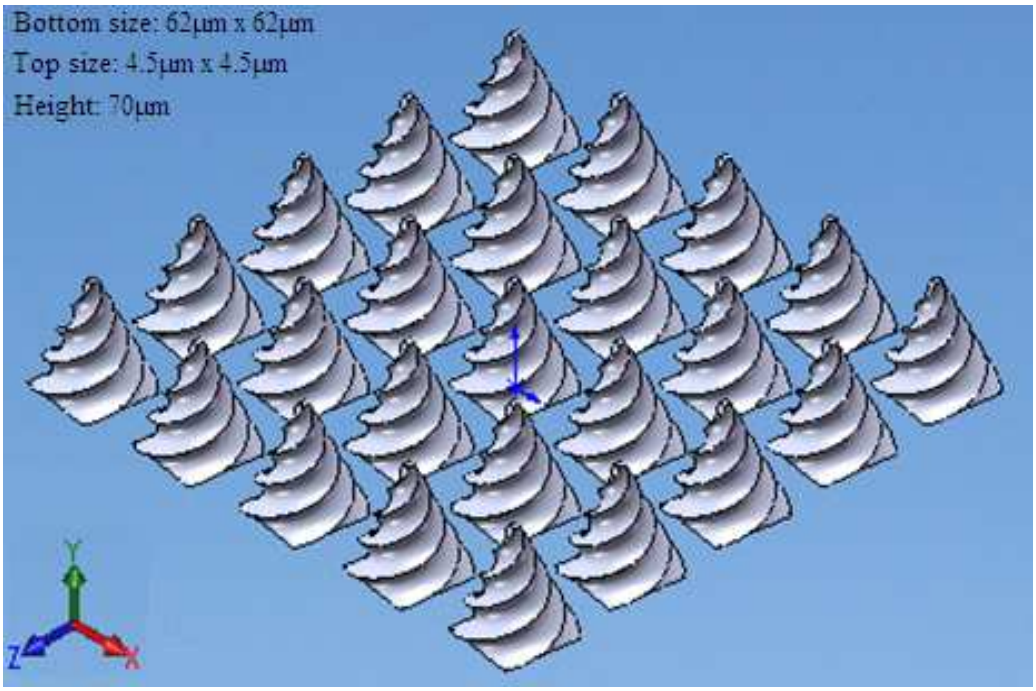

Figure 43: Computer Aided Design (CAD) model of sea-shell type scaffolds.

5.4.4a Parameters and results for PLA-based sea-shell type scaffolds

For the fabrication of the sea-shell type scaffolds we had to slice them in 32 layers of 2.5μm thickness. For the fabrication of the scaffolds, the hatching step was 0.2μm. The laser scanning speed was 3000μm/s and the laser power was 31mW.

After 5 days of cultivation, the cells were fixed, dehydrated and visualized using scanning electron microscopy technique (paragraph 3.9). In figures 44 and 45 are presented the results for PC12 and 3T3 cells respectively.

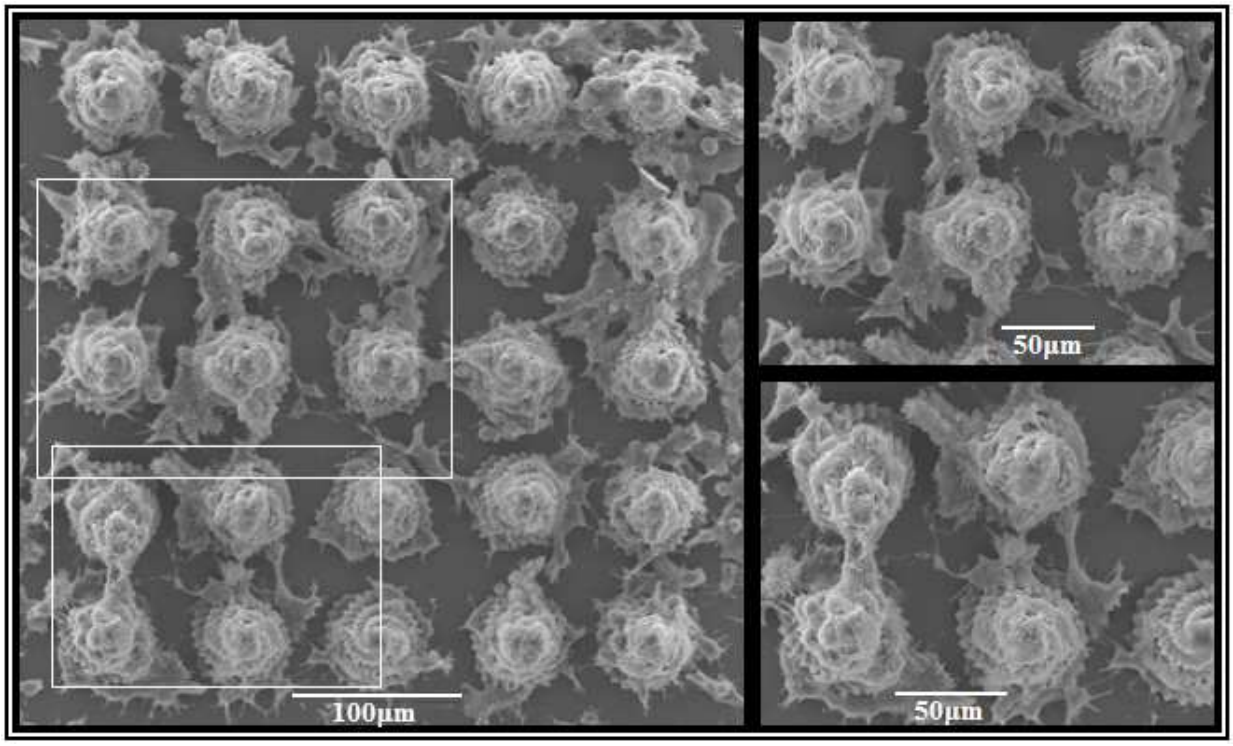

Figure 44: SEM images of neural cells cultured on PLA-based sea-shell type scaffolds after 5 days of cultivation.

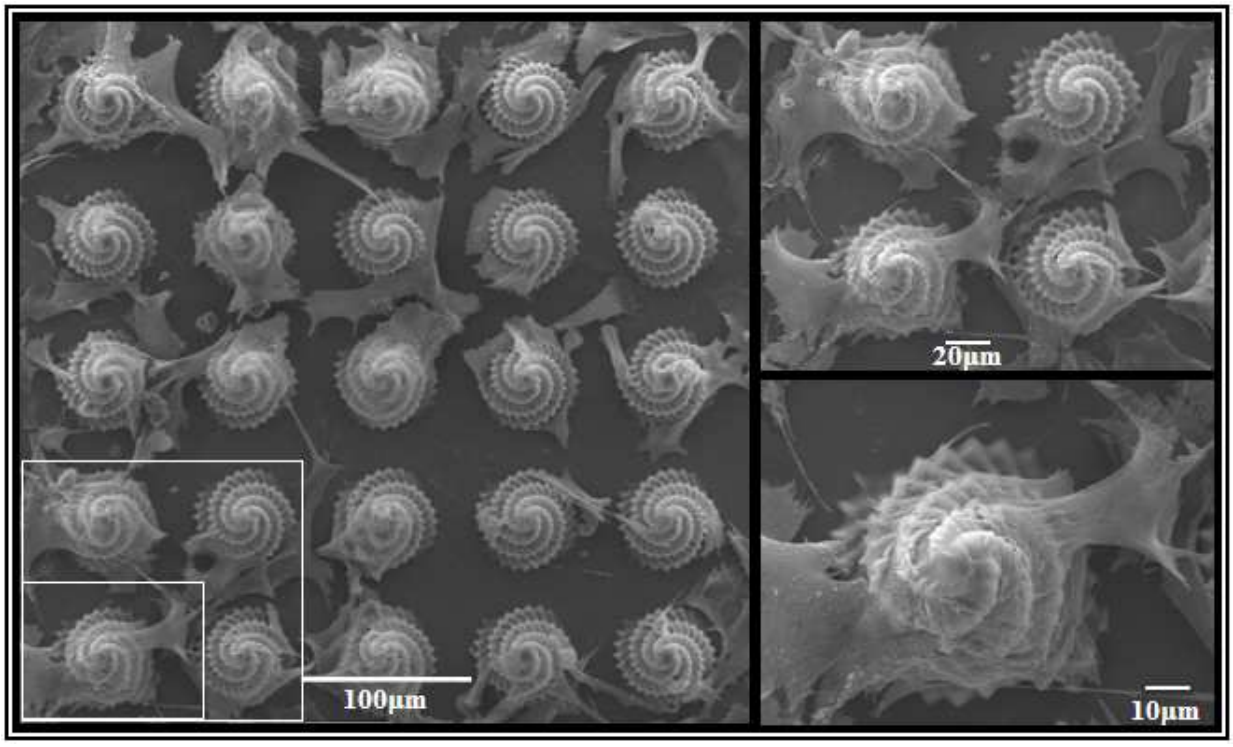

Figure 45: SEM images of fibroblast cells cultured on PLA-based sea-shell type scaffolds after 5 days of cultivation.

In this case, cells were adhered to the scaffolds, which were used as anchors for migration. As it is obvious, cells were developed following the sketch of the scaffold, forming neurons (Figure 44) and filopodia (Figure 45) while gave a 3D network.

5.4.5 Parameters of pyramid type scaffolds fabrication and the results of cells cultivation

The pattern of the pyramid type scaffolds that were fabricated is presented in Figure 46. There is an area of 5x5 pyramids witch sizes are been presented in figure 46.

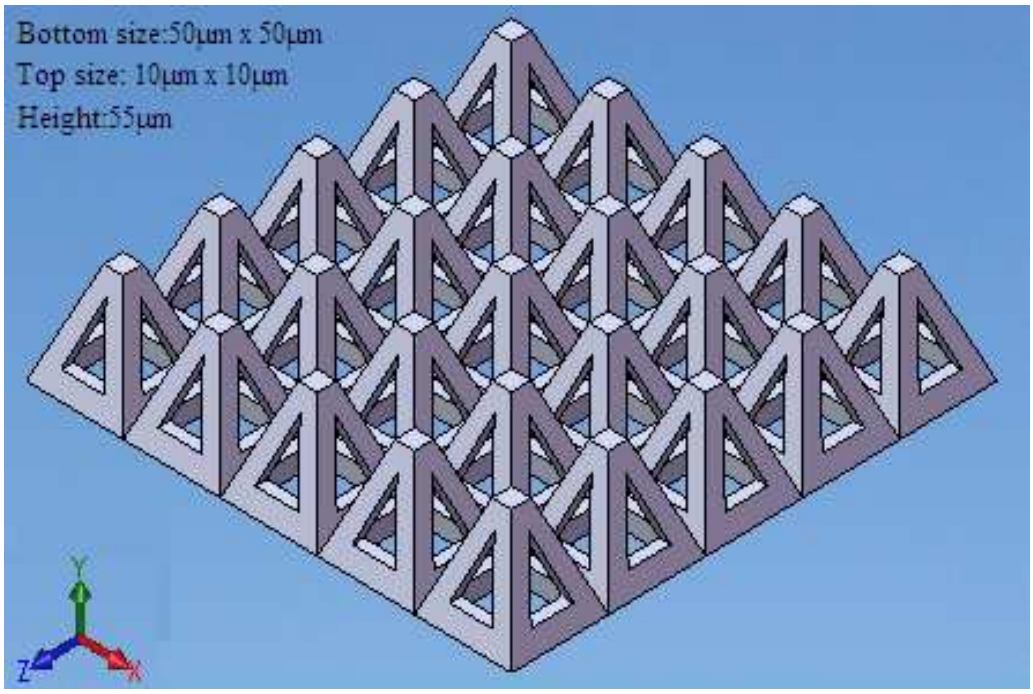

Figure 46: Computer Aided Design (CAD) model of pyramid type scaffolds.

5.4.5a Parameters and results for PLA-based pyramid sea-shell type scaffolds

For the fabrication of the pyramid type scaffolds we had to slice them in 26 layers of 2.5μm thickness. For the fabrication of the scaffolds, the hatching step was 0.2μm. The laser scanning speed was 5000μm/s and the laser power was 28mW.

After 5 days of cultivation, cells were fixed, dehydrated and visualized using scanning electron microscopy technique (paragraph 3.9). In figures 47 and 48 are presented the results for PC12 and 3T3 cells respectively.

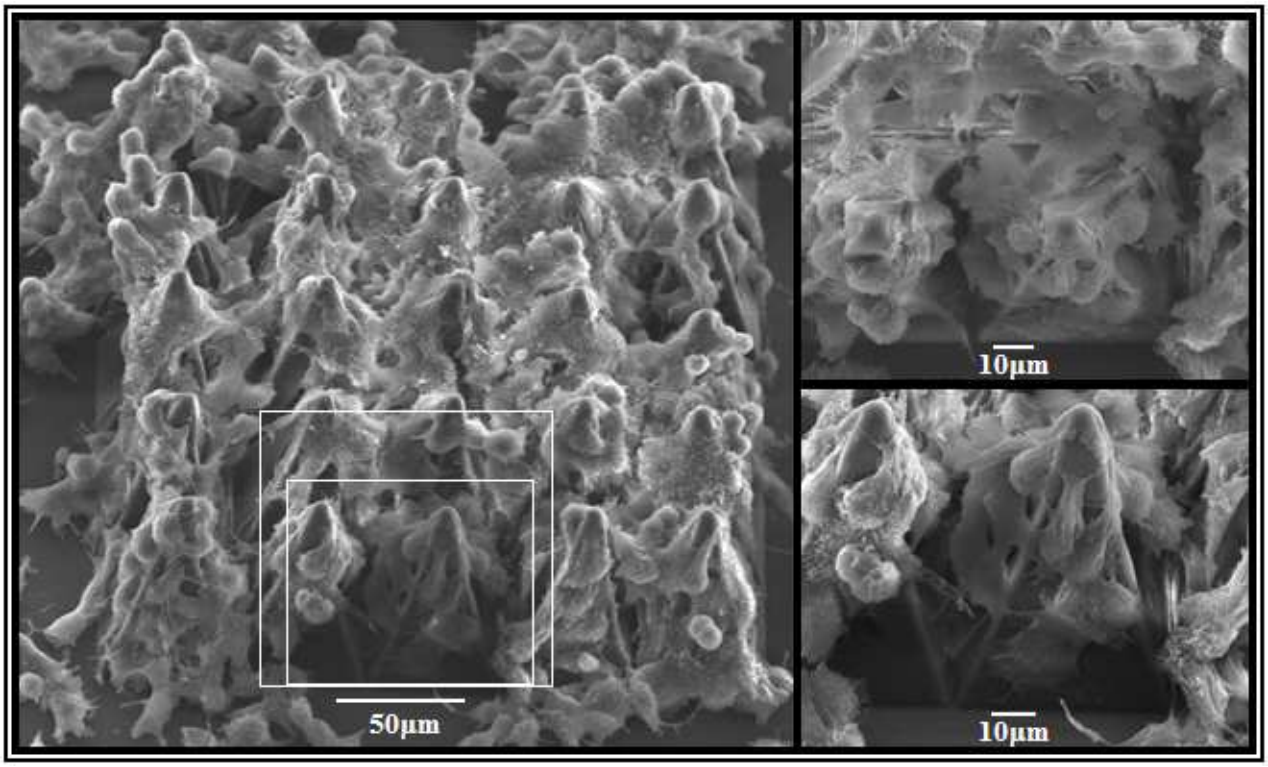

Figure 47: SEM images of neural cells cultured on PLA-based pyramid type scaffolds after 5 days of cultivation.

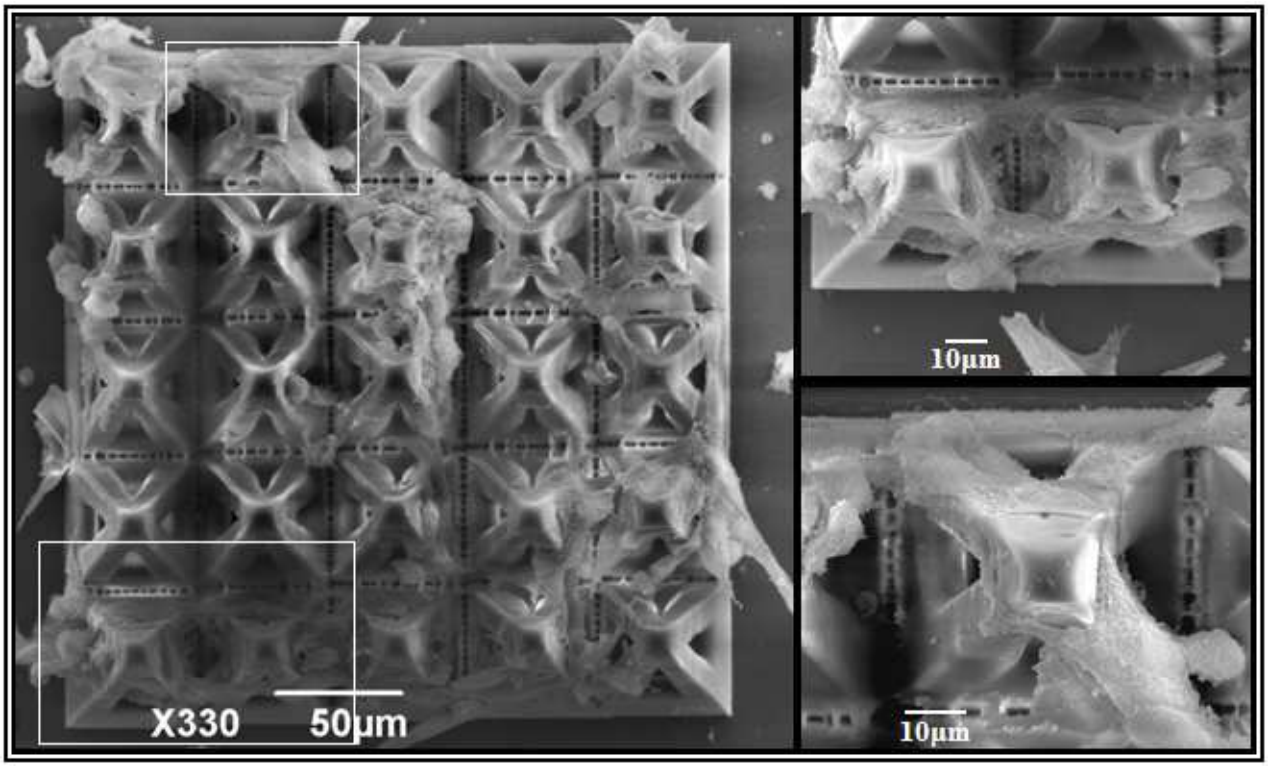

Figure 48: SEM images of fibroblast cells cultured on PLA-based pyramid type scaffolds after 5 days of cultivation.

In this case, cells were bound to the scaffolds, which were used as anchors for migration. As it is obvious, cells were developed following the sketch of the scaffold, forming neurons (Figure 47) and filopodia (Figure 48). Moreover, it is observed that cells use their projections to develope in the porous of the scaffold.

5.4.6 Parameters of guidewires type scaffolds fabrication and the results of cells cultivation.

The pattern of the guidewires type scaffolds that were fabricated is presented in Figure 49. The diameter of the guidewires is 10μm and the distance between to neighbouring wires is 50μm. The dimensions of the scaffold are presented in figure 49.

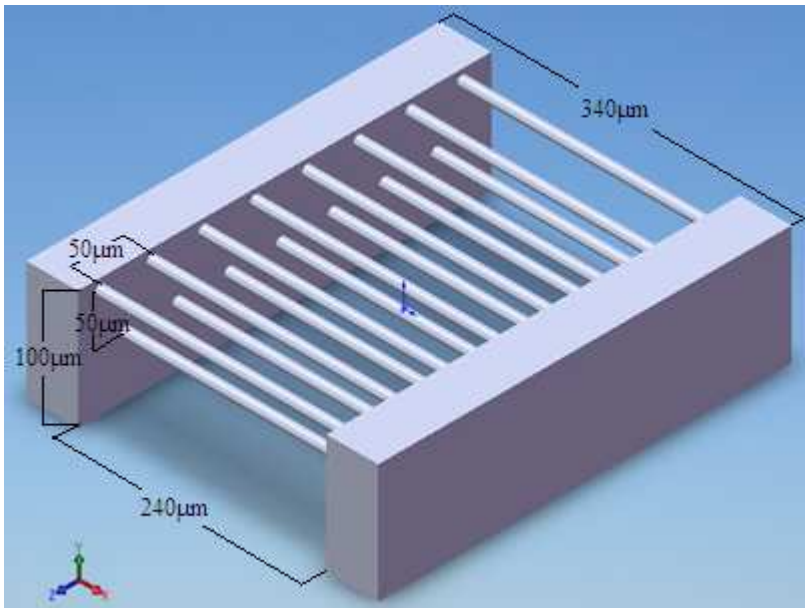

Figure 49: Computer Aided Design (CAD) model of guidewires type scaffolds.

5.4.6a Parameters and results for PLA-based guidewires type scaffolds.

For the fabrication of the guidewires type scaffolds we had to slice them in 20 layers of 5μm thickness. For the fabrication of the scaffolds, the hatching step was 0.2μm. The laser scanning speed was 3000μm/s and the laser power was 31mW.

After 5 days of cultivation, the cells were fixed, dehydrated and visualized using scanning electron microscopy technique (paragraph 3.9). In figures 50 and 51 are presented the results for PC12 and 3T3 cells respectively. Furthermore, in order to verify the neuronal differentiation of PC12 on 3D scaffolds, the presence of class III b-tubulin isotype, a neuronal cytoskeletal antigens, have been studied by immunoflourence experiments. The results are presented in figure 52.

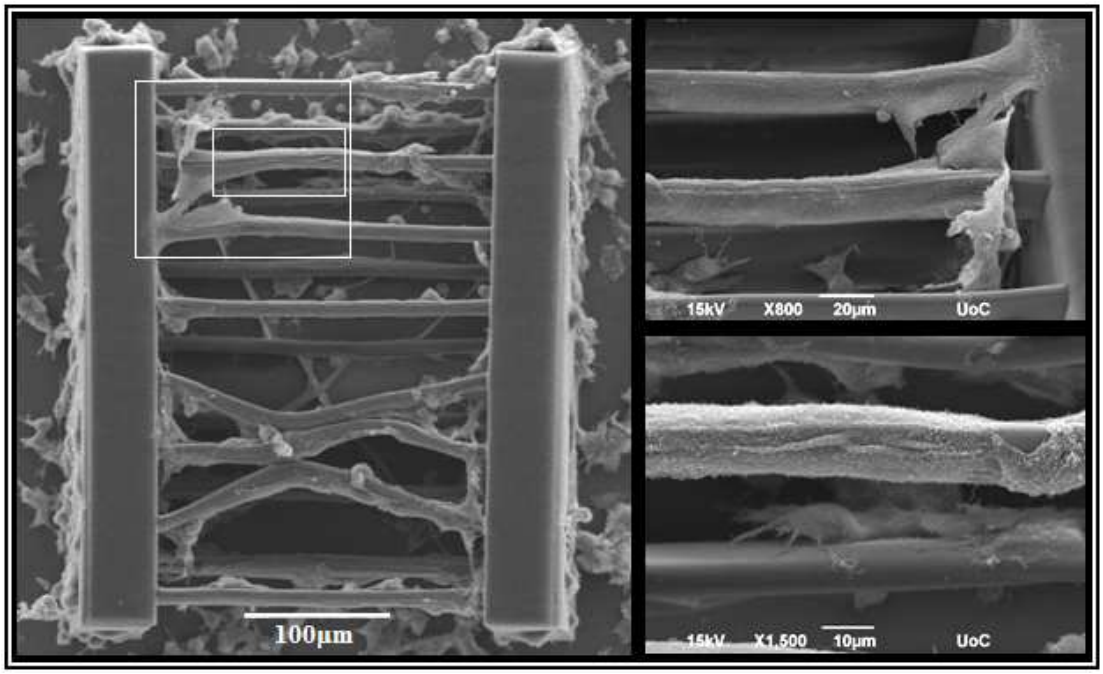

Figure 50: SEM images of neural cells cultured on PLA-based guidewires type scaffolds after 5 days of cultivation.

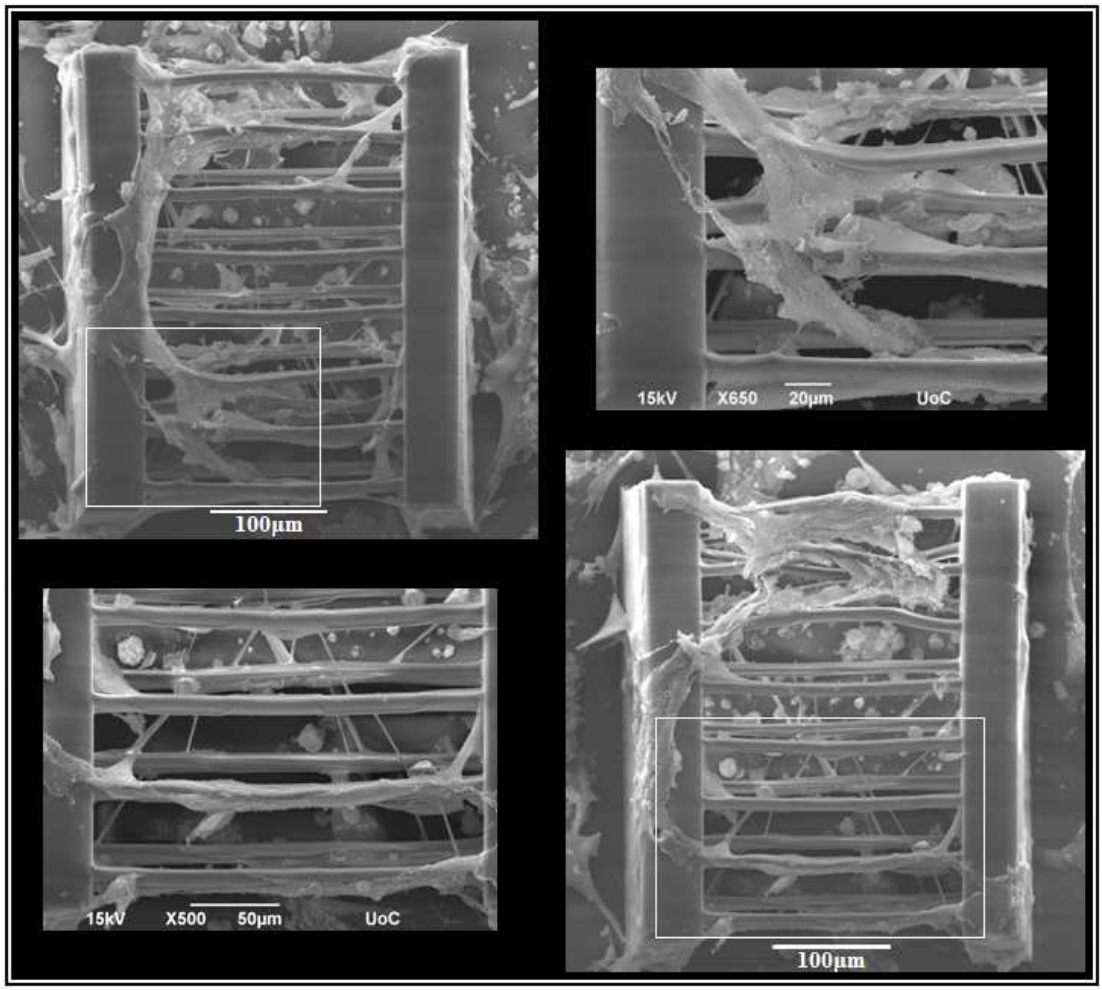

Figure 51: SEM images of fibroblast cells cultured on PLA-based guidewires type scaffolds after 5 days of cultivation.

Figures 50 and 51 indicate that both cell lines attached readily to the scaffolds, and extended their neurites (figure 50) and their filopodia (figure 51) along the guidewires. Moreover, in some cases, we can observe that cells use their projections to fill the empty space between two neighbour lines.

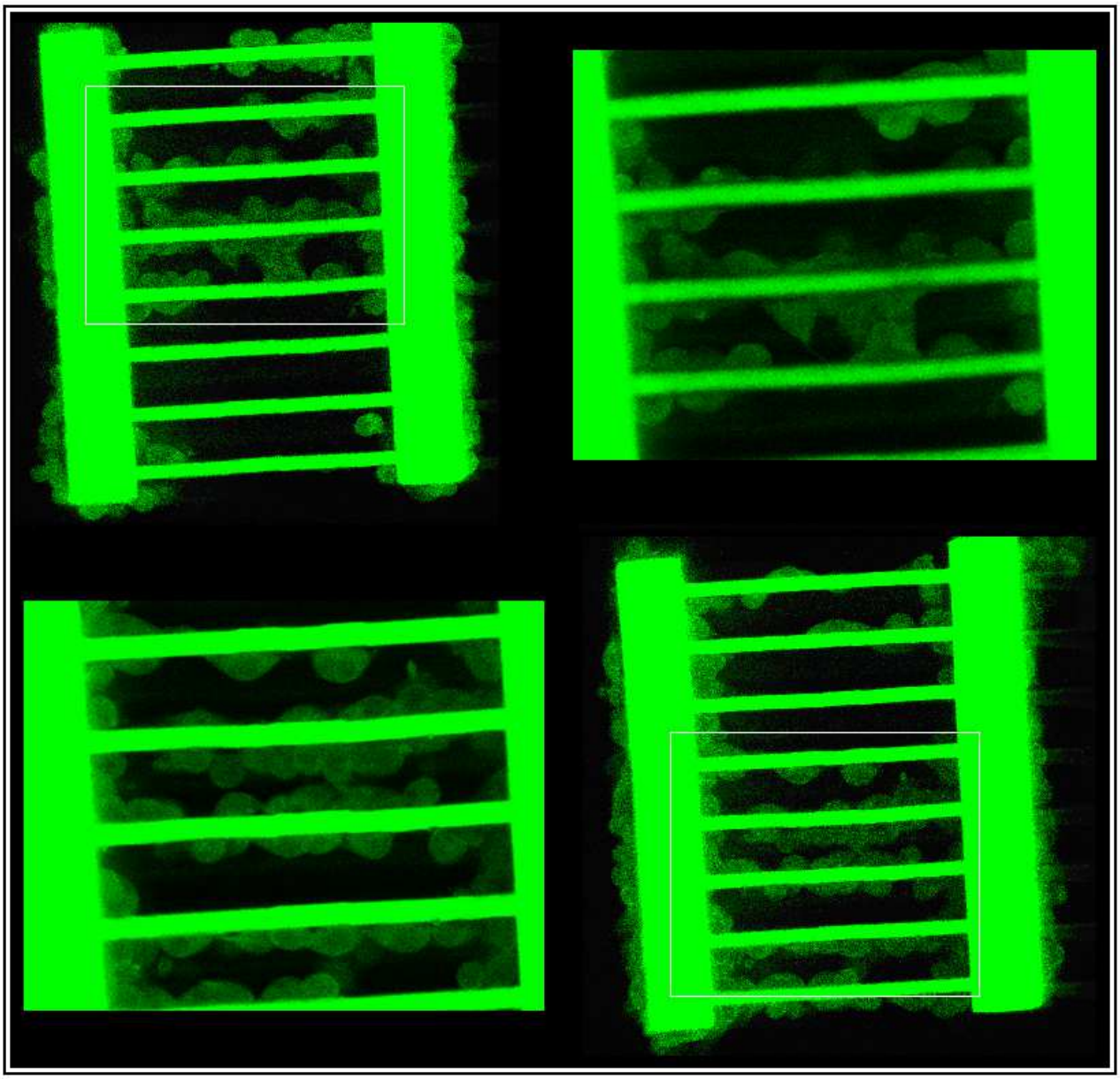

Figure 52: Detection of tubulin in neuronal cultured on 3D scaffolds of PLA-based material, using confocal microscopy analysis. Confocal microscopy images show the distribution of tubulin(green) in neurons cultured for 5 days. Furthermore the autofluorescence of scaffolds (green) is shown in figures too.

In figure 52, we can observe the distribution of tubulin (green) in neurons, that verify the neuronal differentiation of PC12 on 3D scaffolds.

5.4.7 Conclusions for the cultivation on biodegradable 3D Scaffolds

Cell attachment was shown to be further enhanced and facilitated by the proper choice of the shape and size of 3D scaffolds. Thus, in cubic structures the smaller cube volume facilitated cell proliferation as it was easier for the cells to explore the whole surface of the scaffolds, while smaller spacing allowed better cell communication with neighbouring cubes. In the cross-hatched scaffolds, cells preferred the larger structures that allowed cell migration inside the pores. Woodpile-shaped scaffolds were offering more cell adhesion points on the free extremities, facilitated cell migration within the scaffold. In the case of sea-shell type scaffolds and pyramid type scaffolds, cells were developed following the sketch of the scaffold. Finally, in the case of guidewires scaffolds, both cell lines attached readily to the scaffold, and extended their neurites and their filopodia along the guidewires.

5.5 Conclusions

In conclusion, in the first part of this study, two non-biodegradable, organic-inorganic hybrid photosensitive sol-gel materials were used; a Zirconium based and a Titanium based material in four different molar ratios of inorganic to organic part, in order to check the cytotoxicity. For this reason, thin films of these materials were used for cells cultivation. Our cells were attached on films and were healthy, so we led to the conclusion that our materials were not cytotoxic. Moreover, we observed that the type of cells that were used, preferred the materials that were formed harder surfaces. Then, we were used two-photon polymerization technique for the fabrication of three dimensional structures. These structures were used us scaffolds for cells cultivation. Cell attachment was shown to be further enhanced and facilitated by the proper choice of the shape and size of 3D scaffolds. Thus, in cubic structures the smaller cube volume facilitated cell proliferation as it was easier for the cells to explore the whole surface of the scaffolds, while smaller spacing allowed better cell communication with neighbouring cubes. In the cross-hatched scaffolds, cells preferred the larger structures that allowed cell migration inside the pores. Finally, woodpile-shaped scaffolds were offering more cell adhesion points on the free extremities, facilitated cell migration within the scaffold.

In the second part of this study, a new biodegradable polylactide-based material was used for fabricating tissue engineering scaffolds. Neuronal cells (cell line PC12), as well as fibroblast cells (cell line 3T3), were cultivated on two dimensional thin films for checking the cells viability and proliferation and after the encouraging biocompatibility results, 3D complex porous structures were fabricated. Cells development on cubic structures, cross-hatched structures and

woodpile-shaped scaffolds was similar to this on the same scaffolds made of the materials of the first part. In the case of sea-shell type scaffolds and pyramid type scaffolds, cells were developed following the sketch of the scaffold. Finally, in the case of guidewires scaffolds, both cell lines attached readily to the scaffold, and extended their neurites and their filopodia along the guidewires.

Future respective of this study is to observe the best combination of the right choice of mechanical and chemical functonalization properties of the materials, according to the cell type, which will be further used for tissue engineering.